PRODUCTION OF EPOXIDE FUNCTIONALIZED BOEHMITE
NANOPARTICLES AND THEIR USE IN EPOXIDE NANOCOMPOSITES

A THESIS SUBMITTED TO
THE GRADUATE SCHOOL OF NATURAL AND APPLIED SCIENCES
OF
MIDDLE EAST TECHNICAL UNIVERSITY

BY

ANISA ÇONIKU

IN PARTIAL FULFILLMENT OF THE REQUIREMENTS
FOR
THE DEGREE OF MASTER OF SCIENCE
OF
CHEMICAL ENGINEERING

JANUARY 2012

Approval of the thesis:

PRODUCTION OF EPOXIDE FUNCTIONALIZED BOEHMITE NANOPARTICLES AND THEIR USE IN EPOXIDE NANOCOMPOSITES

Submitted by **ANISA ÇONIKU** in partial fulfillment of the requirements for the degree of **Master of Science in Chemical Engineering Department, Middle East Technical University** by**,**

Prof. Dr. Canan Özgen   _____
Dean, Graduate School of **Natural and Applied Sciences**

Prof. Dr. Deniz Üner   _____
Head of Department, **Chemical Engineering**

Prof. Dr. Güngör Gündüz   _____
Supervisor, **Chemical Engineering Dept., METU**

Assist. Prof. Dr. Bora Maviş   _____
Co-supervisor, **Mechanical Engineering Dept., HU**

Examining Committee Members:

Prof. Dr. Ülkü Yılmazer   _____
Chemical Eng. Dept., METU

Prof. Dr. Güngör Gündüz   _____
Chemical Eng. Dept., METU

Prof. Dr. Hayrettin Yücel   _____
Chemical Eng. Dept., METU

Dr. Cevdet Öztin   _____
Chemical Eng. Dept., METU

Prof. Dr. Cevdet Kaynak   _____
Metallurgical and Materials Eng. Dept., METU

Date: 19.01.2012

I hereby declare that all information in this document has been obtained and presented in accordance with academic rules and ethical conduct. I also declare that, as required by these rules and conduct, I have fully cited and referenced all material and results that are not original to this work.

Name, Last name :   ANISA CONIKU

Signature   :

ABSTRACT

PRODUCTION OF EPOXIDE FUNCTIONALIZED BOEHMITE NANOPARTICLES AND THEIR USE IN EPOXIDE NANOCOMPOSITES

Coniku, Anisa

M.Sc., Department of Chemical Engineering

Supervisor   : Prof. Dr. Güngör Gündüz

Co-supervisor : Assist. Prof. Dr. Bora Maviş

January 2012, 130 pages

In the present study the effects of addition of organically functionalized boehmite nano-particles on the mechanical properties of epoxy polymers were analyzed. Nanosize platelets of boehmite powders were produced via a hydrothermal process from the raw material aluminum trihydroxide $Al(OH)_3$ provided by a a chemical supplier, but which in future studies can be replaced by local resources of aluminum trihydroxide available in Seydişehir, Turkey. The ground aluminum trihydroxide particles were submitted to a two-step preliminary ageing procedure in different pH media. Particles were then converted to boehmite nanoparticles via hydrothermal ageing at high pressure and temperature. The product's chemical identity, size, structure and morphology were characterized with XRD, FT-IR, SEM and PSA analyses. By controlling the pH and the ageing time as parameters, hexagonal shaped nanoplatelets were obtained with dimensions ranging from 100 to 500 nm. Aiming at using these nanoparticles into surface coating polymers, the most favorable shape is the plate-like morphology, leading to adopting the last hydrothermal condition in the rest of the study.

The boehmite crystal surfaces are furnished with hydroxyls which can potentially be reacted with epoxy monomers of bisphenol A diglycidyl ether with the help of tin (II) chloride as catalyst through ring-opening reactions. The FT-IR and quantitative analyses indicated that this surface functionalization is possible under a temperature 80 ^{o}C and a weight ratio of 5:1 epoxy monomer to boehmite powder

These novel inorganic/organic hybrid materials were then mixed with epoxy/hardener resin mixture to obtain nanocomposites. The properties of the composites were characterized accordingly with tensile, impact, micro hardness, micro-scratch tests, DMA analysis and observed with SEM analysis.

A deterioration of the tensile strength from the neat polymer was observed, with a distinct trend between the functionalized and non-functionalized boehmite-epoxy polymers. The functionalized polymers showed a less deteriorative character. The tensile modulus instead showed a little improvement of (~4%) in 5wt% loaded polymers. DMA analysis results revealed an improved glass transition temperature in the nanocomposites as well as in storage and loss modulus. As aimed in this work, the functionalized boehmite-epoxy polymers displayed a clear improvement in comparison to both non-functionalized and neat polymers in surface coating properties in hardness and scratch resistance.

Keywords: hydrothermal synthesis, epoxy functionalization, boehmite nanoplatelet, epoxy nanocomposites, scratch resistance.

ÖZ

EPOKSI IŞLEVSELLEŞTIRILMIŞ BÖHMIT NANOPARÇACIKLARIN ÜRETILMESI VE EPOKSI POLIMER KOMPOZITLERDE KULLANIMI

Coniku, Anisa

Master, Kimya Mühendisligi Bölümü

Tez Yöneticisi : Prof. Dr. Güngör Gündüz

Ortak Tez Yôneticisi: Yrd. Doç. Dr. Bora Maviş

Ocak 2012, 130 sayfa

Bu çalışmada yüzeyleri organik bileşiklerle işlevselleştirilmiş böhmit nanoparçacıkların eklenmesiyle üretilmiş epoksi polimer kompozitlerinin mekanik özellikleri incelenmiştir. Çalışma süresince nanoboyutta plaka şeklinde böhmit tozları, başlangıç maddesi olarak alüminyum trihidroksitten hidrotermal yöntemle üretilmiştir. Üretim yöntemi, yöntemin ileride Seydişehir Alüminyum tesisi ara ürünleriyle de sürdürülebilir olması şartı göz önünde tutularak geliştirilmiştir. Hidrotermal süreçte pH değeri ve yaşlandırma süresi kontrol edilerek boyutları 100-500 nm arasında değişen altıgen nanoplakalar elde edilmiştir. Öğütülmüş alüminyum trihidroksit parçacıklar farklı pH değerine sahip ortamlarda ultrasonik karıştırma ile iki aşamalı bir ön yaşlandırma işlemine tabi tutulmuştur. Parçacıklar yüksek basınç ve sıcaklıkta hidrotermal yaşlandırma ile böhmit parçacıklarına dönüştürülmüştür. Ürünlerin kimyasal yapıları, boyutları ve şekilleri, x-ışınları saçınımı (XRD), Fourier dönüşümlü kızıl ötesi spektroskopisi (FTIR), taramalı elektron mikroskobu (SEM) ve parçacık boyut analizi (PSA) ile belirlenmiştir. Ön yaşlandırma evresinde kullanılan sulu çözeltinin pH değerinin parçacıkların son şekillerinin belirlenmesinde önemli olduğu görülmüştür. Asidik değerlerde iğne yapılı nanoparçacıklar oluşurken, ılın (nötr) değerlerden bazik değerlere geçişte ise dörtgen prizmadan altıgen plakalara

doğru bir değişim gözlenmiştir. Çalışmanın ileri aşamalarında altıgen nanoplakaların oluşmasını sağlayan koşullar uygulanmıştır.

Böhmit kristal yüzeylerinde yer alan hidroksil grupları kalay klorür gibi bir katalist eşliğinde halka açılma tepkimeleri sonucunda bisfenol A diglisit eter gibi bir epoksi monomeriyle tepkimeye sokulabilir. Bu şekilde sentezlenmiş melez bir malzemenin ikili özellikler göstermesi beklenir. Anılan tepkime farklı sıcaklık ve epoksi:böhmit oranlarında gerçekleştirilmiş, ve FTIR ve nicel analizler yardımıyla bu şekilde böhmit yüzeylerinin işlevselleştirilmesinin olası olduğu ortaya konmuştur. Çalışmanın ileri aşamalarında tepkime için en uygun koşullar uygulanmış ve tepkime epoksi:böhmit oranı 5:1 olacak şekilde 80°C'de gerçekleştirilmiştir.

Bu yeni inorganik/organik melez malzeme nanokompozit üretimi amacıyla epoksi sertleştirici reçineyle birleştirilmiştir. Kompozitlerin mekanik özellikleri çekme, darbe, sertlik ve çizilme dayanımı testleriyle incelenmiştir. Ayrıca dinamik mekanik analiz (DMA) ve SEM aracılığıyla kompozitlerin termal davranışları ve kırılma yüzeyi biçimleri incelenmiştir. Mekanik özelliklerde beklenen iyileşmeye karşın, özellikle çekme dayanımında saf polimere göre kompozitlerin özelliklerinde bir gerileme gözlenmiştir. Bunun yanında işlevselleştirilerek veya işlevselleştirilmeden bünyeye yapılan eklentilerde, işlevselleştirilen parçacıkların kompozit özelliklerini daima daha az gerilettiği tespit edilmiştir. Bunun yanında çekme modulusu (miyarı) ağırlıkça yüzde beşlik eklentilerde yüzde dört gibi bir ilerleme sağlamıştır. DMA analizlerine göre kompozitlerin camsı geçiş sıcaklıkları fark edilir derecede yükselmiştir. Ayrıca toplama ve kaybetme modulus değerlerinde de ilerleme kaydedilmiştir. En iyi sonuçlar ise sertlik ve çizilme dayancında elde edilmiştir. İşlevselleştirilmiş böhmit nanoparçacıklarının eklendiği kompozitler hem saf polimere göre hem de sade böhmit parçacıklarının eklendiği kompozitlere göre daha iyi sonuçlar vermiştir.

Anahtar Sözcükler: işlevselleştirilmiş nanoboyut böhmit, hidrotermal yöntem, bisfenol A diglisit eter epoksi monomeri, inorganik/organik melez malzeme nanokompozit, sertlik ve çizilme dayancı

To my family and my friends,
for their love, patience and support

ACKNOWLEDGEMENTS

TABLE OF CONTENTS

LIST OF TABLES

TABLES

LIST OF FIGURES

FIGURES

LIST OF SYMBOLS AND ABBREVIATIONS

A_o	Initial cross sectional surface
C	Concentration
d	Diameter
f	Frequency
E	Surface energy
E	Elastic modulus
E′	Storage modulus
E_{max}''	Maximum value of loss modulus
F	Tensile load
L_o	Gauge length
MW	Molecular weight
m	Mass
N	Molarity
n	Mole
ΔS	Change in surface area
ΔT	Temperature change
T_g	Glass transition temperature
t	Time parameter
tanδ	Loss factor - E″/E′
V	Volume
γ	Surface energy density
ε	Normative strain
σ	Tensile stress
ν	Poisson's ratio
$δ^-$	Partial negative charge
$δ^+$	Partial positive charge
ρ	Density

2D		Two dimensional
3D		Three dimensional
ATH		Aluminum trihydroxide
AA		Acetic acid
BADGE		Bisphenol A diglycidyl ether
B.P		Boiling Point
DMA		Dynamic Mechanical Analysis
DIW		Dionized Water
FTIR		Fourier Transform InfraRed spectroscopy
i-POH		iso-Propyl alcohol
NH3		Ammonia
P		Pressure
$\mathbf{P_{d,max}}$		Maximum residual depth for penetration
PSA		Particle Size Analysis
$\mathbf{R_{d,max}}$		Residual depth
SEM		Scanning Electron Micropscopy
XRD		X-Ray Diffraction analysis

Units

Bar	Bar
g/mol	Gram per mol
g/ml	Gram per milliliter
hr	Hour
Hz	Hertz
J	Joule
kV	Kilo-volt

mA	MiliAmper
mg	Miligram
ml	Mililitre
mm	Milimeter
m²	Meter square
N or (mol/ml)	Mol per milliliter
nm	Nanometer
rpm	Revolution per minute
wt%	Weight percentage
µm	Micron-meter
µg	Micron-gram
%	Percentage
º	Degree
ºC	Celsius degree

CHAPTER I

INTRODUCTION

Throughout the history, humankind has continuously been trying to improve quality of life. By combining different materials provided naturally, such as mud and straw, early Egyptian civilization obtained strong and durable buildings. The same logic has been devotedly continued to the present days. Material science and technology has provided humankind with materials not available in nature, making life and technology reach mind-boggling results. Once the plastics were developed, technology hurried to substitute materials which were scarce in nature, but still the plastics alone were not strong enough to keep up with such massive substitution. In order to strengthen and improve rigidity of the plastics, in 1935 Owens Corning developed the first glass fibers. What was once considered as an ill-fated discovery revolutionized whole industries from automotive to electrical, electronics, construction, coatings, etc. [1]. According to Tim Palucka [1], a composite is defined as a combination of two heterogeneous phases, whatever their nature and origin. It is the interface between these phases which defines the degree of enhanced mechanical, physical and chemical properties of the new composite. Focusing on the polymer matrix composites, composites can be classified into three main classes, based on the dimensions of the fillers; macro, micro and nano scale composites. The smaller the size, the more surface area is available for contact between two phases, providing better properties and more stability. Still in the late 1980s a new generation of nanocomposites emerged with improved interface connections through modification of the surface of the nanoparticles.

In the first part of this study nanoscale boehmite platelets were produced from aluminum trihydroxide (gibbsite). Boehmite (AlOOH) particles can be produced with different morphologies and sizes. It constitutes differing proportions of bauxite one of the abundant forms of aluminum ore along gibbsite. Boehmite is known best as being the precursor of γ-alumina, which is widely used as catalyst support or in adsorbents, composite materials and ceramics. Besides γ-alumina related applications, among many other usages, in several studies, boehmite has been used as a filler in plastics to produce nanocomposites in both thermoplastic and thermoset polymers [2, 3]. In the ceramic filler category boehmites have been incorporated to the composites to improve their flame retardant properties, though the effect on mechanical properties has generally been the opposite [4]. Effects of addition of boehmite on the mechanical properties such as fracture toughness, hardness, tensile strength, stiffness, elongation, thermal stability have been studied [5-8]

Boehmite crystals have a double layered structure with oxygens and aluminum cations arranged in an orthorhombic dipyramidal matrix as shown in figure 1.1. The oxygens are organized in cubic closed packing [9-11].
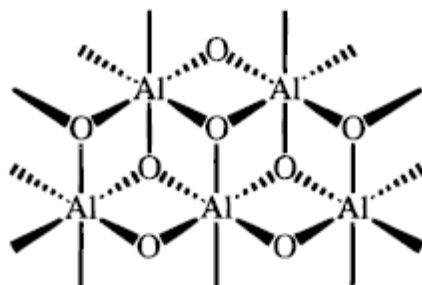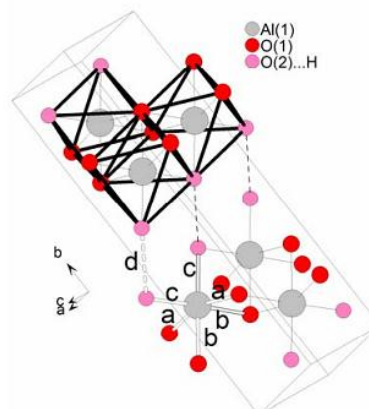
| (a) | (b) |

Figure 1.1 The boehmite structure,(a) schematic of positions of surface atoms in the crystal structure of boehmite. Note that oxygens connected with solid lines lie above and ones with dashed lines lie below the plane Al cations reside. Oxygens above the plane are pointed towards the layer double hydroxide galleries and associated with hydrogens [5], (b) view of a boehmite unit cell along [101] direction: arrangement of edge-sharing AlO_6-octahedra within layers [10]. Hydroxyls pointing to the galleries are shown in pink color and they are hydrogen bonded to the hydroxyls of the next layer.

As shown in figure 1.1.-a, there are two types of oxygen in the boehmite; the ones situated within the layer are shared between four octahedras, whereas the ones on the sides or pointing to the layers galleries are shared by two octahedras. The latter are hydrogen bonded to two similar oxygens on adjacent layers which is shown in figure 1.1-b. The hydroxyl groups present on the outer surface of the crystal make possible the modification of the surfaces with other groups, be it hydrophobic, hydrophilic, etc.

The production of boehmite from aluminum hydroxides have been achieved by several methods, such as sol-freeze drying $AlCl_3.6H_2O$ as raw materials [12], hydrolysis of an aluminum alkoxide under standard conditions, precipitation of inorganic salts like aluminum chloride [13], aluminum nitrate

3

[14] in an aqueous medium with neutralizing agents such as sodium hydroxide [15], urea [16], sodium bicarbonate [17], ammonia [14], etc. Also spray-pyrolysis method [18]and hydrothermal synthesis methods at elevated temperature are available [16, 19-28].

In sol-freeze drying, it is hard to control agglomeration, and the resulting wide size distribution is a major drawback of this method. Additionally the required aging time to precipitate boehmite is longer [12]. On the other hand, the hydrolysis methods stand out to be rather expensive due to the high costs of aluminum alkoxides [19]. The precipitation method involves the extensive need for the control of multiple factors such as pH, temperature or ionic strength in prevention of agglomeration.

Hydrothermal method is the most widely used one when it comes to good control of morphology on nanosize [27, 29] with a direct synthesis of sub-micrometer powders having a narrow size distribution. This method involves a combination of two parameters such as heating the reagent solution at high temperature and pressure up to $300^{\circ}C$ and 100 MPa.

Despite the benefits that nanosize materials contribute to the development of better composites in coating industry, there are specific aspects of nanosize such as high surface area, high Van der Waals interactions which cause high agglomeration level in the composites. As a solution to this, surface modification of the particles has been suggested and applied in the last decade. In this study, the nanosize produced boehmite particles are modified with special organic reagents such as bisphenol A diglycidyl ether, containing very reactive epoxide groups. As a polymer matrix in this study epoxy polymer is used. Epoxies are thermosetting polymers. These polymers are characterized by their extremely reactive epoxy groups, which are planar three-membered rings consisting of two carbon atoms and an oxygen atom shown in figure 1.2.
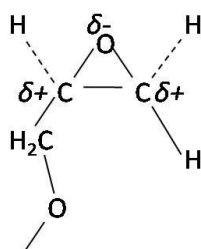
Figure 1.2 Chemical structure of epoxy group.

The reactive nature of this group is induced from the highly strained bond angles together with the polarization of the C-C and C-O bonds. These two factors make epoxy ring more reactive than non-cyclic ethers and more practical in functionalization and curing processes, providing a wide variety of compounds [30].

Once the surface of the boehmite nanoparticles had been functionalized, these novel inorganic/organic hybrid materials were mixed with epoxy/hardener resin mixture to obtain nanocomposites. The resulting composites are expected to possess better mechanical properties, such as scratch resistance, toughness, chemical resistance and thermal stability.

CHAPTER II

LITERATURE SURVEY

2.1 Hydrothermal synthesis of boehmite crystals

Hydrothermal synthesis until the last two decades had been widely used in the industry, especially in the precipitation of gibbsite in Bayer process and the preparation of alumino-silicate zeolites. There have been several studies on the synthesis of nanosize boehmite [19-26].The main advantages of hydrothermal synthesis are the low temperature operation, direct synthesis of sub-micrometer powders having a narrow size distribution. The main mechanisms suggested to control the particle nucleation and growth of the crystals under hydrothermal environments are the dissolution-recrystallization processes, while the complex ions have been considered to be the precursors of the nucleation. By nucleation in the reaction solution, these poly nuclearions tend to form particles of critical size and grow by aggregation. In such reactors, just by controlling pH, temperature and reagent concentrations, it is possible to obtain powders with well-defined properties [31].

The first study of the production of boehmite by the hydrothermal synthesis was done by Bugosh [17], but in later studies modification of the morphology of the produced powders was essayed. Bokhimi et al. [29]by dissolving $AlCl_3 \cdot 6H_2O$ and NH_4OH in distilled water and using reactor temperatures up to 240^oC reported to have obtained thin plates. Tsuchida et al. [20] produced 100nm boehmite platelets from an amorphous hydrated

alumina gel at 255°C after 24 h using different solvents and also introduced the technique of pre-milling the starting material in order to obtain a narrow size distribution of crystalline product.

Li et al. [25] stated to have obtained ultrafine nanofibers with an average diameter of 10 nm. They developed a simple route where the reaction reagents used were aluminum chloride ($AlCl_3 \cdot 6H_2O$) and ammonia ($NH_3 \cdot H_2O$), and as a surfactant cetyltrimethyl ammonium bromide (CTAB). These new powders showed a typical polycrystalline nature. Liu et al. [26]by introducing structure-directing reagent in the acetic acid-sodium buffer solution for the hydrothermal synthesis of boehmites obtained flower-like bunch of boehmite nanowires. Yanigasawa et al. [27] prepared hydrothermally large hexagonal plates with average dimensions of about 4 μm at 250°C for 6 hours. As aluminum source this group used aluminum nitrate $Al(NO_3)_3$ solutions and as hydroxyl group sources sodium hydroxide NaOH was added. In figure 2.1, different boehmite crystal morphologies are shown, each of which was produced under different hydrothermal conditions summarized above.
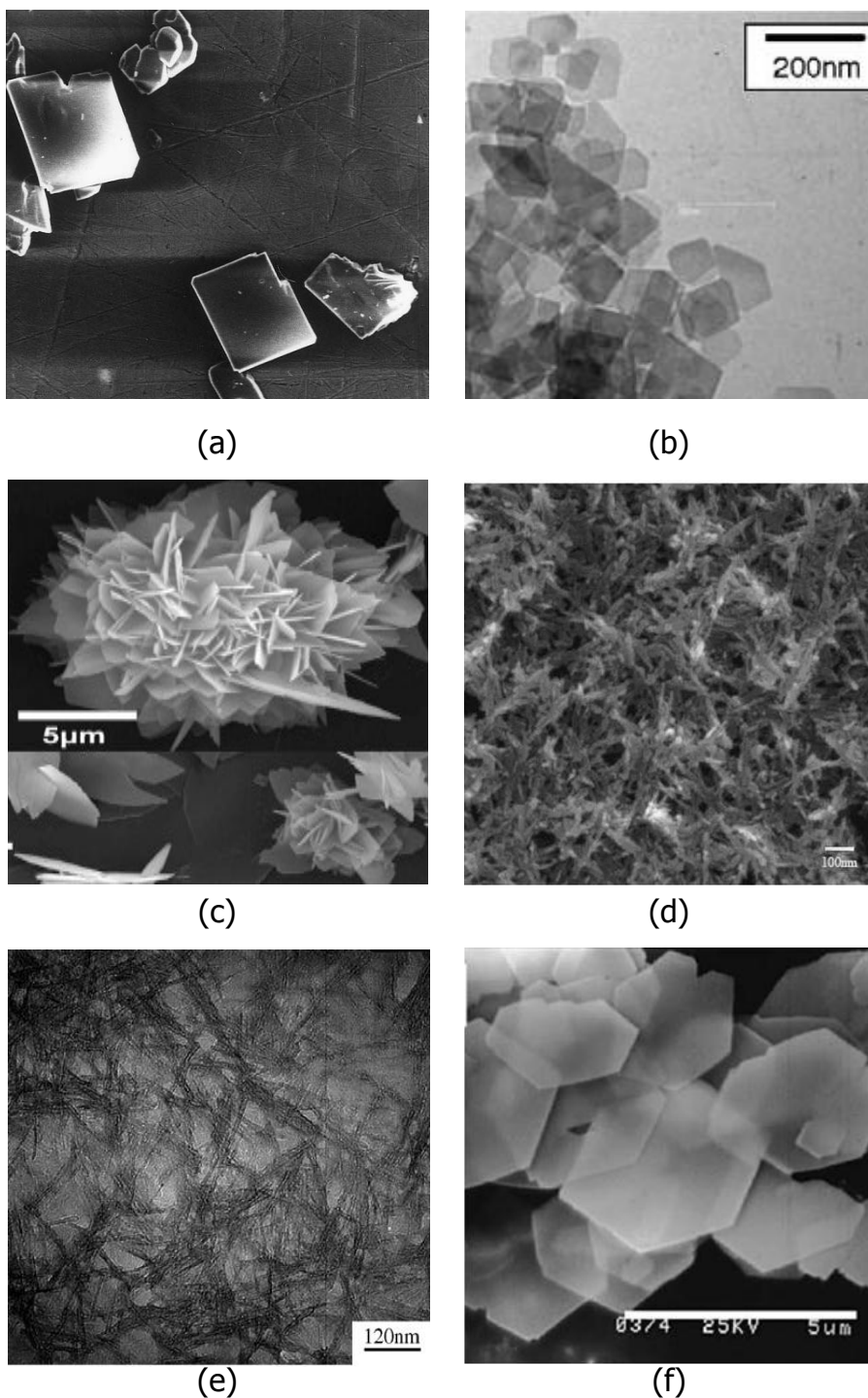
Figure 2.1. Different morphologies of boehmite crystals: (a) rectangle like plates [2], (b) rhombohedral like platelets [3], (c) three dimensional flower-like boehmite superstructure [7], (d) flower-like bunches of boehmite nanowires [8], (e) boehmite nanofibers [14], (f) hexagonal plates of boehmite crystals [15].

2.1.1 Temperature effect on crystal formation

Independent from the aluminum source used, several studies have shown that the formation of boehmite under hydrothermal conditions is highly dependent on the reactor temperature. Mishra et al. [16] introduced urea as neutralizing agent into the hydrothermal synthesis of boehmite with aluminum nitrate $Al(NO_3)_3$ as starting material. They tried several temperatures from 160 to 220°C, observing an amorphous gel precipitation of pseudo-boehmite at 160°C to a well crystallized boehmite at 200°C. While at temperatures below 160°C no precipitation was observed, indicating that no crystalline structure formed at these temperatures.

Bokhimi et al. [29] precipitated boehmite crystals of different sizes at different temperatures, ranging from 23 to 240°C. As starting material hydrous aluminum chloride $AlCl_3 \cdot 6H_2O$ and ammonia solution NH_4OH were used. As the reactor temperature was increased from 23 to 240 the crystallite size grew from 1 to 27 nm.

Yanagisawa et al. [27], using gibbsite mineral as starting material in water environment observed that at temperature 200°C, a little amount was converted to boehmite while at higher temperatures like 230-250°C complete transformation to boehmite occurred. While, using aluminum nitrate as aluminum source and sodium hydroxide as hydroxyl source, they studied the phase transformation starting at room temperature where aluminum nitrate precipitated as bayerite a polymorph of aluminum hydroxide $Al(OH)_3$ to later at a temperature of 150°C crystallized to gibbsite and finally completely transformed to boehmite crystals at 230°C. Beside the temperature effect, they concluded that aluminum nitrate served as mineralizer to obtain larger crystals.

According to Chen et al. [32], at temperatures below 140°C no precipitation product was observed, while from the XRD analysis results as temperature is increased from 140 to 200°C, the crystallinity improved. But according to their FTIR results of the boehmite crystals, as the temperature of the reactor is increased a shifting to lower wavenumbers was observed in the asymmetric (Al)O-H spectra attributed to phase transition from pseudo-boehmite to boehmite.

Studies have revealed that also the morphology of the crystals forming showed a dependency on the reactor temperature. Bugosh et al. [17]operated the hydrothermal process at low temperatures like 140-160°C for long reaction periods as 20 hours under constant stirring. The produced boehmites had morphology of fiber like with a length of 100-200 nm. Sterte et al. [33], investigated synthesis of boehmite crystals in the temperature range 110-160°C. They observed that with higher operation temperatures the crystallinity degree increased along with the particle dimensions.

2.1.2 pH effect on crystal morphology

The presence of impurities and solvent molecules affects crystallization process by intervening in interface interactions. The morphology of a crystal is controlled by the differing growth rates of specific faces of a crystal which are highly influenced by the solvent-solute interactions including Van der Waals, ionic, hydrogen bonds. Using this fact it is possible to design the shape of crystals. Several studies have been done in this direction.

Chen et al. [32], by controlling the pH with neutralizing agent urea, observed that nanowires crystals were synthesized in acidic environment (pH~5) while at basic pH~10 they obtained 2D nanoplatelets.

10

Zhu et al. [34] after obtaining Al(OH)$_3$ as a precipitation product from the solution of NaAlO$_2$ with acetic acid, studied the crystal formation in the hydrothermal process by changing the pH, surfactant and temperature factors in the reaction medium. To control the pH acetic acid and ammonia solution were used, while as surfactant polyethylene glycol. At pH values around 4 or less porous lathes were produced, with the addition of ammonia the shape of crystals changed to thin plates. At pH~6 a mixture of plates and porous laths were obtained, while at pH ≤ 9 only porous plates were observed. They observed also that without the addition of the surfactant and rising of temperature, the crystal growth was very sensitive to pH values.

Another interesting study is that of Okada et al. [35]. They studied the dependence of the boehmite crystal formation on the temperature and the pH of the reaction media. Using two different methods, precipitation and hydrothermal, they tried to produce boehmite from aluminum nitrate and sodium aluminates in precipitation and commercial boehmite in the hydrothermal method. The pH of the reaction media was controlled by the addition of aqueous sodium hydroxide. They observed that pH parameter was more dominant than temperature in the control of the crystal morphology. At temperature around 80°C as the pH got lower ~5 gel-like product was obtained. While the boehmite phase was observed at a pH range of 7 to 10 which was explained with the higher solubility of alumina at these pH values. They stated that higher pH accelerated the rate of dissolution/re-precipitation reaction resulting in larger boehmite crystals. Another important point is the formation of bayerite phase at pH values above 11.

To come to a conclusion with the pH parameter in the hydrothermal synthesis, from the studies presented in this part, it is presumed that at acidic pH and high temperatures, the crystal formation will take place in one direction giving 1D shapes as it is shown in figure 2.2, while at alkaline medium, the formation of crystals shall happen in two directions resulting in

2D shapes. This late result is the one which will be used in the present study, since the main aim is to modify these surfaces by introducing different organic compounds to the hydroxyl groups on the surfaces.
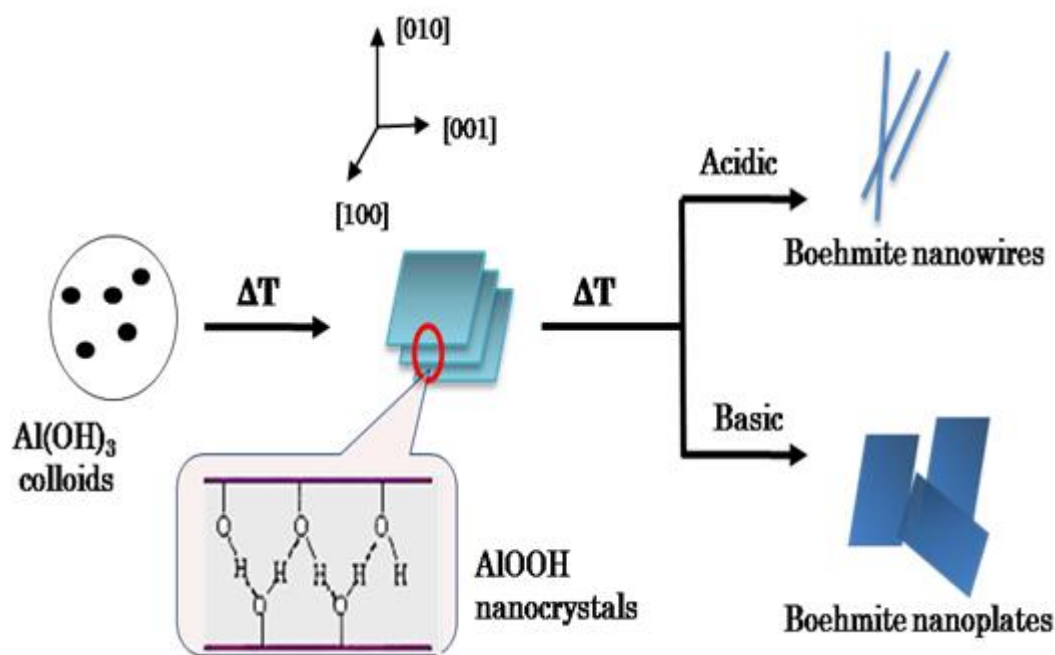
Figure 2.2 Simplified schema of the hydrothermal process and the pH effect on the boehmite products.

2.1.3 Mechanical grinding effect

Besides reaction parameters like pH and temperature, the reagent size is also another criterion to be studied in cases where the feed is a solid rather than a water soluble salt. Tsuchida et al. [2] did grind the gibbsite in a planetary ball mill in air for 2 and 6 hours, before starting the hydrothermal process. They observed that from these ground gibbsite samples, submicrometer boehmite crystals with a narrow size distribution can be obtained. At the same time, Tsuchida implied that the finely ground gibbsite

with an active and meta-stable character is more easily dissolved in the hydrothermal reaction medium, resulting in a faster and more size controllable boehmite production. In milling, ATH was first dispersed in the process control agent, which was isopropyl alcohol (i-POH). According to Suryanarayana et al. [36], there are several factors which urged the utilization of such a process control agent. First, during grinding due to the heavy plastic deformation they undergo, the powders are prone to suffer cold-welding (fusing) which with time cause agglomeration. In order to prevent this phenomena a surface control agent (also indicated as lubricants or surfactants) is mixed up with the powders before the grinding process. The role of this agent is to keep the grinding medium as homogeneous as possible, and also to lower the surface tension. Reducing the surface tension, means increasing the contact surface area of the powders, which will reduce the surface energy as expected from equation 1 [36].

$$E = \gamma \cdot \Delta S \tag{1}$$

Equation 1 is the representation of the energy needed in the size reduction process via physical treatment, where γ is the specific surface energy and ΔS is the increase of surface area. A decrease in surface energy means shorter milling time, which as a result means lower temperatures reached inside the milling chamber and less risks for phase transformations. There is a wide range of process control agents, such as ethanol [37], stearic acid [38, 39] polyethylene glycol [40], ethyl acetate [41]. All of them were used in preparation of alloyed metals. Korhan et al. [42] studied the effect of several organic agents such as ethylene glycol, acetic acid and water in grinding aluminum trihydroxide. A mixture of them gave the smallest size of particles around 400 nm with respect to the shortest time of milling. While grinding with i-POH yielded powders of size around 500 nm.

2.2. Epoxy functionalization

In the last two decades the reputation of nanoscience has become quite eminent. From different studies in nanoscience, it can be seen that introduction of nanoparticles in many systems has proved to be more efficient in comparison to their counterparts with larger dimensions. Still there is much to improve and as the size goes smaller, the more difficult the control becomes. At the same time, there are factors that cannot be neglected even at nanosize. In the case of nanoparticles of boehmite which has an organophobic character, this character is a challenge to be overcome if boehmite is to be incorporated in the organophilic epoxy resins.

In order to obtain a compatibility of these two different characters, many solutions have been provided. The first solutions tried were the ion exchange methods in polymer-clay nanocomposite systems [43, 44]. Another solution and more widely used is the introduction of coupling agents [45-49] such as alkoxysilane monomers as demonstrated in table 2.1. The approach in principle is easy to understand, a monomer with different organic groups is to be reacted with surface groups of the nanoparticles such as hydroxyl groups, while on the other pole a reactive group should be available to react with the monomers or polymeric chains of the resins. Several studies were reported in the last 20 years.

Table 2.1 List of various coupling agents used in nanocomposite systems.
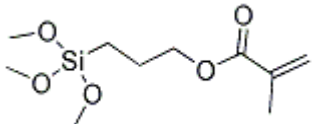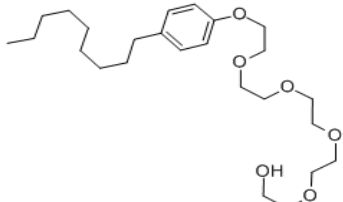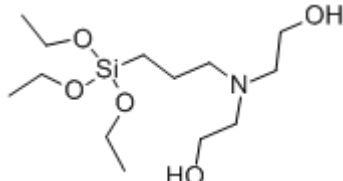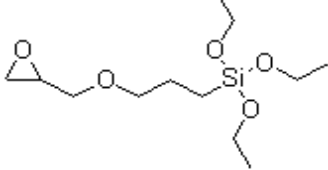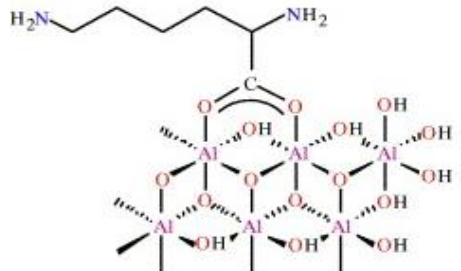
γ-Methacryloxypropyltrimethoxysilane; Silane Coupling Agent	Tan et al. [45]
polyoxyethylenenonyl phenyl ether	Rong et al. [46]
3-aminopropyl triethoxysilane	Tee et al. [47]
3-glycidyloxy propyltrimethoxysilane	Bajaj et al. [48], Shukla et al. [49]
lysine-alumoxane	Callender et al. [50]

Table 2.1 (Cont.d)
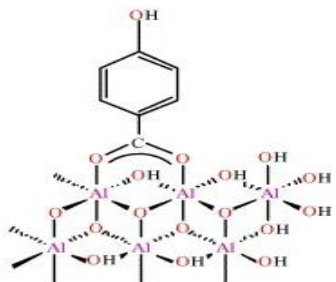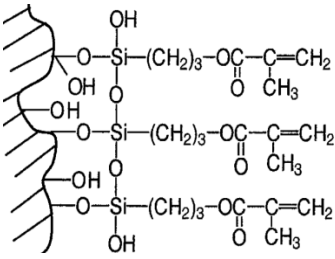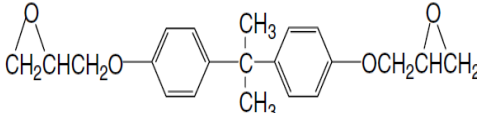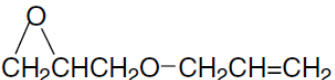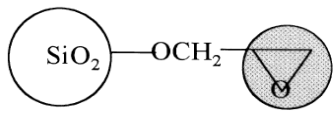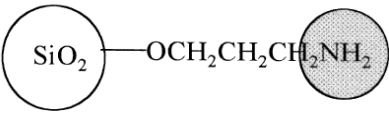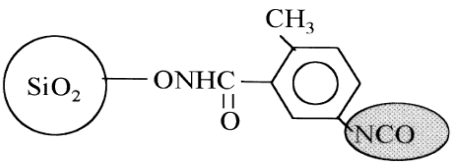
 para-hydroxybenzoate alumoxane	Callender et al. [50]
 Chemical grafting of trimethoxysilyl-terminated propyl methacrylate onto silica nanoparticles	Bauer et al. [51]
 diglycidylether of bisphenol-A	Ying-Ling et al. [52]
 Allylglycidylether	Ying-Ling et al. [52]
 Functionalized with epichlorohydrin	Kang et al. [53]

Table 2.1 (Cont.d)

Functionalized with aminopropyltriethoxysilane	Kang et al. [53]
Functionalized with tolylene 2,4-diisocyanate	Kang et al. [53]

Barron and his coworkers have excelled in their alumoxane preparation [50]. They have succeeded in obtaining stable carboxylate alumoxanes, by reacting boehmite with various carboxylic acids, examples of which are shown in table 2.1. They stated that the carboxylate ligand is covalently bound to the surfacial hydroxide group of the boehmite mineral, providing thus reaction sites when incorporated in epoxy curing. The process is simply demonstrated in figure 2.3.
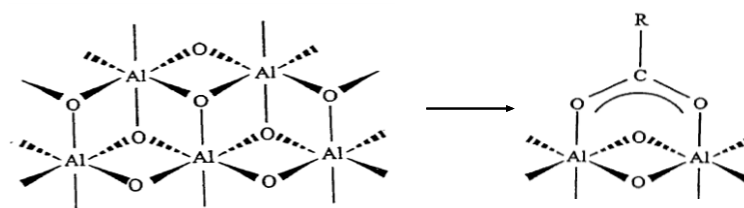
Figure 2.3 Chemical functionalization of boehmite particles with carboxylic acids

Bauer et al. [51] grafted methacroyloxy (propyl)-trimethoxysilane (shown in table 2.1) onto the surfaces of nanosize silica and alumina particles. The modified particles were used as monomers in polyacrylate matrix to improve the scratch and abrasion resistivity of the polymer coating.

Another interesting study is the work done by Kang et al. [53]. They have reported to have successfully modified the surfaces of silica powders with different organic groups such as epoxide ring, amine or isocyanate groups, which are shown in table 2.1. Based on the above short review, it can be seen that in many studies modification of surfaces of silica mineral have been tried to. Referring to the surface hydroxyl groups, silica and boehmite resemble each other in this aspect.

A study of Ying Ling et al. [52] reports to have succeeded, by sol-gel method, the chemical functionalization of nanosize silica particles with oxirane ring of epoxy compounds, also shown in table 2.1. They observed that the epoxy rings successfully reacted with the OH groups of silica with the aid of tin chloride as catalyst. Still what they obtained was more OH group rich surfaces than oxirane groups rich surfaces. The process is shown in figure 2.4.
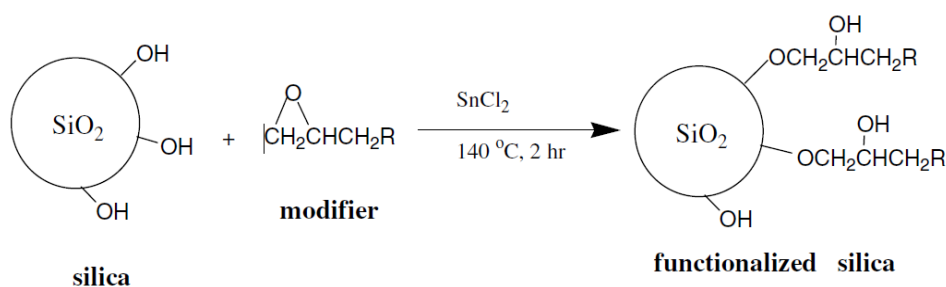
Figure2.4 Surface modification of silica nanoparticles, according to Ying Ling et al.

In this study, the aim is to obtain nanosize boehmite particles with oxirane group-rich surfaces as shown in figure 2.5.
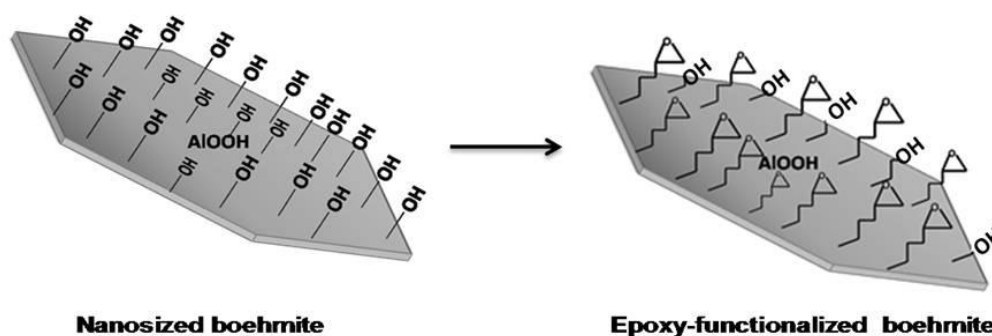
Figure2.5 Functionalization of boehmite nanoparticles with oxirane rings as it is targeted in this study.

2.3 Nanocomposite polymer preparation

The role of epoxy polymers in industry is known to be significant in many fields of industry, finding applications in coating, automotive, construction, electrics, electronics, etc. Epoxy polymer or epoxy resin is characterized with the epoxy groups as shown in figure 2.6.
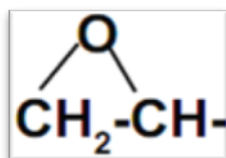
Figure 2.6 Epoxy group

Epoxy resins are produced from the reaction of simple chemicals, available and not expensive [54]. The schema is shown in figure 2.7.
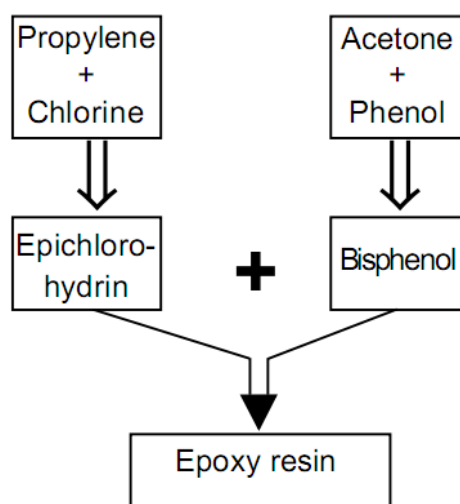
Figure 2.7 Chemicals required for the production of epoxy resin.

Last step of epoxy formation is presented in figure 2.8.Through this last step different epoxy resins are prepared, depending on the ratio of bisphenol A and epichlorohydrine. The smallest epoxy resin of the diglycidyl ether bisphenol A family has a molecular weight of 340 (n=1)and is used quite often in functionalization process [52].
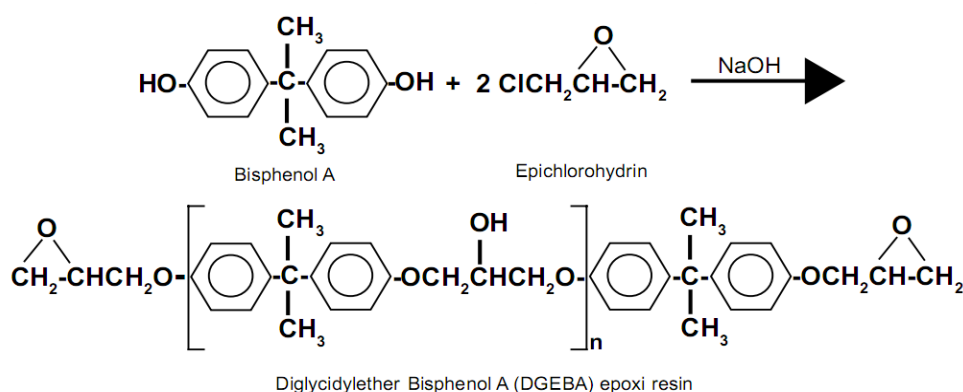
Figure2.8 Final stage of epoxy resin production [54]**.**

The curing of epoxy resins to higher molecular weights is carried out in the presence of curing agents like; amines and amides, which are most commonly used at room temperature, acid anhydrides, imidazoles, boron trifluoride complexes, mercaptans, and metal oxides [54]. These curing agents can be catalytic or co-reactive. In the first case, the curing agent behaves as an initiator for the homopolymerization of the epoxy resin or as an accelerator to the additional curing agents [55]. In the second case, the co-reactive curing agent behaves as a co-monomer during the epoxy curing process. Most of the curing reactions are carried out by nucleophilic mechanisms. Co-reactive class of agents are reactants with active groups such as amine, in primary and secondary amines, hydroxyl group in phenols, thiols, and carboxylic acids, Lewis acid groups as in boron trifluoride complexes or metal oxides, and Lewis bases as tertiary amines [55].

The amine groups, especially primary ones succeed easily in ring opening of very active epoxy group, presented in figure 2.9, starting thus a poly-addition reaction to obtain complex polymers.
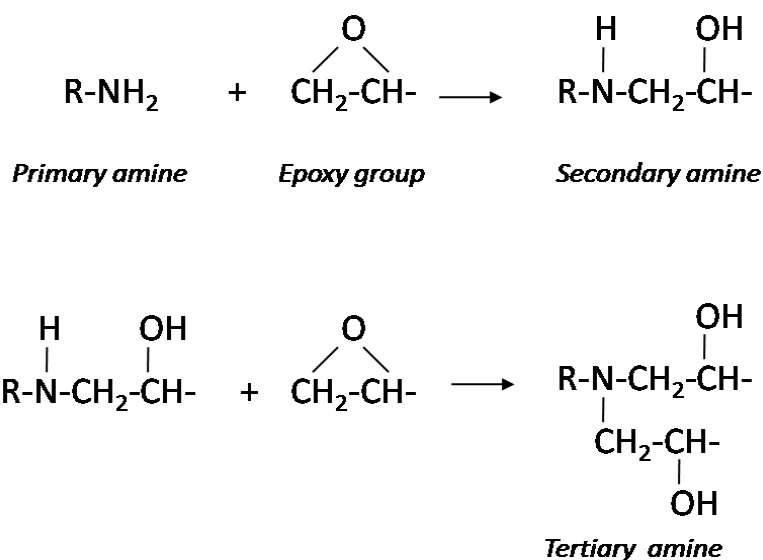
Figure2.9 Starting reaction in the curing process of epoxy resin by a primary amine as a hardener.

The curing process is an irreversible, exothermic reaction, where no by-products are produced and the final product cannot be decomposed back to its reactants. Different epoxy polymers can be obtained according to the hardener type. Because of the different reactive groups on the backbone or side chains of the epoxy polymers such as hydroxyl, epoxy, etc. and the low shrinkage during preparation, these polymers show a wild range of material properties such as adhesion, high mechanical strength, chemical resistance, diffusion density, water tightness, electrical insulation, heat resistance, light stability. Depending on the hardener type used, the epoxy polymers show different final properties according to the required expectations.

Epoxy polymers belong to the thermoset polymer family, whose polymers have a tendency to be harder and brittle. In order to reduce the brittle character of them, modifiers or fillers are incorporated into the polymer matrix. With the introduction of fillers into the epoxy resin, composites are obtained. For the mineral filler class, there exist different types of composites such as micro-composites where micro-scale filler particles are dispersed massively into the epoxy matrix or intercalated nanocomposites where the dispersion happens in a less massive way and some polymer chains are able to penetrate through the filler particles keeping them in a specific order. The last type is the exfoliated nanocomposites in which nano particles are completely dispersed in the matrix in a homogeneous way as single particles, without a specific order [44, 56, 57]. The degree at which the physical chemical and mechanical properties are affected depends greatly on the fillers' nature, size, shape, dispersion quality in the organic matrix. To obtain the best effect induced from a filler, the filler particles should be as small as possible (i.e. nanosize), homogeneously dispersed into the matrix with good adaptation and interaction with the organic phase of the polymer. For a strong interaction between the fillers and the organic part of the polymer, covalent and hydrogen bonding have to be provided. Provided the covalent bonding exists between the inorganic fillers and the

polymer matrix, Becu-Longuet et al. [58] and Haran et al. [59] in their studies, remarked an improved transmission of the mechanical load to the inorganic particles, relieving the polymer matrix and enhancing toughness.

In the case of fillers without any chemical treatment, the tensile properties were negatively influenced, by reducing the tensile strength of the polymer itself. Daniel et al. [60] in their studies of epoxy-clay nanocomposites observed a reduction in the tensile strength. Gonjy et al. [61] as well remarked in their research that the inclusion of non-treated carbon nanotubes into epoxy resin affected positively the elastic modulus but simultaneously decreased the tensile strength of the nanocomposite.

Vogelson et al. [5] described the mechanism that took place in the incorporation of carboxylate-alumoxane nanoparticles into polymer matrix. They described the role of the functionalized nanoparticles as cross-linking agents, generating a hybrid polymer in which the side reactive groups as hydroxyl and amine groups reacted with the resin to create a more complex cross-linking of the polymer. This increased the density of the polymer, which in turn affected positively the mechanical properties as tensile strength [62].

Another observation to be mentioned is the induced effects in the polymer matrix due to differing amounts of particles. Shahid et al. [62] in their studies tried different loadings of the lysine functionalized alumoxanes into the epoxy resin, starting from 3 to 16 weight percent. The best performance in all mechanical properties examined was observed in low loaded polymers, especially for polymers with loaded fillers of less than 5 %.

In conclusion, this research follows the same patterns as many studies mentioned before, in which functionalization is used as an approach to improve the quality of polymer composites. While similar to these researches [45-52], this study, on its own is a well-defined research within its field, in which matching between the reactants has been tried, in other words, epoxy

functionalization is matched to epoxy resins. Up to date, similar studies have used same reactants as in here, but never tried to achieve a matching of organic groups. Ying Ling et al. used bisphenoldiglycidyl A as the epoxy monomer in functionalization step of ceramic materials such silica but no further study is known on the incorporation of these hybrid silica into polymers [53]. The same is valid for boehmite as a functionalized filler but carboxylic acid has been used as a functionalizing unit [50]. Meanwhile, a similarity is observed in the study presented by Vogelson et al. [5] in which carboxylate-alumoxanes are integrated in epoxy resins resulting in improved mechanical and thermal properties while in this study the surface properties are prioritized, such as scratching, hardness, etc.

CHAPTER III

EXPERIMENTAL

In this section, preparation of boehmite crystals, functionalization step and introduction of functionalized boehmite into epoxy resin systems will be explained. Also the materials used and characterization methods will be briefly described.

3.1 Materials

For the hydrothermal process and the grinding route aluminum trihydroxide (ATH) was used as a precursor, ammonia (NH_3) and acetic acid (AA) were used as pH controlling agents and isopropyl alcohol (i-POH) was used as process control agent in grinding step. In each step washing was done with deionized water (DIW).

In the grinding process, the starting material ATH, obtained from Merck, was used without further purification. While the isopropyl alcohol used was of two different grades. For the grinding process control medium pure isopropyl alcohol (from Sigma-Aldrich) and for the washing step technical grade alcohol was used. In the hydrothermal route the highly concentrated ammonia solution (% 32) and glacial acetic acid are used. Both of which are purchased from Merck.

For the functionalization step, synthesized boehmite crystals are the precursor while the functionalizing agent is bisphenol A diglycidyl ether (BADGE) obtained from Sigma-Aldrich. As catalyst in this system, tin chloride was used. Meanwhile the solvent media used was toluene, which was also used in washing procedure together with acetone.

As for the washing step technical grade acetone and toluene were used. In the third step, the resin matrix used is a system of epoxy resin LY 5052 and amine hardener HY 5052, materials which were kindly provided by Barış Electronics Company. Their properties are shown below in tables 3.1 and 3.2.

Table 3.1 Technical data on the reagent used in grinding and hydrothermal process.
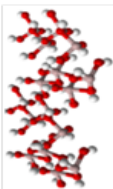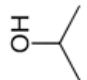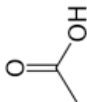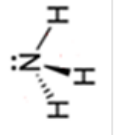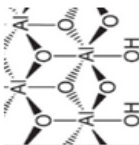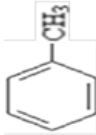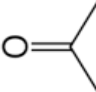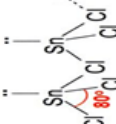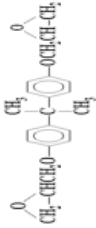
Procedure	Grinding and Hydrothermal step					Functionalization step			
Chemical	$Al(OH)_3 \cdot xH_2O$	C_3H_7OH	CH_3COOH	NH_3	AlOOH	$C_6H_5CH_3$	$OC(CH_3)_2$	$SnCl_2$	$C_{21}H_{24}O_4$
	Aluminum hydroxide	Isopropyl alcohol	Acetic acid	Ammonia	Boehmite	Toluene	Acetone	Tin chloride	Bisphenol A diglycidyl ether
MW (g/mol)	78.0	60.1	60.0	17.0	60	92.1	58.1	226	340
Density (g/ml)	90.0	0.786	1.05	0.880	-	0.865	0.790	-	-
Purity (%)	97.0	99.5	99.8	32.0	-	99.7	99.8	98.0	-
Structure									

Table 3.2 Technical data of reagents used in epoxy resin preparation.

Name	Epoxy resin	Hardener
Nonmenclature	LY 5052	HY 5052
Density (g/ml)	1.17	0.94
Viscosity (mPa.s)	1000-1500	40-60

3.2 Procedure

This study consists of three main parts, each of which include several substeps, all of them are summarized in the figure 3.1 below.

The three main steps are:

I.   Hydrothermal synthesis (including preliminary grinding)

II. Functionalization of boehmite particles with epoxy

III. Incorporation of these organically modified particles into an epoxy resin matrix.

All products were characterized by SEM, FTIR, XRD, DMA, and PSA methods and tensile test, hardness and scratch resistance tests, for which more detailed information, will be given later in this chapter.
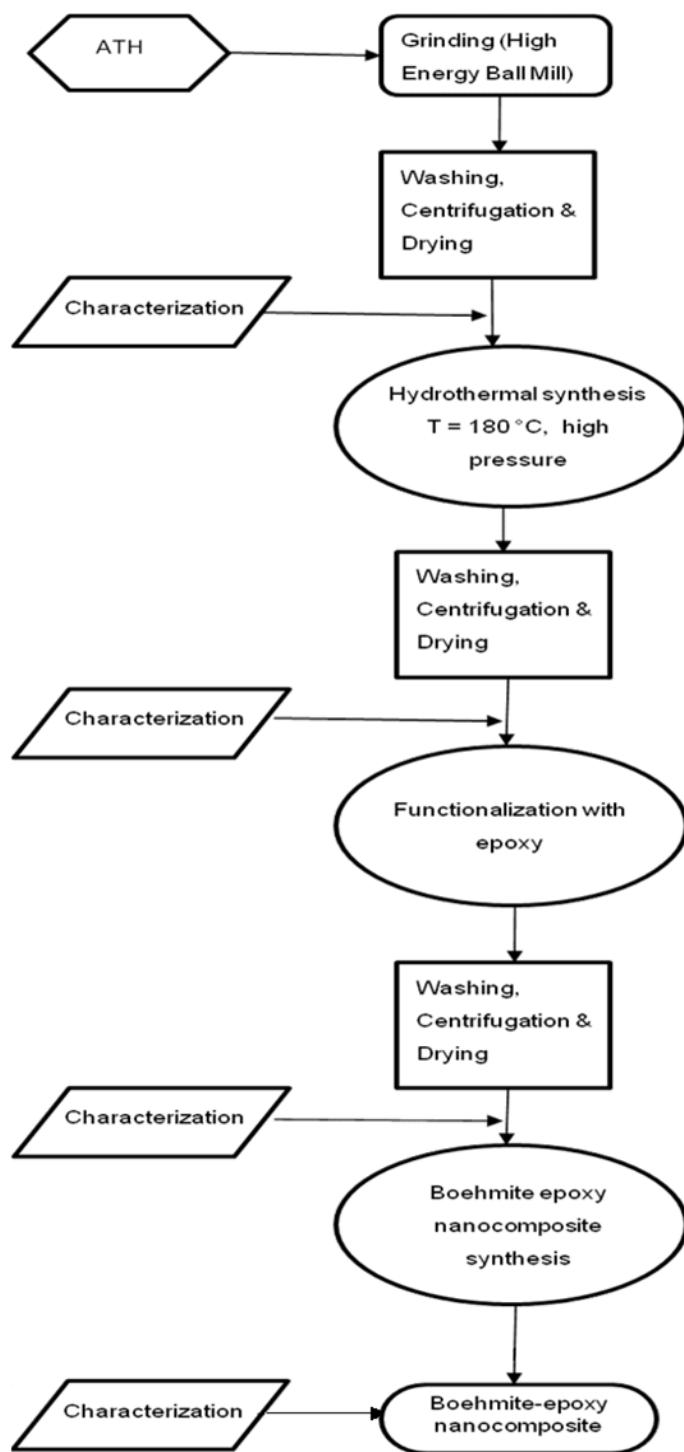
Figure 3.1 A general flow sheet of the experimental procedures of this project.

3.2.1 Grinding Process

The starting material ATH has a size range between 100-150 μm as specified by the Merck as supplier. This is a disadvantage to a great extent in this study, since there is no mixing feature in the hydrothermal reactor used. Also as mentioned in section 2.1.3, the crystallization takes part in colloidal solution at high temperatures and pressure. To obtain a colloidal dispersion, size range should be at sub-micrometer scale, in order to minimize the sedimentation in the hydrothermal reactor. The solution of this problem is apparently using smaller particles, which is possible if the ATH is treated previously by grinding as it is also mentioned in the results of Tsuchida et al. [20]. Moreover, besides obtaining smaller powders, a narrower size distribution can be obtained.

Based on the study by Korhan et al. [42] here, ATH particles were dispersed in i-POH as a process control agent. The reasons to use control agent in this process are:

1) Fast / easy drying

2) Less cementation during drying

3) Lower risk of contamination

Comparing the solubility of ATH in ethylene glycol, isopropyl alcohol (i-POH) and water media; ATH is highly soluble in water, then comes ethylene glycol and it is least soluble i-POH. This can be explained with the variation in size of the molecules, water being the smallest and i-POH being the largest. Also due to organic groups such as $-CH_2-$, both ethylene glycol and i-POH induce less polarity and as the number of C atoms increases the dielectric constant of the medium decreases. For this reason and the steric effect induced from the structure of i-POH, ATH is less soluble in i-POH than in ethylene glycol.

The higher the solubility of an inorganic compound in a medium, the higher the risk of agglomeration as medium leaves particle interconnects, during the drying step. Solubility tends to increase as the radius of curvature decreases (i.e. as the particle size gets smaller). Therefore intuitively, in a process like grinding (or in any process where small particles are taken into a liquid in which they have a slight solubility), as the sizes decrease the effective solubility at the particle interface would be larger, especially in the particle separation and consolidations steps. Considering the grinding liquid medium as a film at the surfaces of particles and in between them (see figure 3.2), no simple drying procedure is capable of getting rid of the films of water in between the particles which are already held strongly in an agglomerated state by the capillary pressure which in fact arises due to this remnant liquid film. Therefore into these films of water there is always enough amount of solubility from the particle interfaces. Even though complete drying has been accomplished, the already-solubilized ions do not go back to the particles, but rather they stay at the interconnection to form an additional layer (structural nature of this layer can be amorphous or semi-crystalline or crystalline depending on the drying conditions like temperature). This is one of the most critical problems in drying. Consequently, with a good solvent, an excessive solubility of Al ions to these particle interconnects would result in the 'cementation' of the 'ground' particles and form larger lumps due to the solubilized matter in between them.
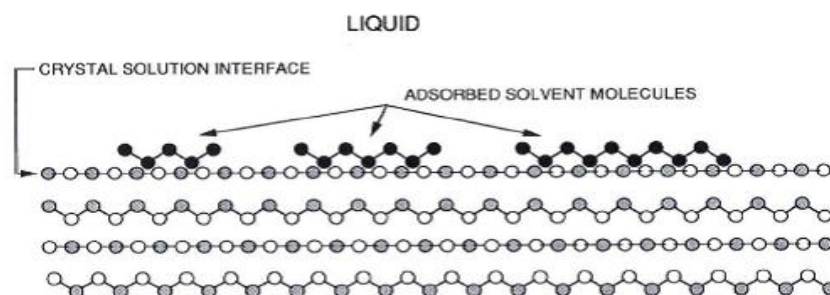
Figure 3.2 Adsorption of solvent molecules onto the crystal solution as a liquid film.

Another important point is the time it takes for the drying process. Comparing the boiling points of the three liquid media, ethylene glycol has the highest B.P (197^oC), which is followed by water with a B.P of 100^oC and ending up with i-POH with 82.6^oC as boiling point. In order for the powders to get dry, more time and more energy is needed for ethylene glycol and water than for i-POH.

3.2.2 Grinding procedure

The ATH powders were dissolved in pure grade i-POH with liquid to powder ratio by moles as 1:2. This mixture was mixed magnetically for 20 minutes until a homogeneous solution was obtained. Later, it was put in the milling chamber together with WC (tungsten carbide) balls of diameter 3 mm (total weight was 622.9 grams). The grinding chamber had a capacity of 125 ml. The ball to powder ratio was kept constant at 12 in all experiments.

The mill type used was a high energy ball mill of the Retsch PM100. An image of the mill chamber is shown in figure 3.3.
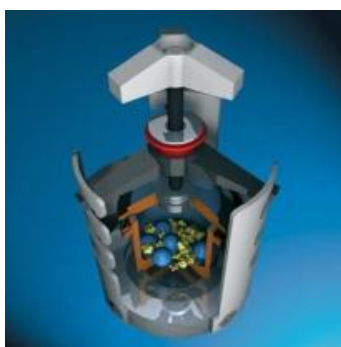
Figure 3.3 Schematics of the mill chamber used in the grinding step.

The grinding time was kept constant for 40 minutes, divided in four cycles of 10 minutes of grinding and five minutes of rest. The speed used was 500 rpm, as advised in the research of Korhan Sezgiker [42]. Subsequent to grinding, ATH was subjected to washing three times with i-POH. As a last part of this procedure, the powders were left to drying at 60°C overnight.

3.2.3 Hydrothermal process

The main factors affecting the hydrothermal synthesis were discussed in Chapter II to a large extent. Based on that preliminary study, with ATH as a precursor the effects of pH controlling agents and the reaction times were inspected. More detailed information on experimented parameters are given in table 3.5. Meanwhile, talking about the procedure; the hydrothermal reactor used is a pressurized stainless steel reactor, maximum capacity of which is three liters. Simplified schematic of this reactor is given in figure 3.4.

1. Gap medium
2. Reaction medium
3. Thermocouple
4. Pressure gauge
5. Temperature controller
6. Heating jacket
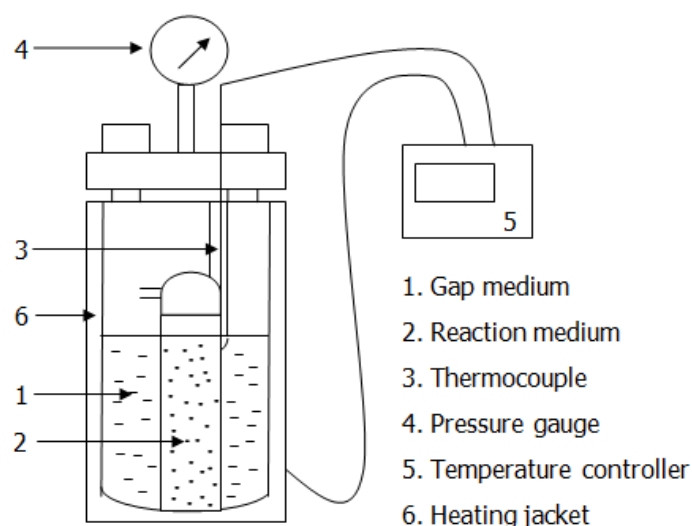
Figure 3.4 A simplified schematics of pressurized reactor system (retrieved from Korhan Sezgiker thesis work [42]).

The reagents used in the hydrothermal reactor were not put into the reactor in direct contact with the stainless steel walls of the reactor. A glass cylinder with a capacity of nearly 400 ml was prepared particularly for this purpose. The reason for not using the whole three liter capacity is that, the volume used should stay in between the minimum and maximum levels allowed in order to prevent any danger due to the high pressure created inside the reactor during the process. Also another reason is the absence of mixing feature inside the reactor. The more reagent is put inside the more difficult is the homogeneity to achieve, more aggregation will then occur. Due to the gap volume created inside the reactor between the glass cylinder and the reactor walls, during the hydrothermal process the volatilization of the liquid reagents takes place. This gives rise to an unwanted change in reactants concentrations during reaction time, which will affect for sure the morphology of the crystals as mentioned in Chapter II. In order avoid this, a gap solution is prepared with the same concentrations as inside the glass cylinder except the ATH in the cylinder, by making sure that once immersed into the reactor together with cylinder, this solution has the same height as the one inside the cylinder. This way during the formation of autogeneous pressure in the vessel by evaporation, concentrations of the aqueous species in the gap and glass cylinder would remain constant.

While regarding the procedure, a different route was followed aiming the control of morphology of crystals. According to the literature research boehmite crystals show a preference in the growing long y-axis. As shown in figure 3.5 the octahedral boehmite layers are located parallel to the x-z plane. The oxygen atoms which are not bonded to hydrogen atoms are shared between the aluminum atoms from four different octahedra, all lying in x-z plane. While the hydrogen bonded oxygens are shared only by half of the number of the octahedra shared by non-hydrogen bonded ones. This fact shows that the interactions along the x-z plane are stronger than the interactions between the oxygen interactions along y-axis between the

octahedral double layers. The oxygen atoms of these surface hydroxyls possess free orbital letting hydrogen bonds interfere and giving rise to crystal growth perpendicular to the octahedral layer. In other words the growth of crystals has a greater tendency to take part along the y axis.
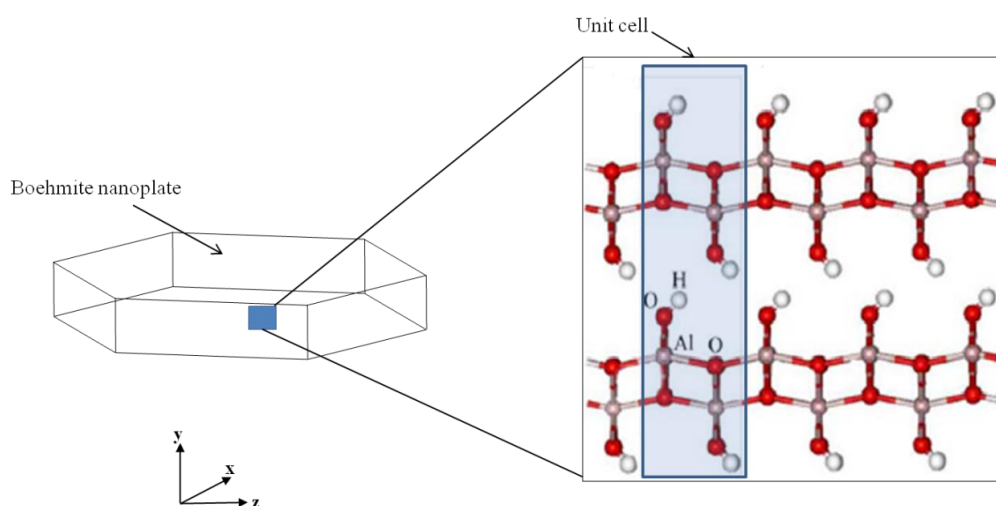
Figure 3.5 Crystal structure of of boehmite. The shaded region is a unit cell of boehmite containing 4 units of AlOOH.

With this information, in this present study a preliminary ageing step is carried out, with the aim of controlling the morphology. The wet-milled and dried ATH powders were left to ageing in acetic acid aqueous solutions for one day under continuous mixing and then concentrated ammonia was added to this solution and again stirred for one day more. First ageing in an acidic media, or in hydrogen rich solution imposes the crystals to grow in one direction only. The hydrogen ions inhibit the hydroxyl groups on the octahedral surface forming two kinds of water molecules. The water molecules formed in the x or z axis (i.e. lateral sides) are chemisorbed water molecules while the water molecules absorbed in the y-axis are physically absorbed whose interactions are way easy to break when compared to chemisorbed molecules. These physically absorbed molecules are vulnerable to crystal cleavage and crystal growth due to the easy rupture of y-plane water-hydroxyl interactions. This leads to a preferential one dimensional

growth in acidic environment (i.e. formation of needle-like morphologies). As the pH is changed to basic by adding NH_3 solution, the hydroxyl groups dominate the solution, so no more one dimensional growth can be observed (i.e. rectangular prisms or rhombohedral shapes form at mediocre pH and platelets form at higher values).

After this two-step pre-hydrothermal ageing the ATH solution is subjected to hydrothermal ageing at a temperature of $180^{o}C$ and an autogeneous pressure which usually varies between 16-12 bars. Due to the presence of acetic acid and ammonia, the pressure value attained in these conditions is higher than the autogeneous pressure that can be reached only by water (around 9-10 bars at $180^{o}C$). Concentration of ATH was kept constant at 10 % weight, while the pH of the reaction medium was controlled with acetic acid (AA) and ammonia (NH_3). Different media were tried and parameters are summarized in Table 3.3. Time was also tested as a parameter with5, 7.5, 10 hours. After the hydrothermal process, the product solution was washed and centrifuged with technical grade DIW and i-POH, respectively and left drying overnight at $60^{o}C$.

Table 3.3 Parameters applied in the hydrothermal process to obtain nanoplatelet morphology**.**

Sample	wt% ATH	wt % AA	wt % NH_3	T (°C)	Time(hr)	Time Pre-aging (hr)	pH initial
HT-1	10.0	5.0	-	180	5.00	-	2.30
HT-2	10.0	-	10.0	180	5.00	-	10.5
HT-3	10.0	5.0	10.0	180	5.00	-	11.2
HT-4	10.0	10.0	10.0	180	5.00	48.0	10.4
HT-5	10.0	10.0	10.0	180	5.00	48.0	9.68
HT-6	10.0	10.0	10.0	180	7.50	48.0	10.0
HT-7	10.0	10.0	10.0	180	10.0	48.0	10.5

Products were characterized with XRD, SEM, PSA, BET, FTIR and also directly titrated in order to determine approximately the number of hydroxyl groups accessible on the surface of the product.

3.2.4 Epoxy functionalization of boehmite particles

As mentioned in hydrothermal procedure part, during hydrothermal synthesis, as the crystals grows, the interactions between double layers is weaker than the in-plane interactions. This is one possible reason that makes these parallel layers vulnerable to crystal cleavage. Consequently, the newly formed crystal surfaces are totally covered with hydroxyls bonded to aluminum atoms. Using this feature, the superficial hydroxyl groups of boehmite crystals can be reacted with active epoxy monomers and cause ring-opening. This creates a hybrid organic-inorganic crystal interface with dual properties. The predicted reaction between hydroxyl groups and epoxy monomer is shown in Figure 3.6.

Nanosized boehmite   Difunctional Epoxy   Epoxy-functionalized boehmite
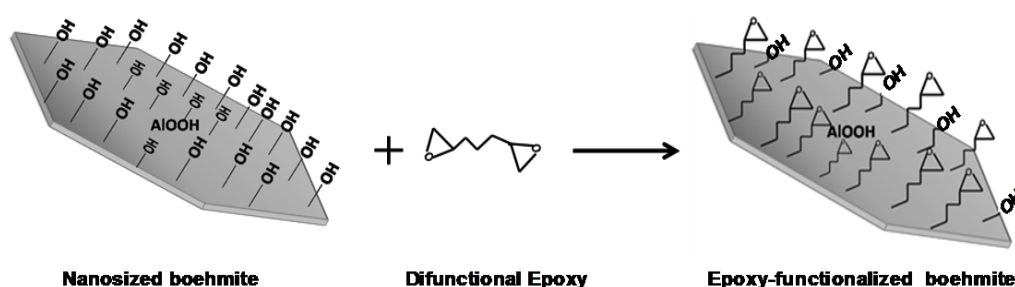
Figure 3.6 Schematics of the reaction between boehmite crystals and epoxy.

The reaction would take place faster using a catalyst like tin (II) chloride $SnCl_2$ [52]. Initially, the boehmite powders were dried overnight at $60^{\circ}C$ under vacuum. This was done in order to get rid of extra superficial water,

which might interfere with the epoxy ring opening causing unwanted side reactions. After this step, BADGE was dissolved in pure toluene for 20 minutes under nitrogen (N_2) atmosphere and heated to a mild temperature in a range between 80 to 100°C, depending on the experiment conditions applied. The temperature was limited to 100°C due to ease of vaporization of toluene, which among other well-known organic solvents (xylene, acetone, etc.) is the most stable with respect to the boiling temperature, which is 110°C. As soon as the temperature was stabilized to the specified one, the boehmite powders and the catalyst were added. By this way the reaction was considered to be started and the conditions of reactions were kept constant for the specified period of time. In this part of the research, several parameters were tried such as time of reaction, weight ratio of BADGE/boehmite, temperature and the effect of catalyst. In table 3.4 the reaction parameters are given and in figure 3.7 the reaction set-up is given.

Table 3.4   Reaction parameters for the functionalization of boehmite particles.

Sample	T (˚C)	BADGE / Boehmite wt ratio	Catalyst ($SnCl_2$) wt %	Time (hr)
EP-4	80	10 : 1	0.1	3
EP-5	100	5 : 1	-	3
EP-6	80	5 : 1	0.1	3
EP-7	100	5 : 1	0.1	3
EP-8	60	5 : 1	0.1	3
EP-9	60	5 : 1	0.1	6

1. Magnetic stirrer-heater
2. Magnetic fish
3. Three-neck round-bottom flask
4. N₂ bubble
5. Boehmite-epoxy solution
6. Inert gas Inlet
7. Condenser
8. Thermometer
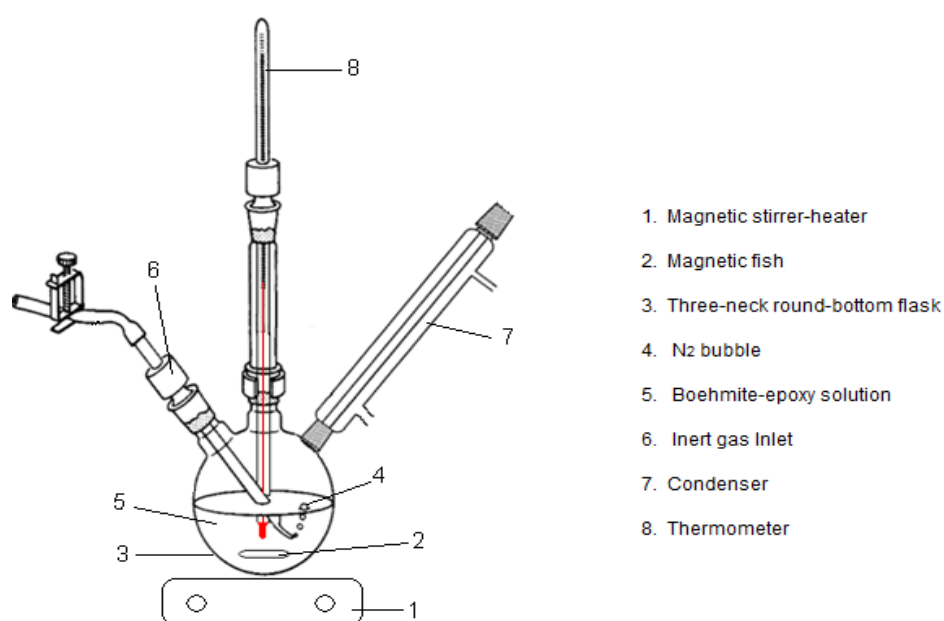
Figure 3.7 Set-up for epoxy functionalization of boehmite particles.

After the reaction the product was washed and centrifuged for several times with technical grade acetone and left to dry overnight at 50°C. The powders were characterized with SEM, FTIR analysis and titrated to determine the presence of epoxy groups on the surface of boehmite powders both qualitative and quantitatively.

3.2.5 Nanocomposite preparation

Functionalized powders were incorporated into the resin matrix system of LY 5052 and HY 5052. As mentioned in material description part the resin and its hardener are supplied from Barış Elektronik Company in Turkey. Here, an extensive description of the way the materials used is given.

The epoxy resin matrix was a two-part system, composed of 100 parts by weight of an epoxy resin and 38 parts by weight of a hardener HY 5052

consisting of a three-amine agent. The hardener HY 5052 serving as a cross-linking agent in curing the epoxy resin is comprised of two primary amines with two functional groups [63].

At this stage, the following comparative approach was followed. The first sets of composite polymers were with the epoxy group functionalized boehmites and the polymer matrix, while the second set was produced from non-functionalized boehmite and polymer matrix. Both sets have the same weight ratios of powders 3, 5 and 10 percent as summarized in Table 3.5. The mixtures were mixed for 20 minutes which is as further as their pot life period allows. In order to get a more homogeneous mixture, the resin system was also subjected to ultrasonic bath for 15 minutes. It is observed that during the solid phase addition bubbles start to form.

Table 3.5　Nomenclature of cured epoxy composites according to composition and weight percentage of powders.

% weight ratio of particles	Functionalized Boehmite	Pure Boehmite
3	FB-EP3	BH-EP3
5	FB-EP5	BH-EP5
10	FB-EP10	BH-EP10

After the mixing, the mixtures were poured into aluminum molds which were previously coated with mold releasing agent. The mold assembly was degassed in a vacuum oven for 15 minutes in order to get rid of the bubbles. During this time, attention was made in order not to have the nanocomposite mixture spilled so that the dimensions of the test samples do not change. As suggested by the Huntsman Advanced Materials Company for the curing systems of LY 5052/HY 5052, the resin system was cured for

24 hours at room temperature and two hours at 100°C. Curing procedure is summarized in figure 3.8.
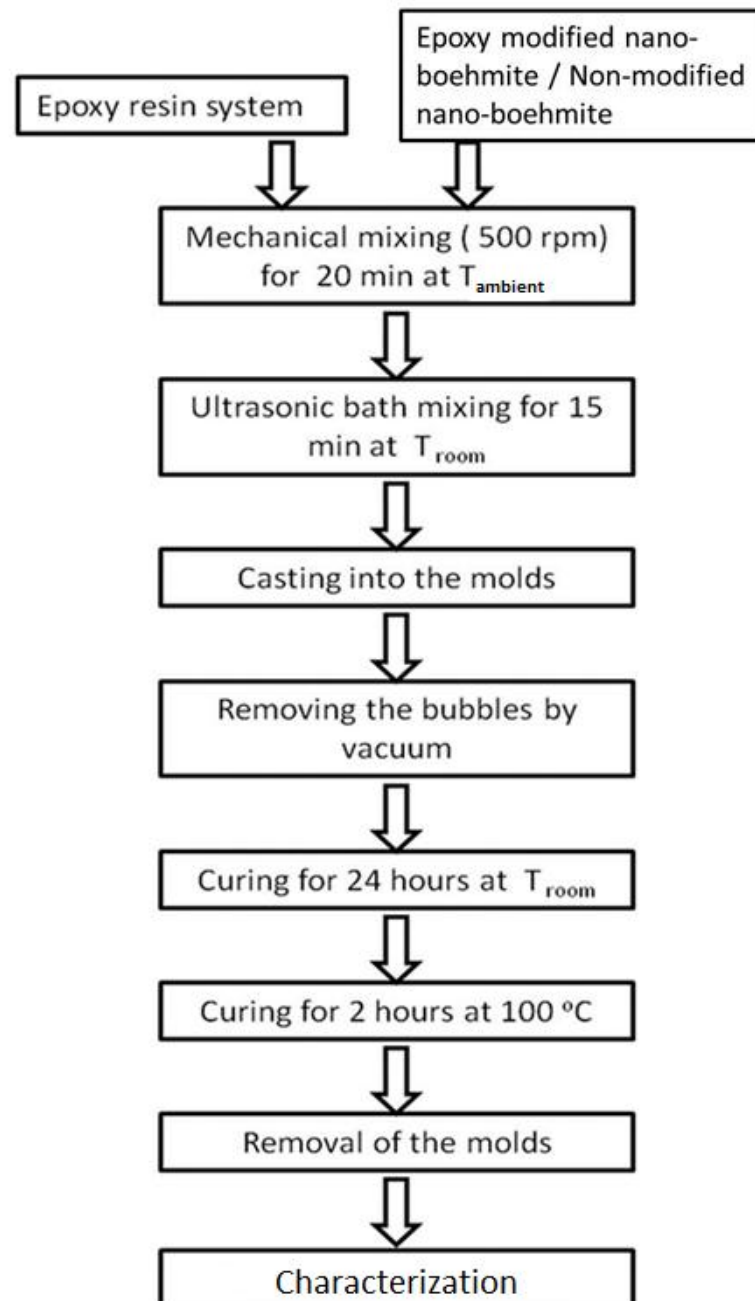
Figure 3. 8   Procedure of incorporation of the modified boehmite nanoparticles into the resin matrix.

3.3 Characterization Methods

As mentioned in the previous parts, after each process step the required analyses have been performed. As a result of these analyses it was possible to characterize the product and decide on with which parameter the rest of the study would be carried out. The characterization methods used in this research are listed below:

- Particle Size Analysis (PSA)
- X-ray Diffraction (XRD)
- Fourier Transform Infrared Spectroscopy (FT-IR)
- Scanning Electron Microscope (SEM)
- Quantitative analysis of OH and epoxy groups on the boehmite powders
- Dynamic mechanical Analysis (DMA)
- Mechanical Behavior tests for polymers
- Hardness Analysis
- Scratch Resistance Tests

3.3.1 Particle Size Analysis –PSA

During the first stages of experiments, beside SEM analysis, to get a better understanding of the size factor, particle size analysis was performed. The analysis was conducted in Chemical Engineering Department at METU, with Malvern Zetasizer Nano Instrument – Model No: ZEN3500, Malvern Instruments Ltd.). The test samples were carefully prepared in aqueous solutions with a mild acidic pH range between 2.5 and 3.5. The acidic environment was achieved with addition of acetic acid solution. A detailed description of the procedure is given in thesis of Korhan Sezgiker [42].

3.3.2 XRD analysis

XRD analysis can be used to determine the crystal structure of materials. The positions and intensities of the diffracted X-rays give information about not only the crystal structure, but also used to characterize the particle size, orientation, or disorder in synthesized structures. The analyses were performed in the department of Metallurgical and Materials Engineering (METU)witha Rigaku model X-ray diffractometer (Model No: RIGAKU – D/Max-2200/PC). The radiation used was Cu-Kα with a step interval of 0.02 degrees, at 40 kV and 40 mA.

3.3.3 FT-IR analysis

For each part of this study obtained products; ATH (ground powders), boehmite nanocrystals, functionalized boehmite nanoparticles, were characterized with FT-IR spectroscopy. The tests were performed in Mechanical Engineering Department at Hacettepe University, with IR Prestige-21 SHIMADZU FT-IR spectrometer. Before characterization, samples were well mixed in 200 mg of KBr salt (with a very low weight percentage of 2%) and ground into a homogenous and refined entity. The mixture was thenvacuum pressed into a pelletand characterized with the spectrometer within the wavenumber range between 400 and 4000 cm^{-1} with 4 cm^{-1} resolution.

3.3.4 SEM analysis

Morphologies of the synthesized particles were studied with SEM microscope (Quanta 400F - Field Emission SEM instrument, in Central Laboratory, at Middle East Technical University and Bilkent University Institute of Material

Science and Nanotechnology – National Nanotechnology Research Center). Through these images, information on the size, shape, morphology and distribution was collected.

3.3.5 Quantitative titration analysis

The quantitative analysis for the estimation of hydroxyl and epoxy groups present on the boehmite surface was performed with titration. For the determination of hydroxyl groups in boehmite crystals a back titration method was used [53].The procedure was as follows:

In an Erlenmeyer flask, 2 g of boehmite powder was mixed in 80 ml of 0.05 N NaOH solutions. The flask was sealed well and left overnight in constant stirring. Later 10 ml of this solution is titrated with0.05N HCl solution. Concurrently, blank titration of 10 ml of 0.05 N NaOH solution without boehmite powders is performed. The data are collected in table 3.6. The calculations are shown in Appendix A.2 for both OH group and epoxy group titration processes.

For the estimation of end epoxy groups a method adopted by Neville and Lee was used [64]. One gram of functionalized boehmite powder is added to 100 ml of pyridine with 0.02074 mol HCl solution. They were heated for 20 minutes (T=40°C) and back-titrated with 0.05 N NaOH solution. Phenol phthalein was used as the indicator. Another solution produced with the same method as described above was used for blank titration.

Table 3.6 Volumetric data for the titration process of boehmite solution.

Surface OH group estimation				Epoxy End group estimation			
V_{sln}	$V_{Blank-sln}$	V_{HCl}	$V_{HCl-Blank}$	V_{sln}	$V_{Blank-sln}$	V_{NaOH}	$V_{NaOH-Blank}$
10 ml	10ml	30 ml	5.5 ml	100 ml	100 ml	205 ml	194 ml

3.3.6 Dynamic mechanical Analysis - DMA

The dynamic mechanical analysis was performed in Central Laboratory at METU, with a Perkin Elmer Pyris instrument. The polymer sets were constantly subjected to an oscillating load with a frequency of 1 Hz. The cured epoxy polymer specimens were 10 mm long, 5.7 mm wide, 4 mm thick. The measurements were performed in a bending mode or with single cantilever. Viscoelastic properties such storage modulus, E', loss modulus, E" and tangent delta, tanδ were observed as a function of temperature only, with a scanning rate of 3°C/min within a temperature range between 30 and 200°C. Storage modulus is a measure of storable energy during the oscillation period. As a property, it is more related to the solid state of matter, being a measure of elasticity of elastomers. The loss modulus is a measure of the energy dissipated during the oscillation period and it defines more the liquid phase of the matter or the viscous character. Tanδ is a derived property and called the loss factor. It is defined as the ratio of loss modulus to storage modulus, E"/E'.

3.3.7 Mechanical behavior tests for polymers

The tensile tests were performed in Chemical Engineering Department at METU, according to ASTM D 638 standards[65]. The machine used is BESMAK A.S. U-type instrument. The epoxy polymers were cured in spoon-like dog-bones in aluminum molds. For each set of polymers 5 specimens were tested. The dimensions of specimens are tabulated in table 3.7.

Table 3.7 Tensile Test specimen dimensions.

Gauge length, L_o	Width	Thickness
33 mm	6 mm	4 mm

As specified by Grellman et al.[66] for brittle materials, whose elongation at break is less than 10 %, a cross-head speed of 5 mm/min is suitable. Tensile tests are classified as quasi-static method, where the load is applied very slowly with a constant uni-axial cross-head speed until fracture. From the deformation the matter experiences during this test, elastic deformation, plastic deformation, linear and non-linear visco-elastic deformation related information can be obtained. The recorded load-extension diagrams give various information such as tensile stress, σ and strain, ε as defined in equations 2 and 3:

$$\sigma = \frac{F}{A_o} \qquad (2)$$

$$\varepsilon = \frac{\Delta L_o}{L_o} 100\% \qquad (3)$$

Tensile stress is the tensile load (F) per unit of initial cross sectional surface, A_o. The elongation due to the external load application is related to the initial gauge length, L_o. Besides tensile stress and strain, elastic modulus and toughness can be evaluated. Elastic modulus is related to the elastic region of the specimen which is located at the initial linear part of the stress-strain curve. It is calculated as a constant slope in the linear region of stress-strain curve following Hooke's Law. In this region, deformation is reversible and so after applied force is removed, sample can turn to its original shape. The elastic modulus is defined by equation 4:

$$E = \frac{Stress(\sigma)}{Strain(\varepsilon)} \qquad (4)$$

Finally, toughness is the area under the stress-strain curve with unit of energy per unit volume.

3.3.8 Hardness Analysis

Hardness property was first defined on metals, as the resistance against indentation by a harder body. The test procedure stands for a hard indenter pressed down onto the surface of the specimen under continuous data collection. Micro-indentation measurements of hardness were performed at room temperature with CSM micro scratch tester in METU Central Laboratory. The indenter used is a diamond micro Vickers rectangular pyramid. For the sake of practice, the Poisson's ratio (ν) is assumed to be constant at a value of 0.30.

3.3.9 Scratch Resistance Tests

The surface planes of the polymers were characterized with CSM micro scratch tester in METU Central Laboratory. The tester's procedure is simply described in figure 3.9. A controlled scratch with a sharp tip is applied onto the polymer surface. The type of indenter used is a Rockwell type diamond with a radius of 100mm.The load applied to the surface is progressively increased from 0.5 N as an initial value to 25 N for a distance of 5 mm. The loading rate used is 49 N/min. The critical loads are collected by means of an acoustic sensor and also observed with a built-in optical microscope. The test enables collection of applied force, the friction force and the penetration depth.
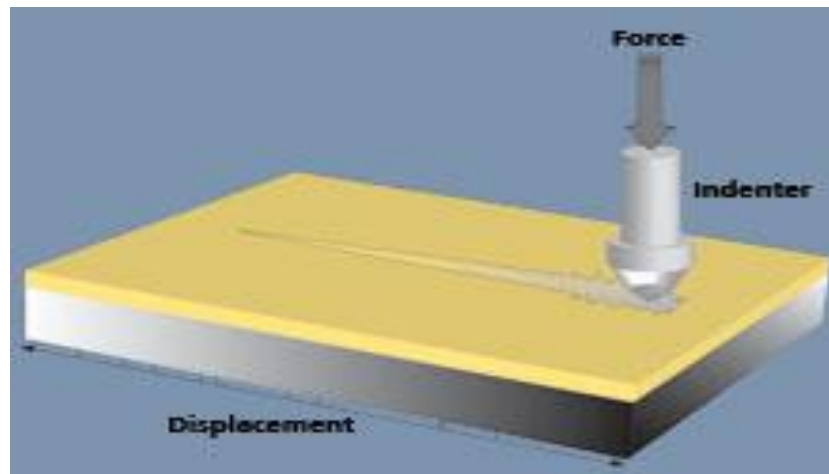
Figure 3.9 Mechanism of scratch resistance testing on polymer surface.

(*Reference: CSM Instruments SA Company, www.csm-instruments.com, retrieval date: 27/06/2011*)

CHAPTER IV

RESULTS AND DISCUSSION

4.1 Grinding Process

As mentioned in the chapter 3.2.1, intending to get a good dispersion of particles during hydrothermal reaction, the ATH particles were ground by high energy milling to achieve sub-micron particle sizes. Due to contamination risks of the ATH from abrading grinding media (refer to section 3.2.1 for details), wet grinding was carried out with i-POH.

In figure 4.1 result from the particle size analysis is presented. As-received ATH had a size between 100-150 µm. The ground powders on the other hand, reached a bimodal size distribution with 115 nm and 412nm being the average diameters.

Size Distribution by Volume

Record 6: A_gr_AA_2.68 6
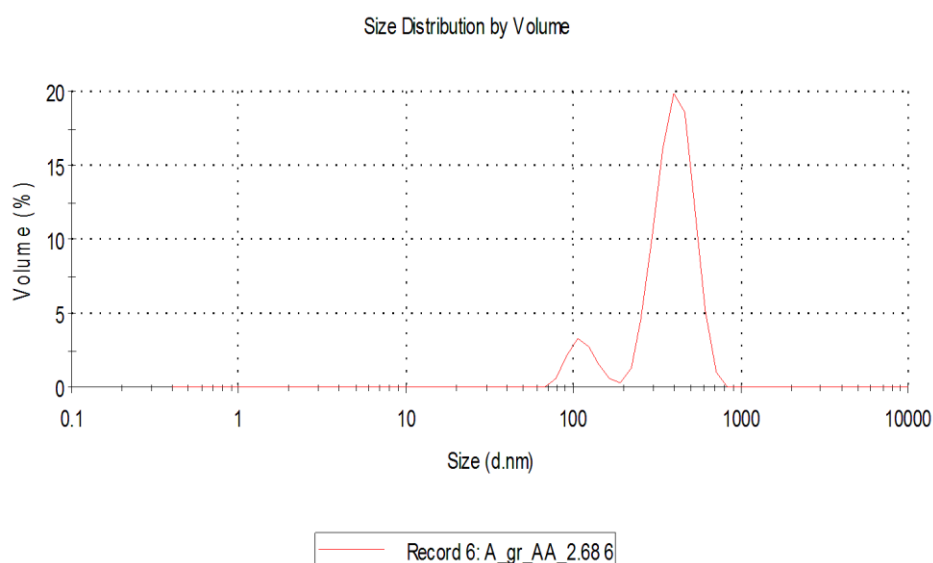
Figure 4.1 Cumulative particle size distribution of ATH particles subjected to a one-step high energy ball milling.

Besides particle size, effect of milling on crystal structure and possible changes in chemical structure of the particles were examined with XRD and FT-IR analysis, respectively. Results are given in figures 4.2 and 4.3.
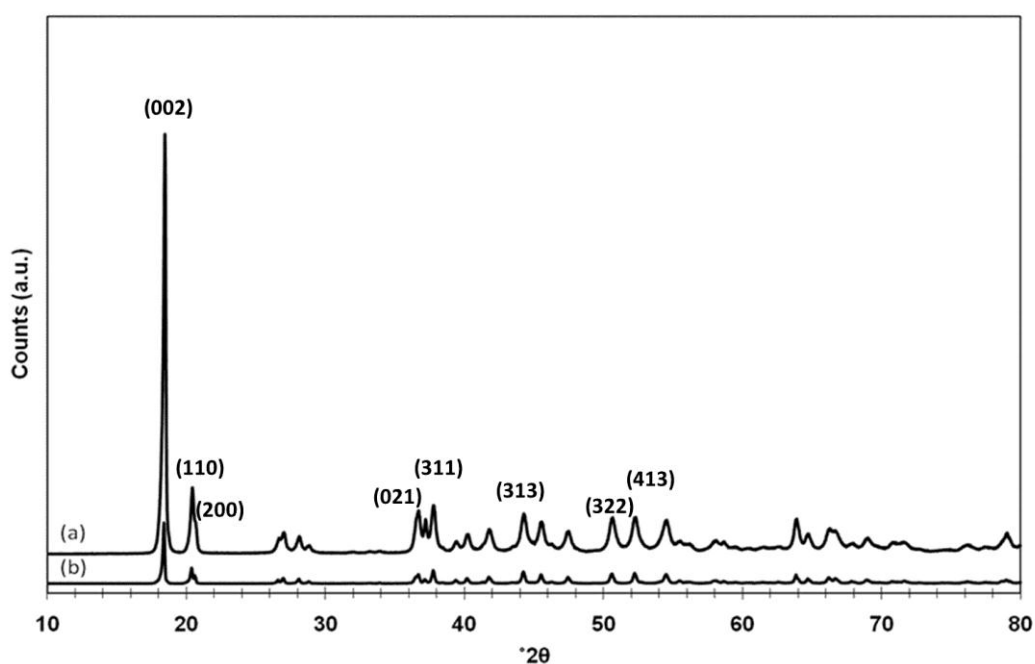
Figure 4.2 XRD patterns for (a) ground ATH particles and (b) as-received ATH powders.

Ground ATH conserved its typical gibbsite structure, which is identified with main peaks appearing at 18.38, 20.38, 37.12° 2θ values. These peaks represent the (002), (110) and (311) planes, respectively and no additional peaks appear upon grinding. More detailed data on the results of XRD are given in table A.1 (Appendix A.1). On the other hand, the peaks observed in ground ATH showed a significant peak broadening with respect to the as-received sample, which is due to the decrease in particles sizes. The expected relative intensities (given in table A.1 in Appendix A.1) in both samples remain similar.

Results obtained from FT-IR analyses are given in figure 4.3. It can be confirmed that the chemical structure is not altered during wet grinding with i-POH.
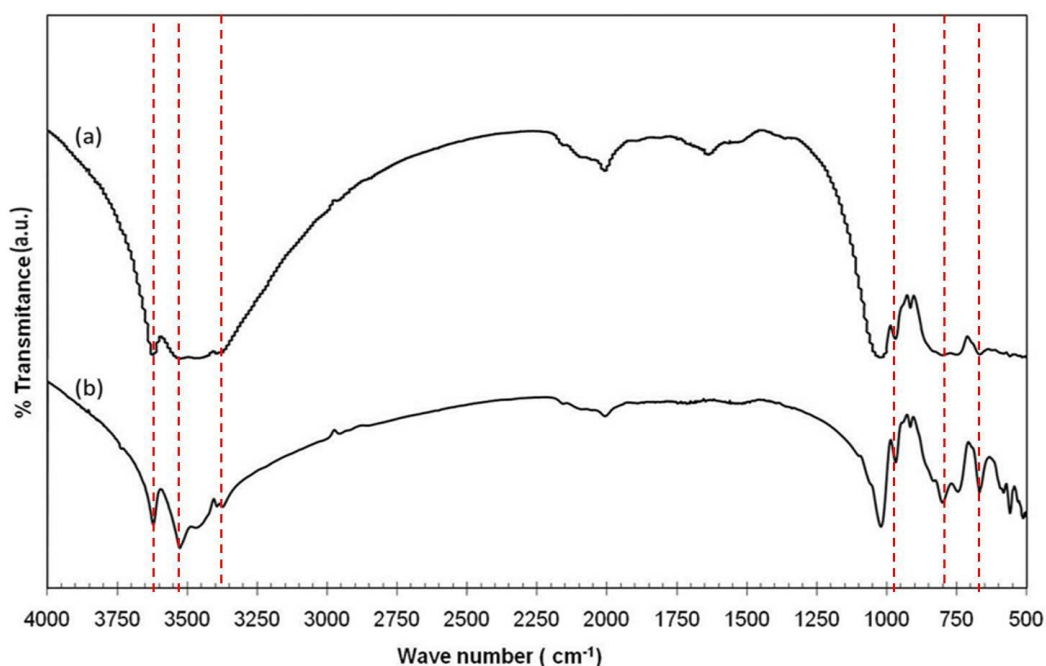
Figure 4.3 FT-IR spectra of (a) as-received ATH and (b) ground ATH.

The hydroxyl stretching vibrations are observed in both ground and as-received ATH. A sharp peak at 3618 cm^{-1} is attributed to the vibrations coming from the interlayer hydroxyl group of synthetic gibbsite. This is in

accordance with the data reported by Liu et al. [67]. While in the study reported by Tsuchida et al. [20] νOH stretching vibrations of the interlayer O-H groups begin to fuse into a broader band, which is observed similarly with the peaks at 3518, 3450 and 3377 cm^{-1}. In the region 2000-1500 cm^{-1}, weak and overtone peaks were observed. This is in accordance with the study made by Bhattacharya et al. [68]. Such bands are attributed to δ-vibration of loosely bound water molecules on the particles' surface. This disturbance is observed most in the ground particles which can be explained with the washing step carried out after grinding. The other intense region 1000-900 $cm^{-1}$is attributed to δ-deformation from OH bending vibration, which has conserved its characteristic peaks in both cases. Whereas in the 900-500 cm^{-1} region, the peaks are attributed to out-of-phase (OH) vibrations [69]. These have merged into broader bands in ground sample showing the weakening of hydrogen bonds between the layers. This has also been confirmed in the study of Tsuchida et al. [20]. The sharp peaks located at low wavenumbers (i.e. 499, 447, 409 and 405 cm^{-1}) are attributed to Al-O-Al bending deformations, and they are present in both samples.

4.2 Hydrothermal process

In the hydrothermal process step aluminum source used was the ground ATH from the first step and concentrated aqueous acetic acid and ammonia solutions were used to adjust pH. From the beginning to the end of the hydrothermal process reagents are expected to evolve towards a chemical equilibrium which can be described by the equations 6-17 as proposed by Hakuta et al. [35].What may look like a simple equation (i.e. the overall reaction described by eqn.5), is actually quite a complex system comprising the formation of around 30 complexes including the acid-base equilibrium between acetic acid and ammonia:

$$Al(OH)_3 \rightarrow \gamma\text{-}AlOOH \tag{5}$$

$$Al(OH)_3 + H_2 \overset{K_{S0}}{\longleftrightarrow} Al^{+3} + 3\ OH^- + H_2O \tag{6}$$

$$2H_2O \overset{K_w}{\longleftrightarrow} OH^- + H_3O^+ \tag{7}$$

$$CH_3COOH + H_2O \overset{K_A}{\longleftrightarrow} CH_3COO^- + H_3O^+ \tag{8}$$

$$NH_3 + H_2O \overset{K_B}{\longleftrightarrow} OH^- + NH_4^+ \tag{9}$$

$$Al^{+3} + 2H_2O \overset{K_{S1}}{\longleftrightarrow} Al(OH)^{+2} + H_3O^+ \tag{10}$$

$$Al^{+3} + 3H_2O \overset{K_{S2}}{\longleftrightarrow} Al(OH)_2^+ + H_3O^+ \tag{11}$$

$$Al(OH)_3 + 2H_2O \overset{K_{S3}}{\longleftrightarrow} Al(OH)_4^- + H_3O^+ \tag{12}$$

$$Al^{+3} + 3OH^- \overset{K_{S4}}{\longleftrightarrow} AlOOH + H_2O \tag{13}$$

$$Al(OH)^{+2} + 2OH^- \overset{K_{S5}}{\longleftrightarrow} AlOOH + H_2O \tag{14}$$

$$Al(OH)_2^+ + OH^- \overset{K_{S6}}{\longleftrightarrow} AlOOH + H_2O \tag{15}$$

$$Al(OH)_3 \overset{K_{S7}}{\longleftrightarrow} AlOOH + H_2O \tag{16}$$

$$Al(OH)_4^- + H_3O^+ \overset{K_{S8}}{\longleftrightarrow} AlOOH + 3\ H_2O \tag{17}$$
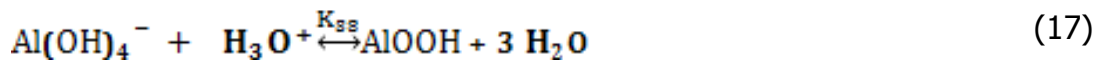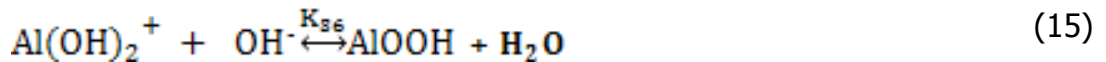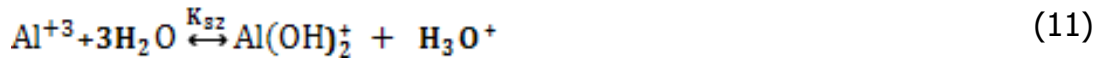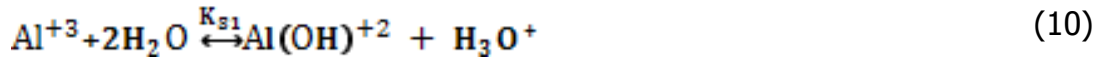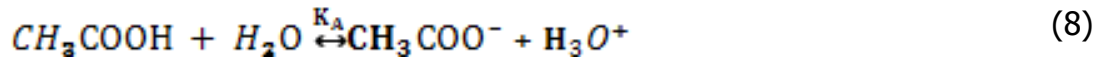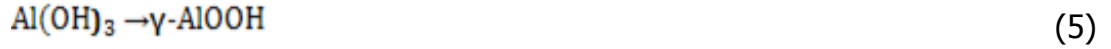
As confirmed by Yanagisawa et al. boehmite crystals appear after nucleation which is the rate controlling step [35]. The hydrothermal boehmite formation from gibbsite is described by a dissolution-precipitation mechanism [35]. As soon as the ATH crystals start to dissolve mainly according to equation 6 at high temperatures attained in the pressurized vessel, depending on the pH level determined by the equations 7-9;

different complexes are expected to form according to equations 10-12. The dominant species will again depend on the pH level. There are also other complexes that can possibly form which are not given here, nevertheless for the scope of this thesis these three are found sufficient. Simultaneous to the dissolution and complex formation reactions, a number of reprecipitation reactions can be defined by the equations 13-17, all of which lead to the thermodynamically most stable solid species, i.e. boehmite, at the temperature the reactions were carried out (180°C).

Even though hydrothermal process products' identity was partly predicted based on literature research, particles were analyzed with FT-IR results of which are given in figure 4.4. The crystal structure and particle size and morphologies were examined with XRD and SEM respectively (figures 4.5, 4.6 and 4.7).
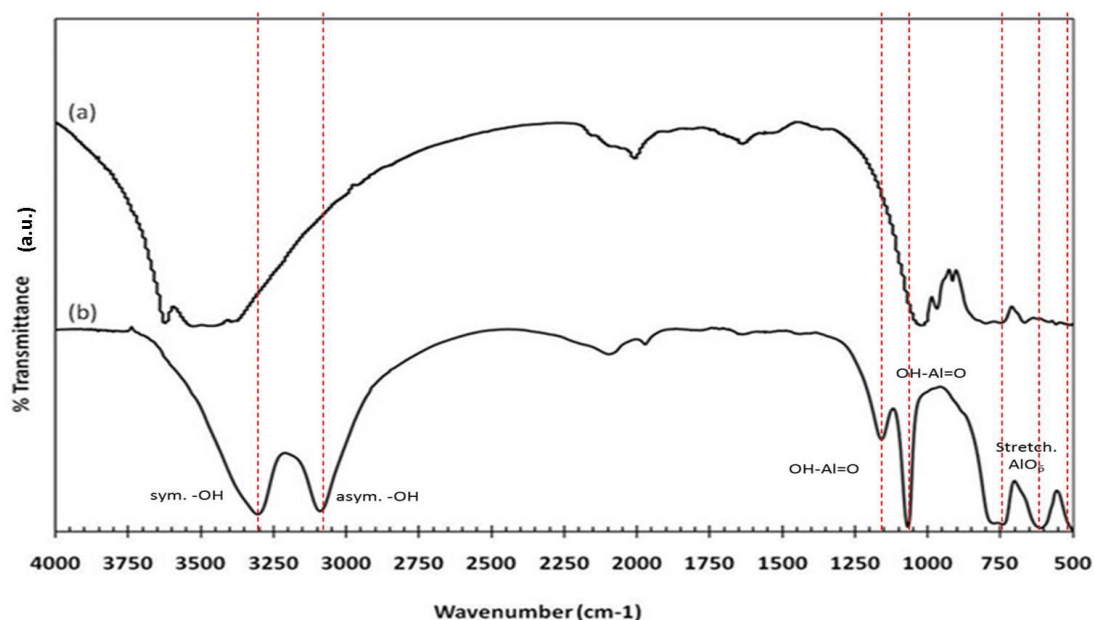
Figure 4.4 FT-IR results for (a) ground ATH powders and (b) hydrothermal product HT5.

According to the pure boehmite FT-IR spectrum, the dominating peaks characteristic of boehmite phase were same as those reported in other

studies [70],[71]. There are four intense signals at 486, 615, 670 and 760 cm^{-1}, explained as the stretching vibrations of Al-O-Al in the distorted AlO$_6$ octahedron. While the peaks at 1074 and 1163 cm^{-1}are due to the angle bending and angle deformation (wagging) of the H-bonds present in the octahedral structure of boehmite (OH-Al =O). The asymmetric and symmetric stretches of the interlayer OH groups are seen at 3294 and 3094 cm^{-1}, respectively.

In figure 4.5, XRD results from hydrothermal product and ground ATH are compared. ATH powders displayed the typical X-ray diffraction pattern of gibbsite at 2θ values of 18.40°, 20.38°, and 37.12° which represent (002), (110), and (311) reflections, respectively. The product from the hydrothermal process displayed a different pattern, matching the diffraction pattern of orthorhombic boehmite crystals (JCPDS card 21-1307) [32, 72], with the dominant peaks at 14.58°,28.26°, 38.42°, and 49° 2θ values with respective indices of (020),(120),(031), and (051)/(200). For detailed information refer to data intableA.1 and A.2 in Appendix A.1.
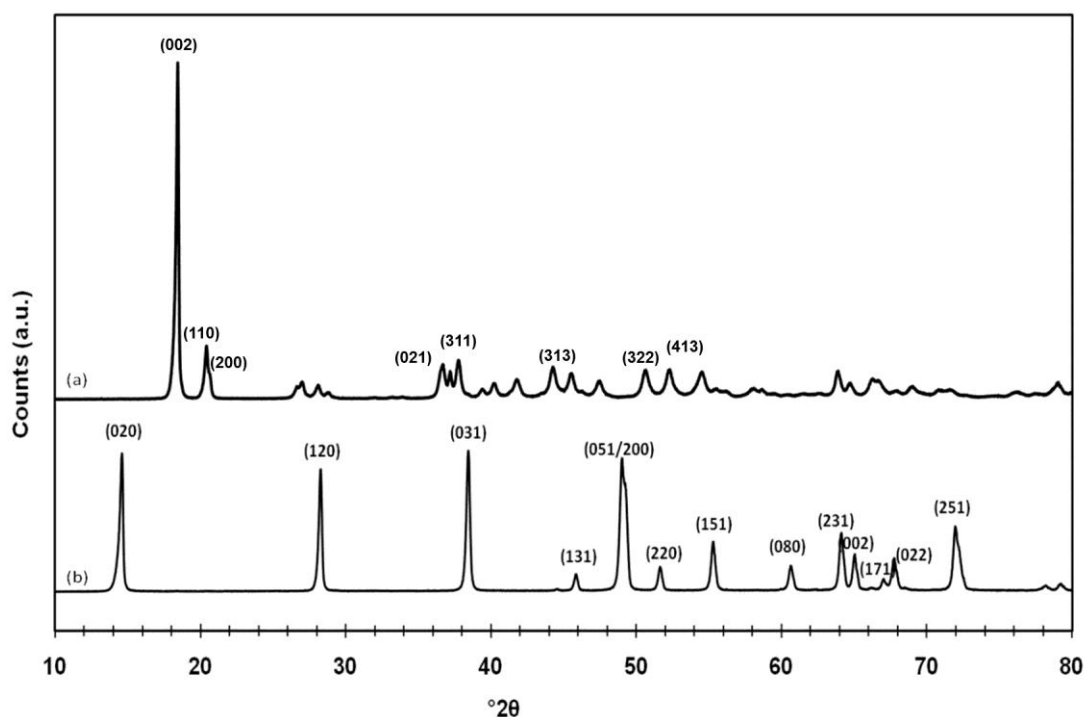
Figure 4.5 XRD results of (a) Ground ATH, (b) Hydrothermal product after 10 hours digestion (HT7).

4.2.1 Residence time in the reaction vessel

Effect of residence time in the reaction vessel on the boehmite crystals' growth was studied with XRD analysis. Results are given in figure 4.6. It is observed that as residence time increases from 5 to 10 hours, the crystallite sizes decrease to nearly 43% of the largest crystallite size observed in sample HT5 across (020) planes (d_{020})(summarized in table 4.1 and figure 4.6).
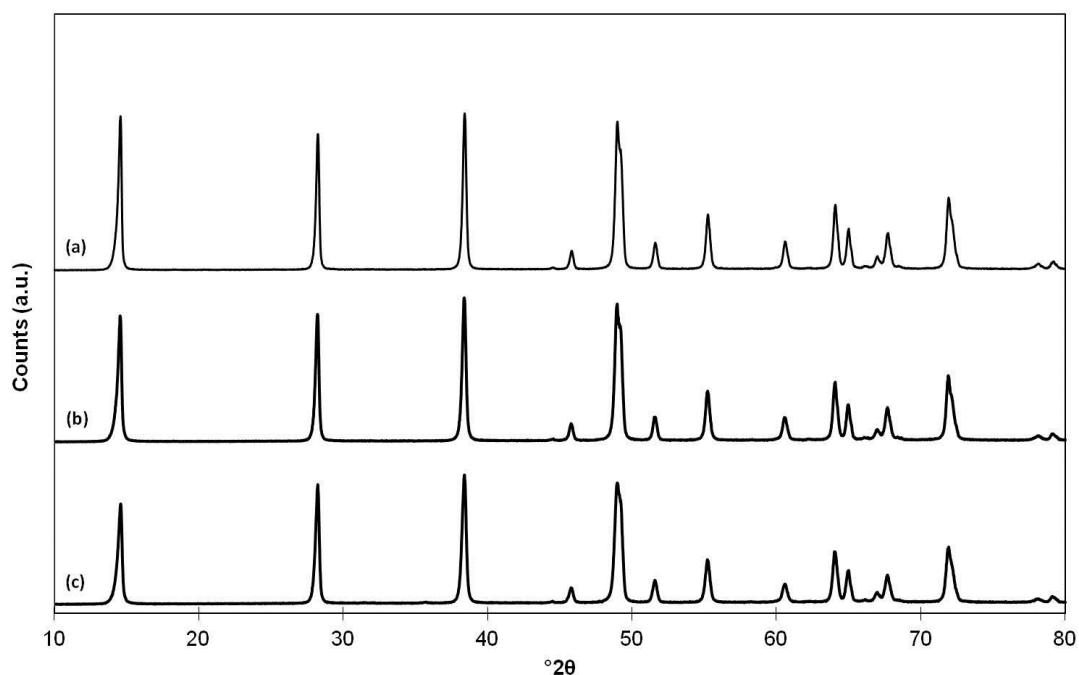
Figure 4.6 XRD results for different residence times; (a) Hydrothermal product after 10 hrs (HT7),(b) Hydrothermal product after 7.5 hrs (HT6), and (c) Hydrothermal product after 5 hrs (HT5).

Table 4.1 Results of the average crystallite size calculations from boehmite particles, using Scherrer formula [42].

d_{vol} (nm)	HT5 (5hrs)	HT6 (7.5 hrs)	HT7 (10 hrs)
d_{020}	14.8	9.36	8.52
d_{120}	16.8	10.4	12.3
d_{031}	6.82	6.55	5.22

4.2.2 Reaction Medium Effect - pH

Another parameter studied in hydrothermal process was the pH of aging and hydrothermal medium as listed in table 3.5. It was observed that pH of the medium had a considerable effect on crystals shape as shown by the SEM analysis results given in figure 4.7.
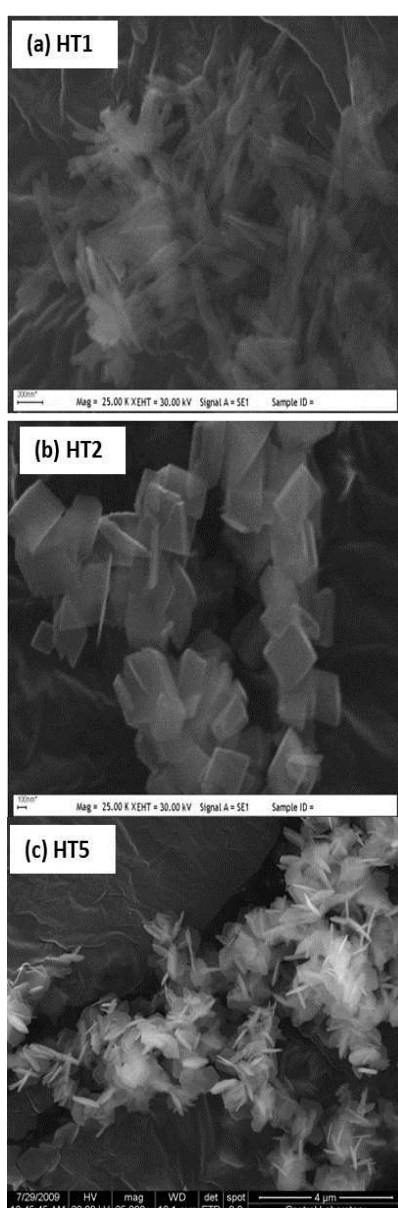
Needle-like crystals
Parameters:
No aging
t_{rxn}: 5 hrs
pH: 2.3
pH adjusted only by addition of acetic acid.

Rectangular prisms
Parameters:
No aging
t_{rxn}: 5 hrs
pH: 10.5
pH adjusted only by addition of ammonia.

Hexagonal plate-like crystals
Parameters:
24hrs aging
t_{rxn}: 5 hrs
pH: 9.68
pH adjusted by addition of acetic acid and ammonia. An acidic aging period was applied in between.

Figure 4.7 SEM micrographs of the hydrothermal products digested in different media in which pH was varied.

In HT1 (fig. 4.7.a) and HT2 (fig. 4.7.b) before the hydrothermal process no pre-aging was carried out and the pH was controlled by addition of only one pH regulator. Due to acidic pH, products in HT1 were needle-like as predicted and in agreement with Chen et al. [6] and Zhu et al. [34].While in products of HT2, the morphology observed was more like rectangular prisms. In HT5 however, a preliminary aging was carried out before the reactants were put into the reaction vessel and pH was regulated with acetic acid and ammonia. The result was hexagonal boehmite nanoplatelets as shown in fig.4.7.c and also in figure 4.8 at a higher magnification.
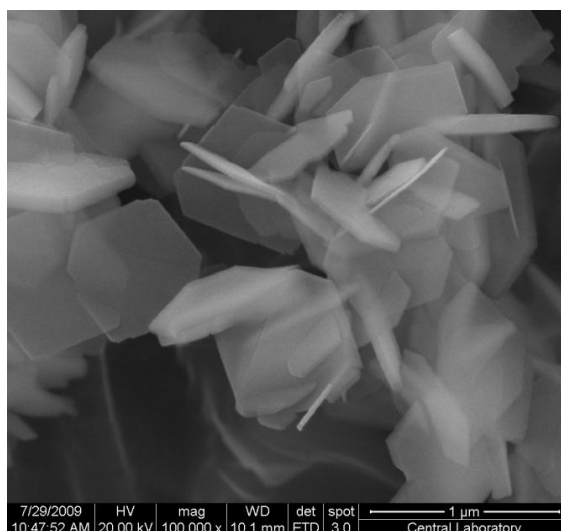
Figure 4.8 Hydrothermal process product HT5at a higher magnification displaying the hexagonal nanoplatelet morphology attained under the stated conditions.

In Figure 4.9, the particle size analysis (PSA) of the product after the hydrothermal process is shown. It shows a bimodal distribution and smaller distribution can be ascribed to the shorter dimension of the platelets (i.e. thickness) while the larger could be assumed to give the hexagonal platelet surface dimensions as its circular equivalent. According to this the platelets had an average diameter distribution of 519 and 148 nm. This could also be

verified by the SEM result given in figure 4.8. These hexagonal nanosize crystals were found satisfactory for one of the main goals of this study which was obtaining high specific area/volume ratio crystals by producing boehmite in platelet form. These particles would then be incorporated into epoxy polymers.
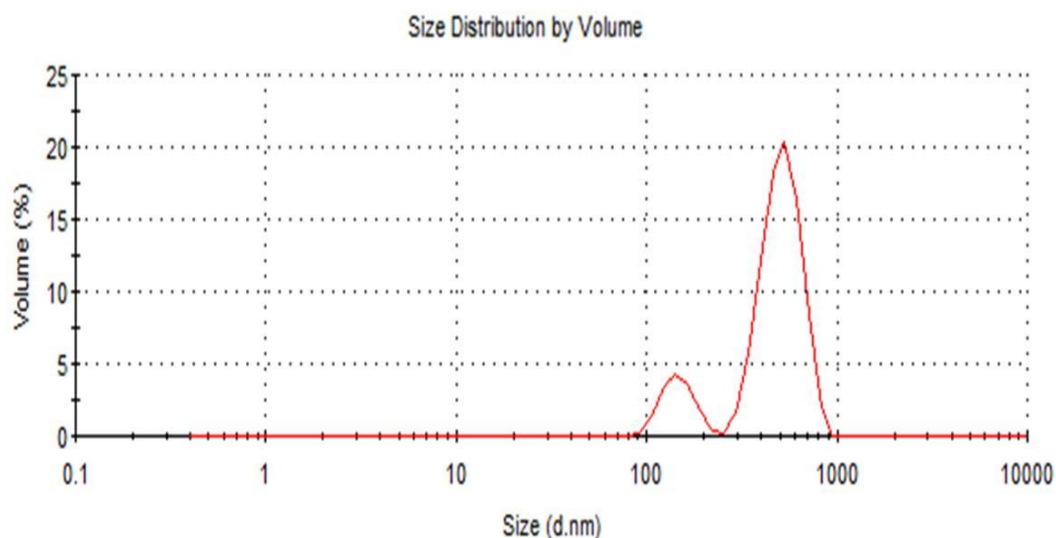
Figure 4.9 Cumulative particle size distribution of hydrothermally produced boehmite particles from HT5 set.

4.3 Epoxy Functionalization

During hydrothermal synthesis, as the crystals grows, the interactions between double layers gets weaker than the other interactions. This is one possible reason explaining the vulnerability of these parallel layers to crystal cleavage. Consequently, the newly formed crystal surfaces are totally covered with hydroxyl groups bonded to aluminum atoms. Using this feature, the surface hydroxyl groups of boehmite crystals are meant to react with the epoxy monomer under the influence of $SnCl_2$ catalyst which behaves as a mild Lewis acid and causes ring-opening of the very active

epoxy ring, creating thus a hybrid organic-inorganic crystal with dual properties. In figure 4.10 the possible mechanism occurring during functionalization can be suggested to be like,
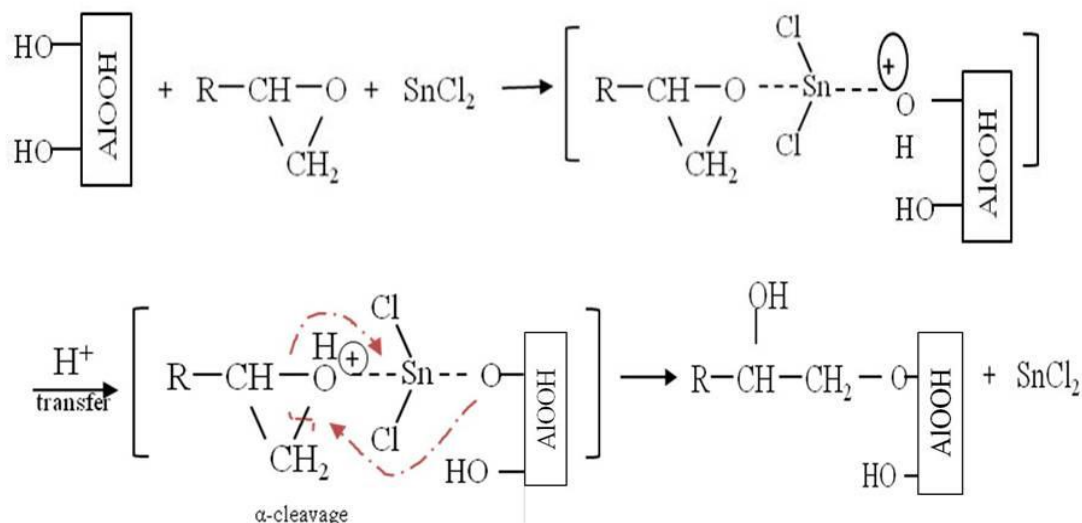
Figure 4.10 Reaction mechanism of functionalization and the role of tin chloride as a catalyst. Note that in di-epoxides the 'R' groups have an additional epoxide ring that would remain unreacted depending on the reaction conditions.

In figure 4.11 the SEM results after functionalization are given. It is observed that the functionalized plates are much better dispersed than the as-prepared boehmite plates. This is a fact which can be attributed to the presence of the organic ligands on the surface of plates, which in this case the unreacted epoxide ring. Due to its negative polarity, the oxygen atom in the epoxide rings extending out at the end of di-epoxides repel each other, which means that the epoxide rings on opposite plates have a tendency to repel each other, and thus causing an increase in the dispersion quality as observed in SEM results.

61

(a)   (b)
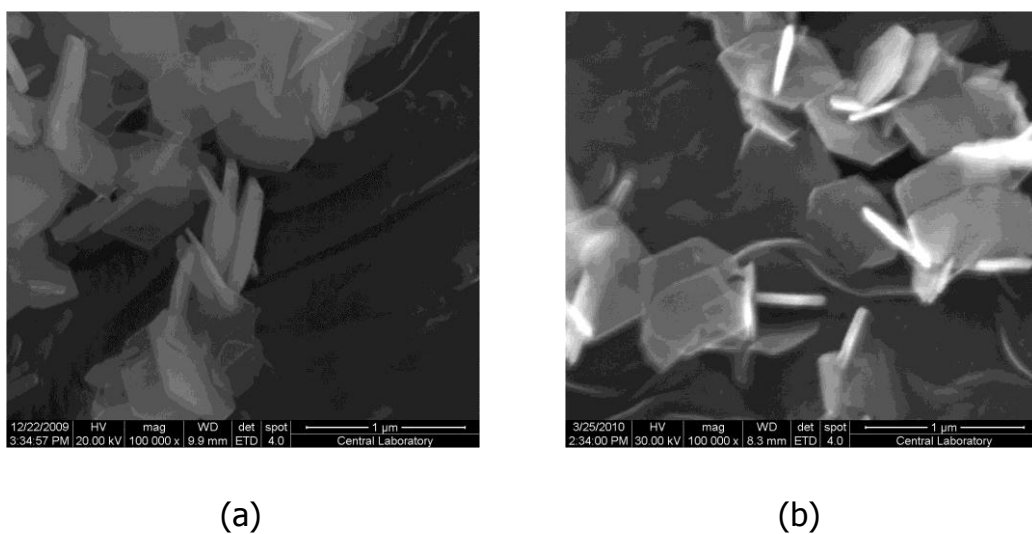
Figure 4.11 SEM analysis of (a) as-prepared boehmite particles and (b)
epoxy functionalized boehmite particles.

In figure 4.12 the expected structure of the functionalized boehmite plate surface is given. According to this schema, the formation of the aliphatic linkage, the remaining epoxide rings are the essential groups which should be traced in the FT-IR data analysis in figure 4.13.
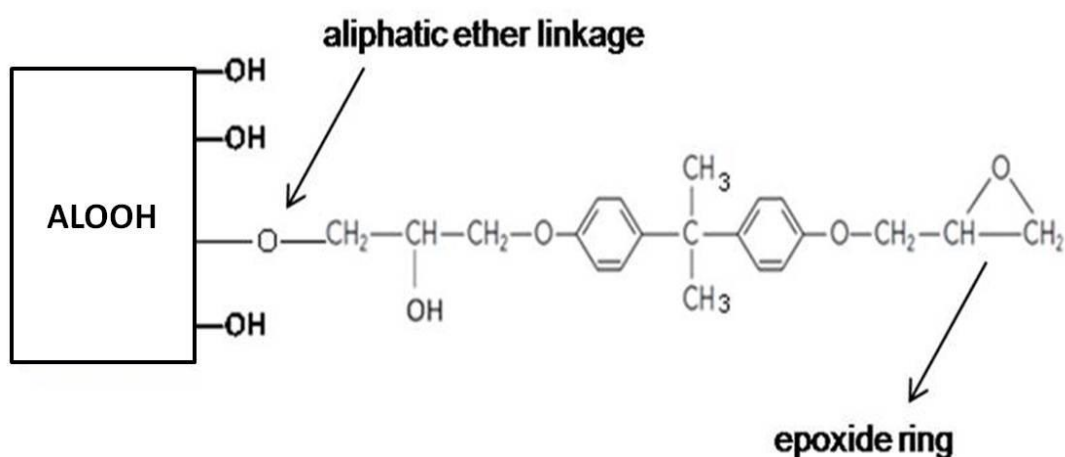
Figure 4.12 Epoxy functionalized boehmite surface.

Unlike the as-prepared boehmite, the FT-IR spectra of the functionalized boehmite shows a great variety of signals in the 1400-1800 and 2600-3000 cm^{-1} zones, attributed to the organic groups reacted with the surface hydroxyls of the crystals. At the same time, the typical strong peaks observed in boehmite spectrum shifted and broadened in the hybrid boehmites, which can be taken as a sign of the presence of other group frequencies such as the peaks at ~800, 1050, 1180, 1270 cm^{-1}. The broadening of the peaks is most probably due to overlapping of frequencies of different vibrations of the organic groups with the boehmite vibrations. The peaks observed in the epoxy functionalized-boehmite sample, EP6are listed and explained in table 4.2. The key hints that indicates that the functionalization was successful and that there are epoxy groups on the boehmite surface, are the asymmetric stretching of CH$_3$ at 2969 cm^{-1}, asymmetric stretching of the backbone -CH$_2$- group at 2925 cm^{-1}, symmetric stretching of -CH$_3$, aromatic C-H stretching at 2871 cm^{-1}, the Al-O-CH$_2$-symmetric stretch (aliphatic) at 2840-2860cm^{-1} and the shoulder at 881cm^{-1}.
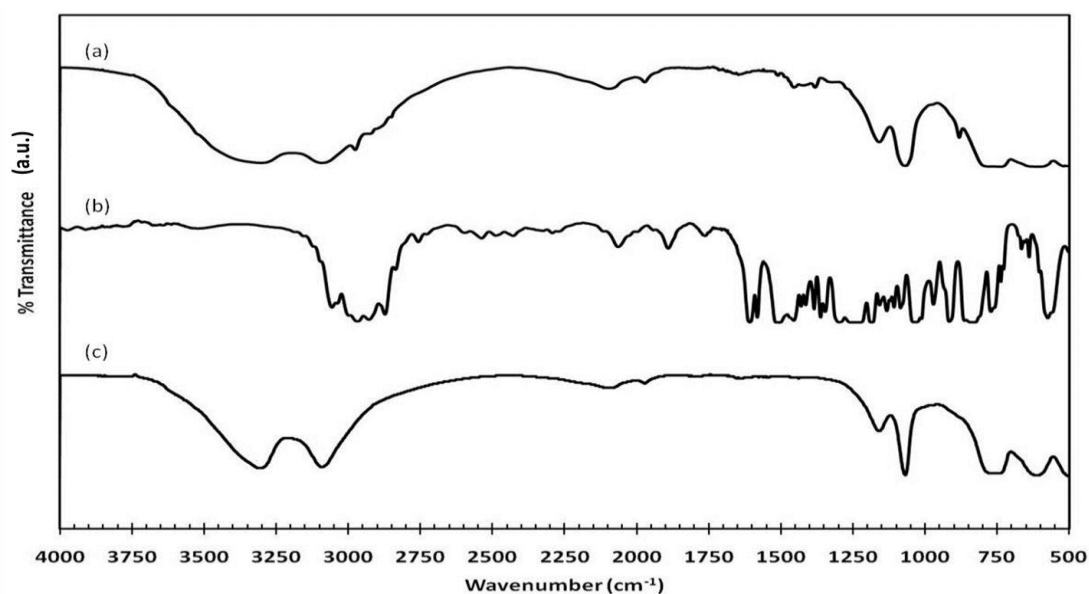
Figure 4.13 FT-IR spectra for sample EP-6 in comparison with the pure reagents; (a) experimental product EP-6, (b) BADGE and (c)as-prepared boehmite.

Table 4.2   List of main peaks observed in the functionalized boehmite surfaces and their attribution.

Observed Wavenumber (cm $^{-1}$)	Assignment (cm $^{-1}$)
s 3300	• Asymmetric stretching of OH groups at 3295 [70],[71]
s 3100	• Symmetric stretching of OH groups at 3094 [70, 71] • Symmetric Phenyl C-H stretching vibrations at 3038 [72] • Asymmetric vibration of CH_2 in the epoxy group at 3057 [72]
m 2970	• Asymmetric stretching of CH_3 at 2969 [73]
m 2924	• Asymmetric stretching of in the backbone CH_2 at 2925 [74]
w 2870	• Symmetric stretching of CH_3, Aromatic C-H stretching,2871[73]
w 2850	• Al-O-CH_2- symmetric stretch (aliphatic) at 2840-2860 [73, 74]
w 1510	• Breathing of benzene ring at 1500-1520 [75]
w 1487	• Asymmetric deformation of CH_3; CH_2 scissoring vibrations at 1483-1492 [76]
w 1471	• Asymmetric deformation of CH_3; CH_2 scissoring vibrations at 1470-1472 [76]
m 1450-1460	• Deformation band of CH_2 in the oxirane ring at 1460 [77] • Deformation band of aromatic C-H [74]
w 1367-1388	• Symmetric deformation of gem-dimethyl group [78]
w 1263-1281	• C-O-C in phase stretching (ring breathing) of oxirane ring at 1240-1280 [79]

s – strong, m - medium, w- weak, sh– shoulder

Table 4.2 (Cont.d)

Observed Wavenumber (cm $^{-1}$)	Assignment (cm $^{-1}$)
s 1163	• Angle deformation (wagging) of the H bonds in the octahedral structure of boehmite (OH-Al =O)[70, 71] • Rocking vibrations of CH_3 groups at 1160-1190, in-phase CH_2 stretching of oxirane ring at 1170-1180 [74, 79]
s 1074	• Angle bending of the H bonds in the octahedra structure of boehmite (OH-Al =O) [70, 71] • Phenolic C-O stretching at 1065 , aliphatic C-O stretching in the oxirane ring at 1040 [79, 80]
sh 881	• Out of phase stretching of oxirane group at 860-890[79]
s 720-800	• Overtoning of stretching vibrations of Al-O-Al in the distorted AlO_6 octahedron [70, 71], • Symmetric stretching of oxirane ring 720-840, • Asymmetric stretching of oxirane ring at 810-850 [81], • Out of phase phenolic C-H deformations at 831 [72] • CH_2-C_2H_3O (epoxy ring) stretching at 772 [79]

s – strong, m - medium, w- weak, sh – shoulder

Besides the FT-IR analysis, titration analysis was performed both, qualitatively and quantitatively. In the qualitative analysis, the color of the titration medium turned pink when HCl reacted with the ether group of epoxy on the boehmite particle surface, proving that there are epoxy end groups on the surface of the boehmite particles. With the quantitative titration analysis, calculation details of which are given in Appendix A2, the number of surface OH groups and the number of epoxy end groups were

evaluated. According to the tests, it is assessed that there is 0.0049 mol OH groups per gram non-functionalized boehmite and 0.00055 mole epoxy end group per gram funtionalized boehmite of sample EP6.

4.3.1 Effect of Temperature On Functionalization
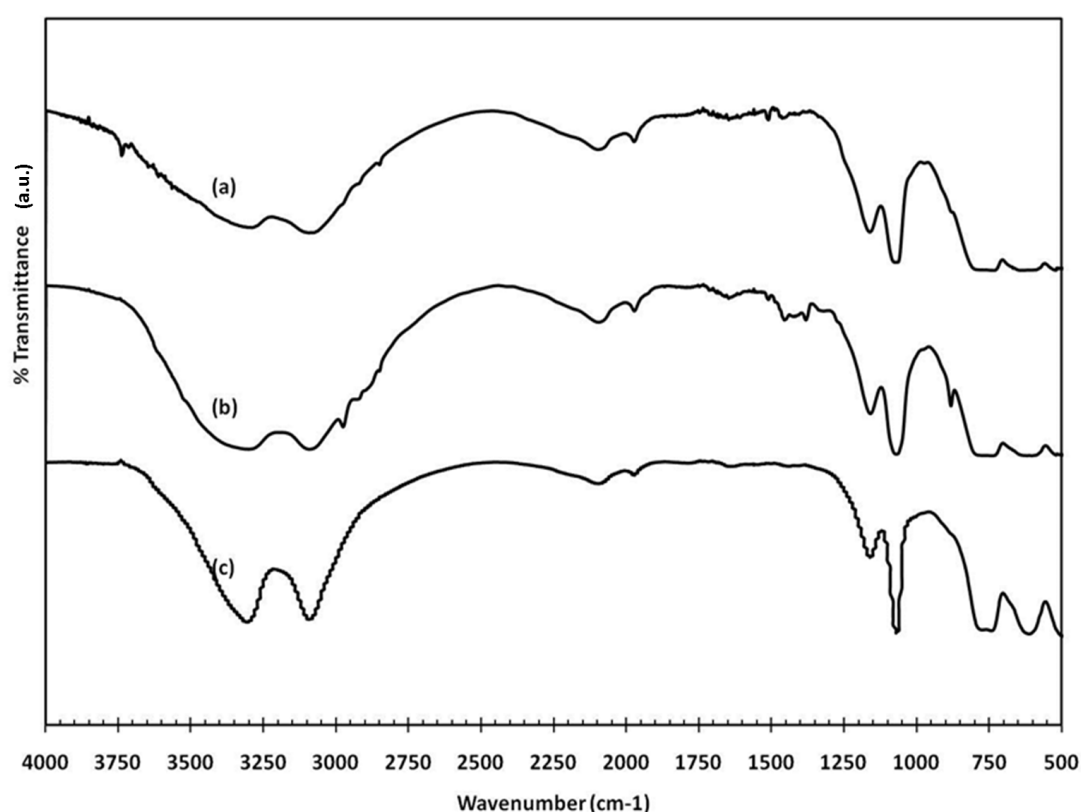
Figure 4.14 FT-IR results reflecting the temperature effect (a) EP-7(T: 100°C), (b) EP-6 (T: 80°C) and (c) EP-9 (T: 60°C).

According to Wu et al. and Ying-Ling et al. [52, 82], the process of functionalization can be performed at a temperature range of 140-200°C, without serious instability caused by the solvent. In the present study the temperature range was kept at a temperature range between 60-100°C. This constraint is because of the low boiling point of toluene. The FT-IR analyses

results given in figure 4.14, reflect the temperature effect. The curve (c) belonging to sample EP-9 performed at reaction temperature of 60°C, lacks the typical assigned shoulder resulting from –CH-O-CH$_2$out of phase stretching vibrations in the oxirane ring (880 cm^{-1}), the asymmetric stretching of CH$_3$ at 2969cm^{-1}, asymmetric stretching of the backbone -CH$_2$- group at 2925 cm^{-1}, symmetric stretching of -CH$_3$, aromatic C-H stretching at 2871cm^{-1} and the Al-O-CH$_2$- symmetric stretch (aliphatic) at 2840-2860 cm^{-1}. Compared to other temperatures, EP-9 also lacks the variety of peaks in the 1700-1300 cm^{-1} range in which lies the bands of the organic groups from epoxy. The clearest evidence of functionalization is observed at 80°C while at 100°C; the primary peaks proving the occurrence of the reaction seem to be weaker and not that dominant as in 80°C. However it is difficult to say that functionalization carried at 100°C is less successful than the one carried at 80°C, because, many peaks might have been eclipsed by the strong peaks of boehmite at the same wavelengths. Nevertheless the peaks characterizing the benzene group vibrations and aliphatic groups are visible in the 1300-1700 cm^{-1} range. To conclude, both temperatures 80 and 100°C are efficient for the reaction to take place. Use of higher temperature can be expected to lead to toluene escaping to atmosphere during the reaction, reducing the amount of solvent required for the reactants to be active. Therefore to be on the safe side, the functionalization experiments for further stages were performed at 80°C, avoiding risks from toluene evaporation as a solvent at higher temperatures.

4.3.2 Effect of ratio of reactants

In this study, different from the approach of Ying-Ling et al. [53] in which the feeds' weight composition was a ratio of 7:3 or 6:4 of epoxy functionalizing unit to silica, compositions which were in much higher excess

were used, such as 5:1 or 10:1 BADGE to boehmite. This measure was taken because of the low temperatures in which the reaction took place. In both cases, as shown in figure 4.15, there is a strong evidence of organic groups on the boehmite surfaces evidenced from the appearing interactions in the 1300-1700cm^{-1}range. Still there are differences between these two samples, which are observed mainly in the 3000-3300 cm^{-1}, 1200-1400 cm^{-1}, the shoulder at 880 cm^{-1}, and the finger print zone for boehmite 400-700 cm^{-1}.
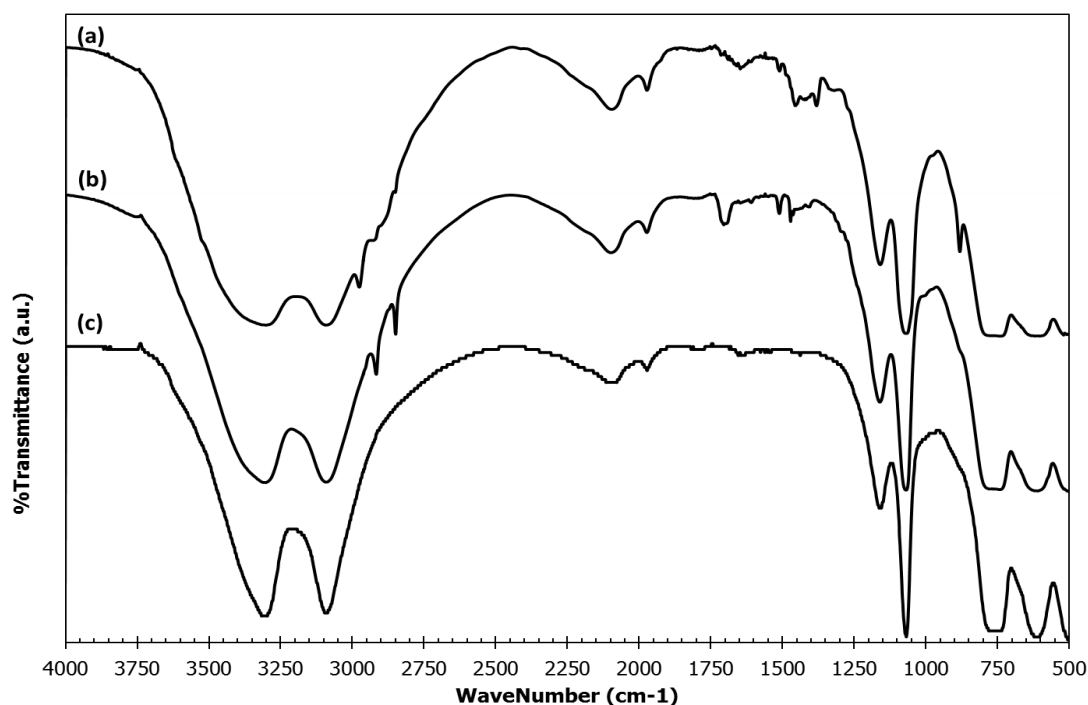
Figure 4.15 FT-IR spectra reflecting Epoxy:Boehmite weight ratio dependency in functionalization; (a) EP-6 (R: 5:1, t: 3 hr, T: 80°C) (b) EP-4 (R: 10:1, t: 3 hr, T: 80°C) and (c) as-prepared boehmite.

As mentioned in table 4.2, the region of 3000-3300cm^{-1} in both samples, EP4 and EP6, reflects the boehmite typical bands but EP4 profile is more loyal to pure boehmite profile of that zone. Meanwhile EP6 sample has stronger intensity in these two bands, with the vibration of the secondary

alcohols being added to the interlayer OH vibrations and also epoxy group vibrations. The same argument follows the fingerprint zone for boehmite between 400-700 cm^{-1}. In EP4 FTIR spectrum, the fingerprint zone of boehmite is less affected from the organic groups compared to that in the spectrum of EP6 where the main peaks are greatly widened due to the superposition of other group absorptions besides the boehmite's. In the 1200-1400 cm^{-1} zone, many peaks observed in EP6 and pure BADGE are less strong in EP4. Also the shoulder in 880 cm^{-1} is very weak in EP4. Using a ratio higher than 5:1 did not seem an efficient approach, therefore this ratio was fixed in further experiments.

4.4 Polymer preparation

Before starting the discussion of this part of the study, there are two phenomenons necessary to be discussed: dewetting and crazing effects, which are schematically explained in figure 4.16.

(a)   (b)
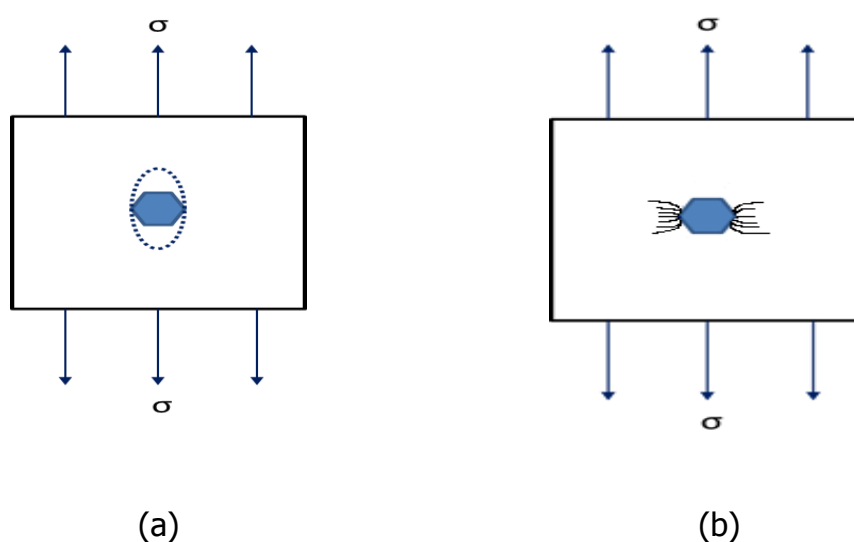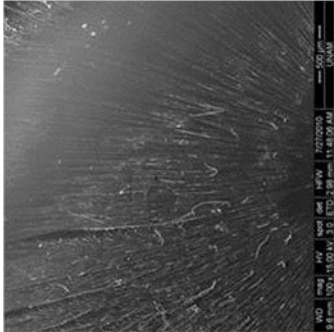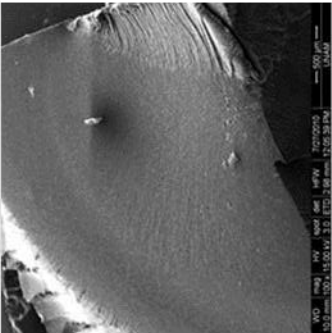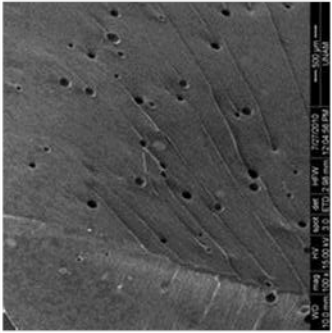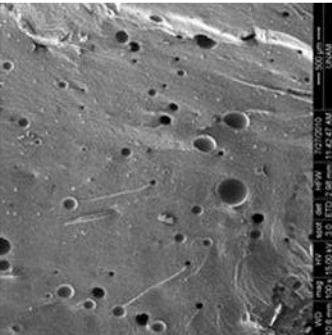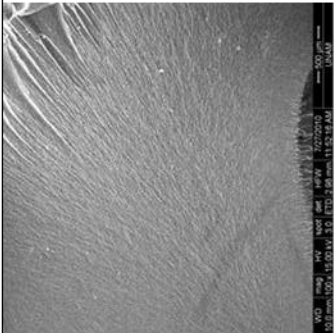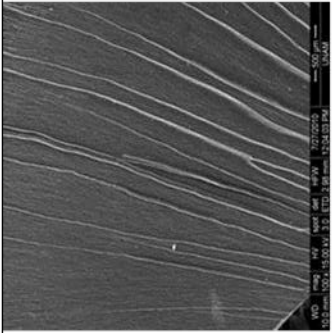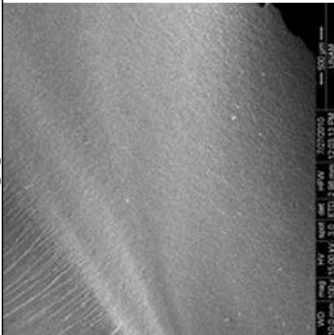
Figure 4.16 Dewetting effect (a) and crazing effect (b) occurring under stress to a nanoparticle in a polymer matrix.

As illustrated in figure 4.16 as a tensile stress is exerted on the polymer matrix, owing to different modulus of polymer and the particle, a stress concentration is created which will cause dewetting and cavitation at the sharp edges of the particle. Once dewetting happens the stress is concentrated at the equator of the particles as shown in figure 4.16-a, causing cracks and crazing. In brittle polymers such as the one prepared in the present study, the cracking phenomenon is quite frequent and the presence of particles in the matrix serves as crack initiator and decreases the impact strength [83].

Besides the possible effects of crazing and dewetting on mechanical properties, use of nanoparticles can also lead to some negative effects in composite properties. As the size of particles decrease, surface area and surface energy increase as well. This in turn triggers a larger particle-particle interaction, adherence and agglomeration. In the present study, because of the nano-dimensions, the particles exhibited a higher tendency to form agglomerates, especially in highly viscous resins with weight ratio larger than 3% (at the moment of mixing before curing) since their presence increases the viscosity according to Nielsen et al. [83] and as a result it is more difficult to obtain a good dispersion. Therefore the higher the amount of particles, the greater was the agglomeration as exemplified in figure 4.18. Because of the increase in viscosity, there is a higher tendency for air entrapment within the prepared samples, lowering the density, causing voids and affecting all mechanical properties.

In figure 4.17, SEM micrographs are given for each set of polymers prepared (refer to table3.7 for details of samples). The pictures were taken from fracture surfaces of the polymers (after being instantly broken). In the first column the samples in which the non-functionalized boehmite particles incorporated in the epoxy matrix are presented. In the second column, the polymers with functionalized boehmite particles are presented.

Figure 4.17 SEM micrographs of pure epoxy polymer (a), non-functionalized boehmite-polymers (b,d,f) and functionalized boehmite-polymers (c,e,g) (all micrographs were taken with ×100 magnification).
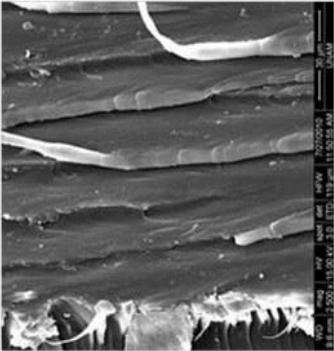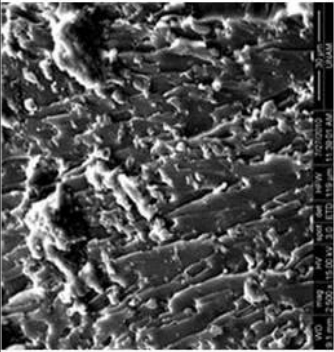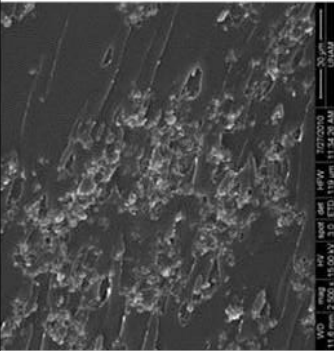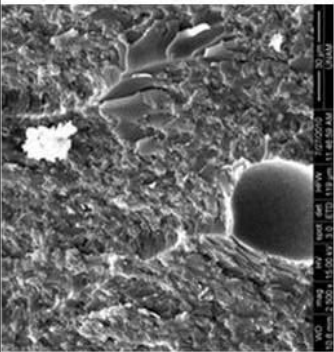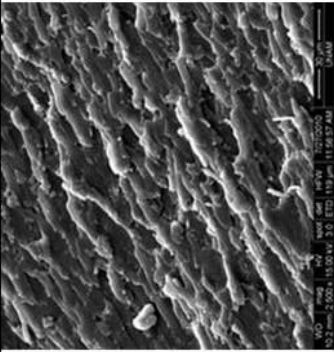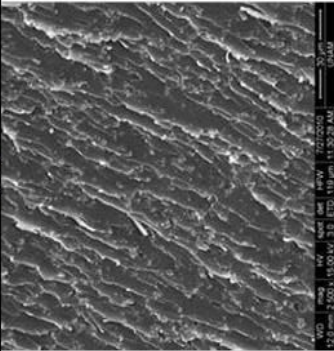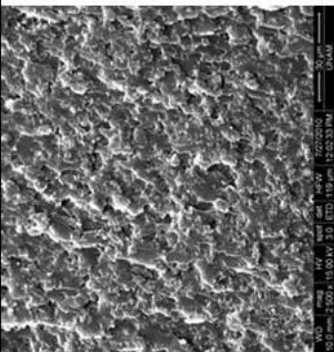
In the non-functionalized boehmite-polymers, due to organo-phobic character of the boehmite particles, a higher agglomeration tendency was observed even by naked eye during introduction of these powders into the polymer matrix. This phenomenon was clearly seen in figure 4.17 for non-functionalized boehmite-polymer sample of 10% weight ratio. The creation of a multiphase in the epoxy matrix gives rise to the dewetting and crazing effect. This phenomenon in turn causes voids and crazing as observed in figure 4.17.d and 4.17.f. Here the higher non-functionalized boehmite concentration caused a denser agglomerate concentration and higher concentration of voids and crazes. The presence of voids in the matrix is expected to decline the mechanical properties at a large extent.

The opposite is observed in the functionalized boehmite set. Due to the epoxy groups on the boehmite surface, these functionalized powders seem to be dispersed in a more homogeneous way and less agglomeration is observed in figure 4.18 (c, e, g) when compared to their non-functionalized homologues given in figure 4.18 (b, d, f). In figure 4.18 the surfaces given in figure 4.17 are shown at a higher magnification.

The EP5 set shows a different pattern from the other classes, exhibiting fine lines originating from the crack initiation region during the fracture of the polymer sample for the SEM analysis.

Besides comparing homologue polymer sets, another interesting observation is seen between the pure epoxy polymer surface and the nano-composite surfaces. Referring to figure 4.18 (a), the pure epoxy interface shows that the polymer has a fibrilar and layered structure, with layers distinguishable from each other. This is one of the reasons why epoxy polymers are brittle. In the nano-composite set this feature is less obvious and softened with the particles being well incorporated into the polymer matrix, especially in the functionalized boehmite-epoxy polymer set, shown in figure 4.18 (c, e, g).

Figure 4.18 SEM micrographs of pure epoxy polymer (a), non-functionalized boehmite- polymers (b, d, f) and functionalized boehmite-polymers (c, e, g) (all micrographs were taken with ×2500 magnification).

73

Dynamic Mechanical Analysis Results

Another test performed on the produced polymers was the Dynamic Mechanical Analysis. In table 4.3 the data obtained from these tests are summarized. In the storage modulus graph given in figure 4.19 there were 3 distinct regions which could be observed from 25 to 180°C. At temperatures lower than 70°C the polymer is stiff and keeping its solid structure with an accordingly high modulus and low tan (δ). As the temperature increases, the polymer softens and in the third region (>120°C) the material behaves like a soft rubber and has a low modulus. It is between these two temperature ranges where the glass transition occurs and referred as α-relaxation. The DMA graphs for each polymer set are given in Appendix A.3.

In table 4.4 several parameters retrieved from the storage modulus, and loss factor (tanδ) graphs in Appendix A.3are summarized. One of these is the glass temperature which is determined from the maximum of loss modulus E″ value and storage modulus (E_{50}') values from the glassy region measured at 50°C and E_{180}' from the rubbery region measured at 180°C.According to Nielsen et al. [83] using the temperature of $(\tan\delta)_{max}$ will give an approximate value of T_g since the temperature of $(\tan\delta)_{max}$ is more sensitive to cross-link density, filler content or blend morphology than T_g. The closest value to refer as T_g is the maximum of loss modulus.

Table 4. 3. DMA results of the set of polymers tested with different weight ratios of functionalized and non-functionalized boehmites.

	$T_g(^oC)$	$tan\delta_{max}$	$E'_{50}(10^8Pa)$	$E'_{180}(10^8Pa)$	$E_{max}''(10^8Pa)$
PURE	85.5	0.767	17.6	0.737	2.12
BH-EP3	114	0.672	20.8	0.857	2.55
FB-EP3	110	0.637	18.5	1.02	2.19
BH-EP5	112	0.662	17.9	0.671	1.93
FB-EP5	109	0.688	19.6	0.849	2.25
BH-EP10	112	0.598	19.5	1.23	2.45
FB-EP10	104	0.699	21.6	1.05	2.64

In all the polymers, there was only one transition region, which means there is only one phase in epoxy matrix despite the fact that increasing weight ratio of the powders were introduced in the polymer matrix. This means that they were dispersed at a degree acceptable for the polymers to keep their identity.

The storage modulus versus temperature plots in figures 4.19, 4.20 show that the storage modulus decreased as temperature increased or as the polymer approached the glass transition and found its minimum at rubbery region. As the temperature increased, the bonds in the polymers chains got less stable and the polymer chains gained a higher mobility, involving cooperative motions. This caused the storage modulus to decrease and the polymer became rubbery.
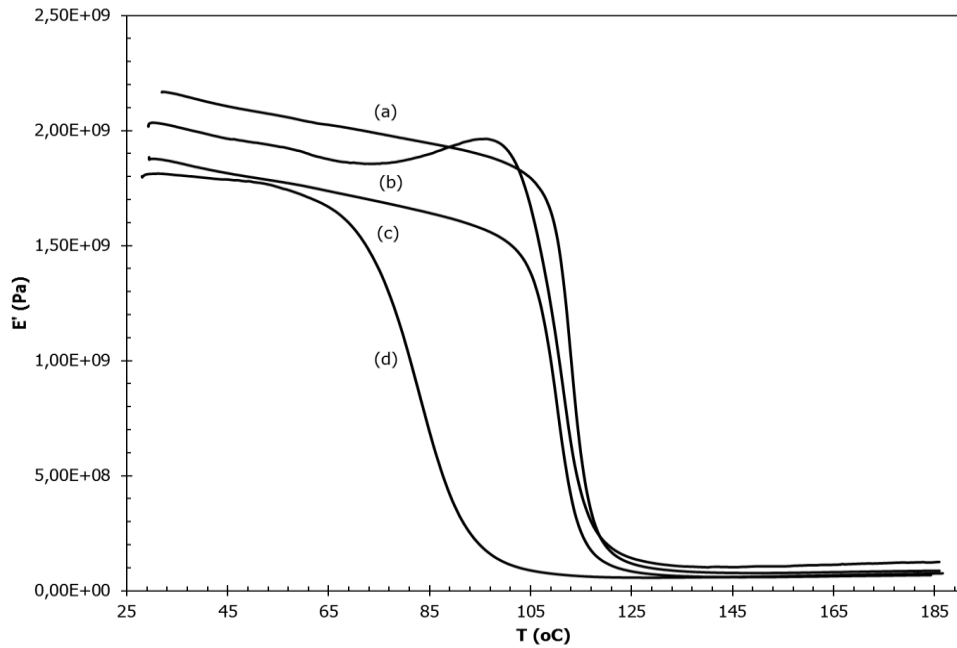
Figure 4.19 Storage modulus as a function of temperature for non-functionalized boehmite-epoxy polymer set:(a) BH-EP10 (b) BH-EP3, (c) BH-EP5, and (d) pure epoxy polymer.
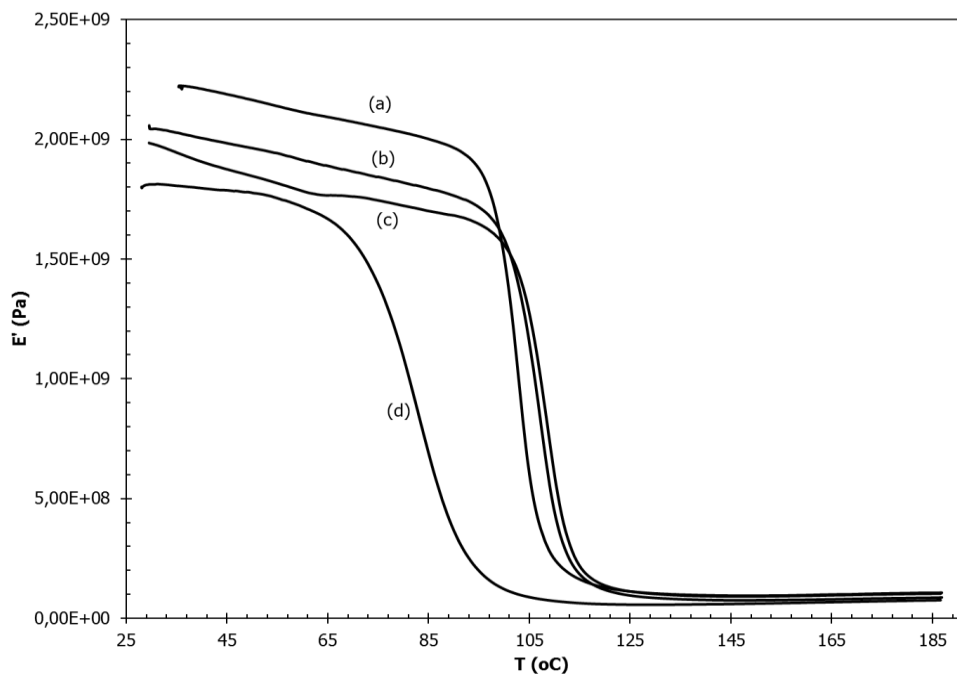
Figure 4.20 Storage modulus as a function of temperature for the functionalized boehmite-epoxy polymer set: (a) FB-EP10 polymer set, (b) FB-EP5, (c) FB-EP3 polymer set, and (d) pure epoxy polymer.

In both graphs 4.19 and 4.20, the storage modulus curves for the nanocomposites were greater in all three regions. This is due to the presence of boehmite particles which have a higher storage modulus and it was contributing to the storage modulus of the neat epoxy matrix. As the amount of powders increased, the storage modulus increased respectively, which implies a more rigid polymer. This was exactly the case for functionalized nanocomposite set, while for the non-functionalized composite set there was no particular trend related to weight composition. The same was true also for other properties. In the functionalized boehmite-polymer set there was always a distinct regularity in the trend of the all the parameters with respect to increasing weight percent of the ceramic.

An increase in glass transition temperature was observed in both composite sets. This is explained with the presence of inorganic domain which restricts the mobility of organic polymer chains during glass transition. The increase in Tg is higher in non-functionalized composite sets, where the inorganic phase is more persistent. Meanwhile, the Tg of functionalized composite sets were lower than the non-functionalized sets but higher than the pristine polymer. This is explained with the fact that the organically modified particles behave as polyfunctional crosslink centers, which allows the particles to be incorporated in the network formation without much constriction as in the non-functionalized set case. On the other hand, it is observed that parallel with the agglomeration index increase, glass transition temperature decreases with the higher weight ratio of fillers. This result is stronger in the functionalized composite polymer set, which is attributed to the plasticizer effect these agglomerates exert on the network, behaving as oligomeric intermediates with their epoxy/hydroxyl functions.

The BH-EP3 set has the highest storage modulus before glass transition and the highest glass transition temperature. This phenomenon is explained with the better dispersion quality of the powders when compared to higher

weight ratios but when it comes to comparing with the same weight ratio functionalized polymer set, FB-EP3; it is explained with the higher remnant stiffness degree. The functionalized polymer, due to its better compatibility with the polymer network, retains a character similar to the matrix polymer and shows a better ability to adapt to the polymer by not being just a host particle but behaving as a part of the system.

Tensile properties

The tensile tests were performed for each set of polymers. The tensile strength, elastic modulus (or tensile modulus) and maximum strain at fracture point for all samples are summarized in table 4.4. All the data for each set of polymers with images of the tensile test samples after the test was performed are given in appendix A.4. The tensile strength (stress) and the strain were obtained from the data on the stress-strain plots while the tensile modulus was calculated from the slope of same plots. Toughness values were calculated from the area underneath the stress-strain curve in the plastic region.

Table 4. 4 Tensile test results for the pure, functionalized and non–functionalized boehmite-epoxy polymers.

Sample	BH content (Wt. %)	Tensile Strength (MPa)	Tensile modulus (MPa)	Toughness (10^6 J/m^3)	Strain at Fracture (%)
PURE	-	63.9	753	2.91	12.6
BH-EP3	3	41.7	750	1.14	6.82
FB-EP3	5	42.0	770	1.00	6.72
BH-EP5	10	35.3	729	0.76	6.15
FB-EP5	3	52.0	767	1.56	8.06
BH-EP10	5	49.3	780	1.14	7.70
FB-EP10	10	31.7	717	0.35	5.53

The tensile test results given in figure 4.21 showed a deterioration of tensile strength with the addition of the both types of particles. As stated in Pham's review [84] of epoxy polymers, the impact strength together with other mechanical properties such as tensile and flexural strength tend to decrease with the introduction of hydrated aluminum oxide fillers. This phenomenon has been treated vigorously by Nielsen et al. [83]. Nielsen explained it with the dewetting and crazing effect described in figure 4.16.
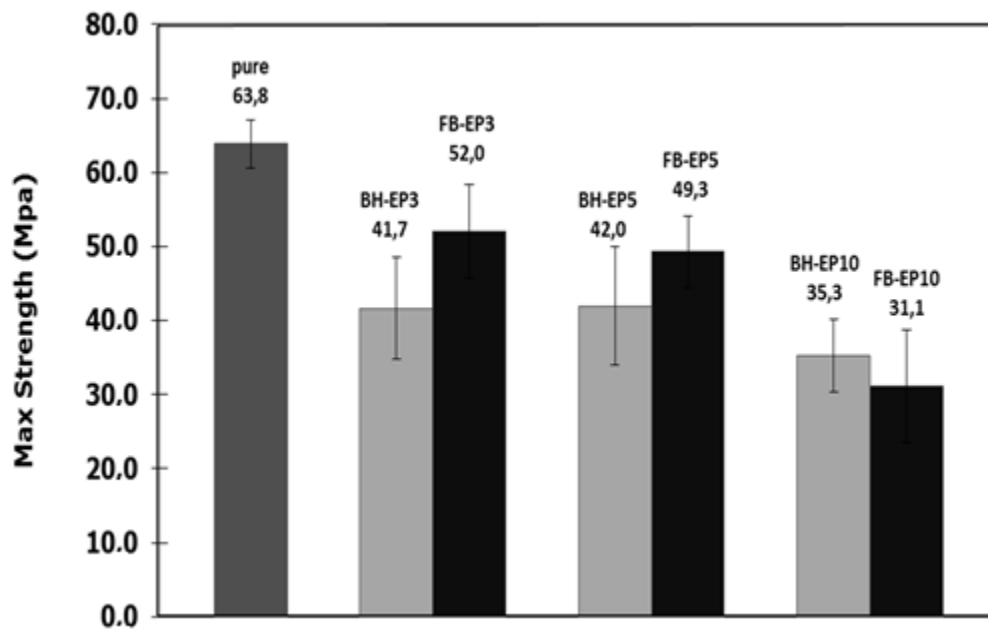
Figure 4.21   Tensile stress data for each set of polymers.
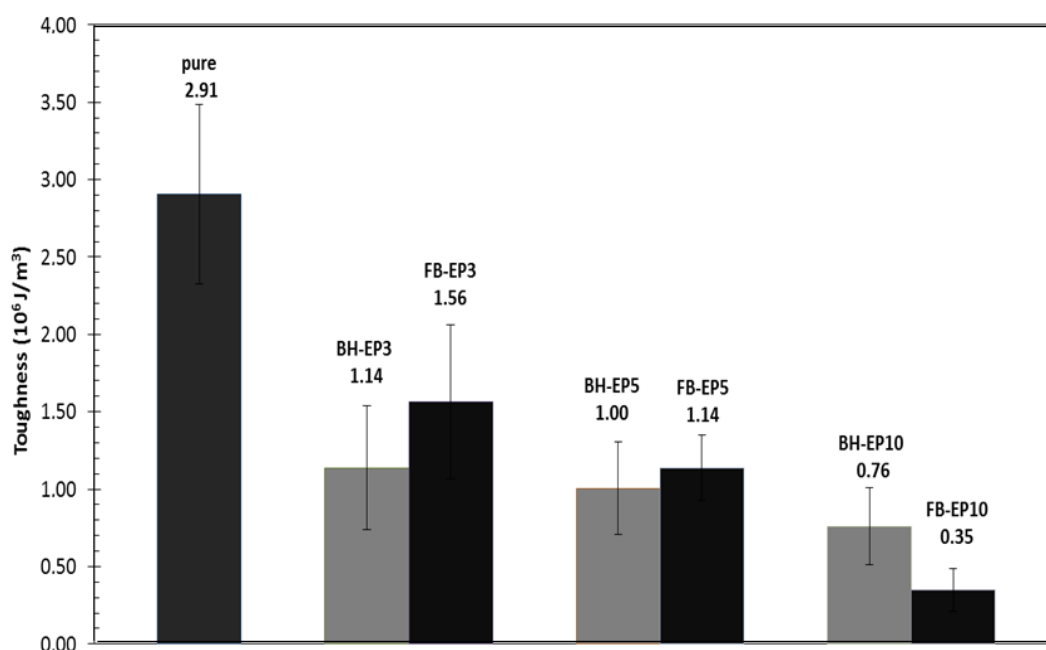
Figure 4. 22 Toughness data for each set of polymers.

As illustrated by the results given in figure 4.21, as a tensile stress is exerted on the polymer matrix, due to different modulus of polymer and the particle, a stress concentration is created which causes dewetting and cavitation at the poles of the particle. Once dewetting happens the stress is concentrated at the equator of the particles as shown in figure 4.16, causing cracks and crazing. In brittle polymers such as the present samples, the cracking phenomenon is quite frequent and the presence of particles in the matrix serves as a crack initiator and lowers the impact strength.

Beside the crazing and dewetting effect, as the size of particles decreases, surface area and surface energy increases as well. This in turn triggers a larger particle-particle interaction, adherence and agglomeration. This effect is clearly observed in toughness results given in figure 4.22. In the present test, because of their nanosize dimensions, the particles exhibited a great tendency to form agglomerates, especially in highly viscous resins (the moment of mixing before curing). Since their presence increases the

viscosity according to Nielsen et al. [83], as a result it becomes more difficult to obtain a good dispersion. So the higher the amount of particles, more agglomeration is observed (refer to SEM analysis in figure 4.17). Because of that, more bubbles were entrapped along with the agglomerates, lowering the overall density and affect the mechanical properties adversely. The modulus, tensile strength and toughness values were observed to decrease as the amount of air entrapped increased with the increased agglomeration.

The functionalized boehmite particles incorporated in the epoxy resin showed a less detrimental effect than the non-treated boehmite particles in the tensile and hardness tests. This is due to two main reasons; the epoxy groups on the particles' surface may have succeeded to be incorporated into the polymer matrix during the curing process and the other explanation is the organophilic character of these particles enables a better dispersion in the matrix.

An interesting phenomenon is observed in all the epoxy functionalized boehmite-polymer composite fracture test results for the 10 weight % samples. In comparison to lower particle percentages such as 3 and 5 weight percent, the 10 wt% samples displayed much lower improvement than the non-functionalized counterpart polymers. This is due to the interaction of the surface epoxy groups on the boehmite nanoplates during the curing process. Because of the nanosize particles, as explained above it is more difficult to obtain a proper dispersion at 10 wt% particle concentration, which in turn triggers the epoxy groups on the surface of the boehmite platelets to react with paralleling epoxy groups across the other boehmite platelets. This might have given way to a higher degree of agglomeration than the counterpart polymers.

The elastic constant E modulus (tensile modulus called here) in the tensile test specimens was determined as a secant modulus, representing the

elastic and linear-viscoelastic deformation range of the specimens in the tensile test diagrams. In other words, it includes the range of deformation between 0.05 – 0.25% of the total strain between strain gages [66].

Figure 4.23 Tensile modulus for each polymer set, with respect to the weight percentage of functionalized and non-functionalized boehmite particles in the epoxy matrix.

In figure 4.23, the tensile modulus for each polymer set is presented. A higher modulus is observed in the functionalized particles-polymer composite matrix than the untreated particle-polymer composites as observed in the 3 and 5 wt % cases, while in the 10 wt% case an opposite effect is observed. In the 3 and 5% cases, the lower modulus in the non-treated particle-polymer composite is probably because of the stronger hydrostatic forces among the particles, leading to increased crazing and dewetting effect. A similar trend was also observed in the maximum strain at fracture point. The functionalized nanocomposites show a higher degree of strain under stress than the non-functionalized composites as given in figure 4.23.
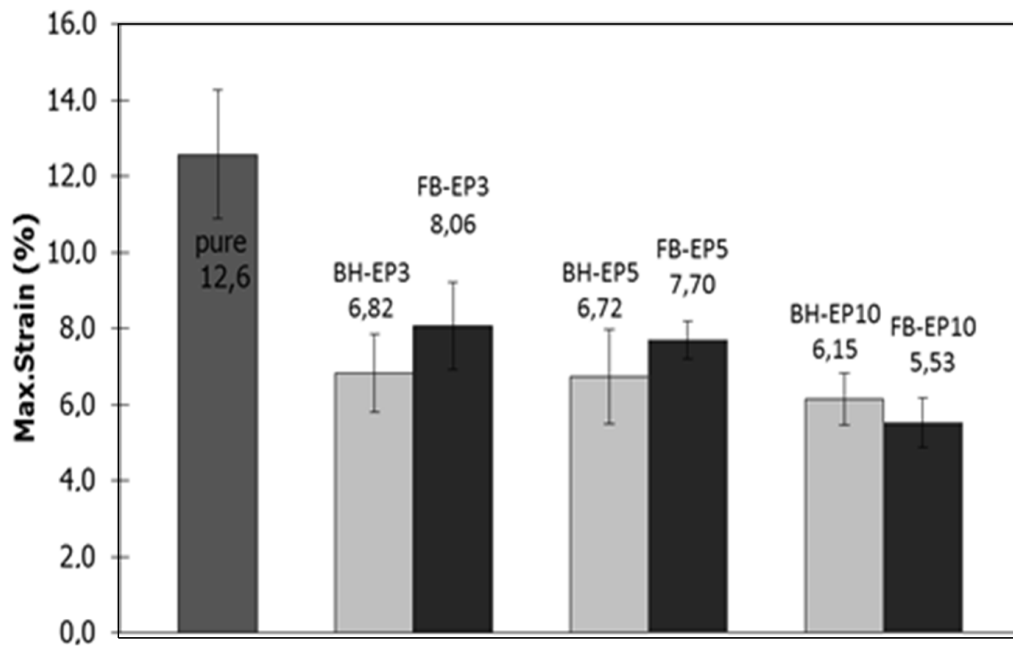
Figure 4. 24 Maximum strain at fracture for each polymer set, with respect to the weight percentage of functionalized and non-functionalized boehmite particles in the epoxy matrix**.**

Impact Test Results

Charpy impact tests are high speed fracture tests measuring the energy to break a specimen under the test conditions provided. The specimens are deformed within a short time and therefore exposed to high strain rates. Since non-toughened epoxy resin matrices are classified as brittle materials, they exhibit a high sensitivity to notches and local inhomogeneities. The impact energy of notched specimens, for example, is generally much lower than that of un-notched specimens. This phenomenon occurs from the fact, that notches act as stress concentrators, and most of the deformation takes place in the neighborhood of the notch tip where a higher apparent strain rate occurs in comparison to that in similar un-notched specimens. It can be stated that the same effect may be induced by particle agglomerates, which

remain as stress concentrators within the matrix, if the mixing provided is not adequate. If the incorporated particles act as strong stress concentrators, the impact energy absorption quality of the epoxy matrix is expected to decrease significantly as more particles are introduced. The results of the tests are shown in figure 4.25. It should be noted at this point that the use of un-notched specimens in this study emphasizes the measurement of the energy to initiate a crack which adds to the energy required to propagate a crack through the material.
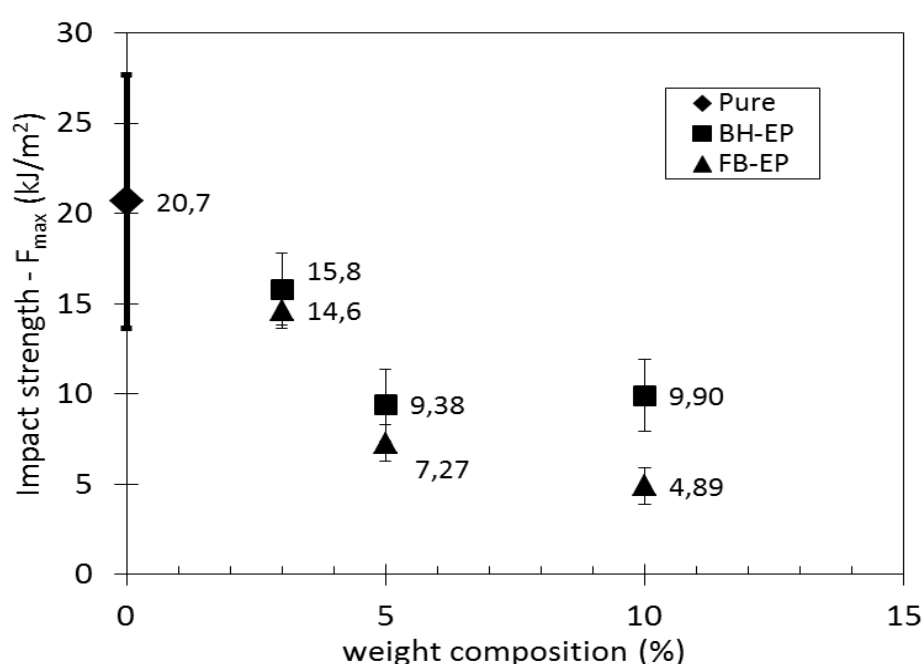
Figure 4. 25 Impact strength of each polymer set, with respect to the weight percentage of functionalized and non-functionalized boehmite particles in the epoxy matrix.

Different from the resulting trends in other mechanical tests, in impact test the epoxy-functionalized boehmite-epoxy nanocomposites show lower impact strength than the non-functionalized boehmite-epoxy nanocomposites. Opposite result were expected since the epoxy groups on the boehmite surfaces make it possible that they are incorporated into the epoxy matrix at a better degree than the non-functionalized boehmite

particles. This should diminish the stress concentration on the boehmite particles. Nevertheless, the results did not follow such trend.

Hardness Test Results

In figure 4.26, the indentation hardness test results are summarized. The tests were performed in micro scale using a Vickers indenter. As the weight percentage increases for the 3 and 5 wt.% cases, a higher hardness was recorded, while for the 10 wt.% sample in functionalized boehmite epoxy resins the effect was even higher, improving the hardness by 18% with respect to the pure resin. In the non-functionalized boehmite composite tests, the hardness declined from 243 to 127 MPa or by 47%.

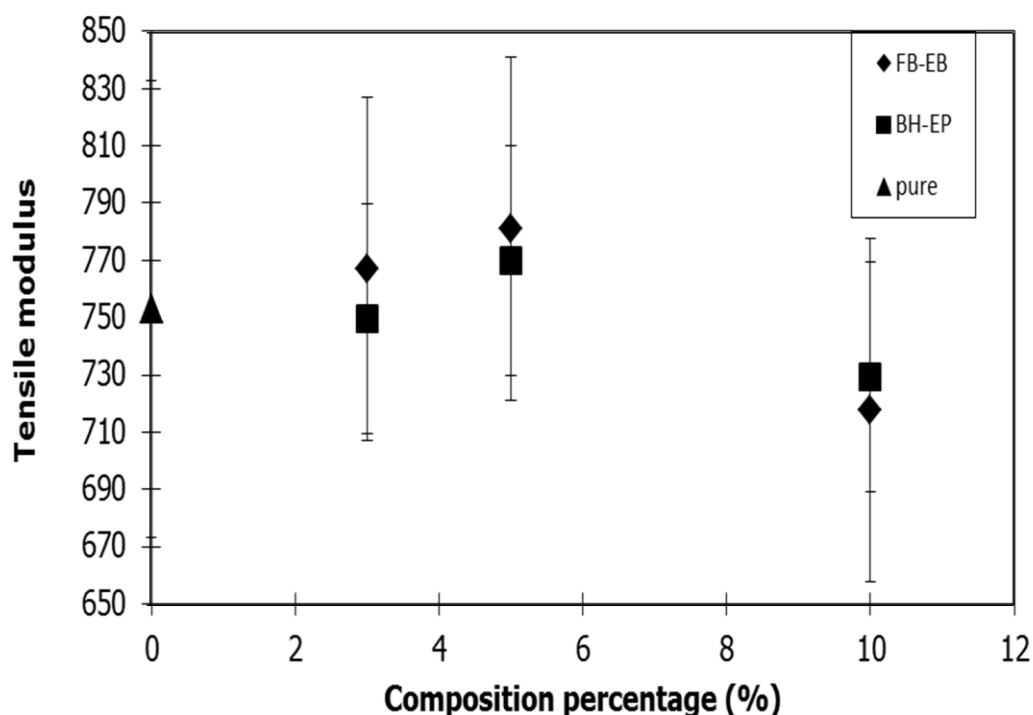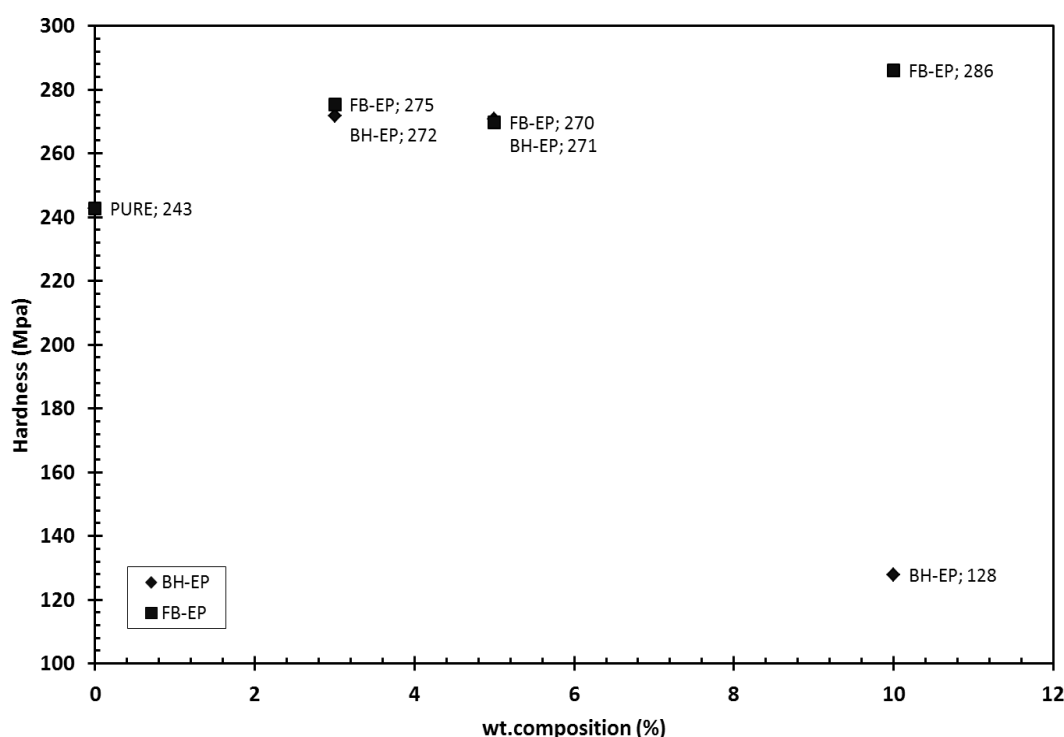**Figure 4.26** Hardness test results for each polymer set, with respect to the weight percentage of functionalized and non-functionalized boehmite particles in the epoxy matrix.

Scratch Resistance Results

The scratch resistance of the composites was also investigated. The residual depth and penetration depth profiles are presented in Appendix A6 for each set of polymers. The maximum depth for both residual and penetration depth are tabulated in table 4.5.

Table 4.5 Maximum residual depth for penetration $P_{d,max}$ and residual depth $R_{d,max}$ from the scratch test results of each set of polymers.

	$P_{d,max}$ (μm)	$R_{d,max}$ (μm)
PURE	128	25
BH-EP3	128	38
FB-EP3	72	20
BH-EP5	71	27
FB-EP5	133	20
BH-EP10	88	42
FB-EP10	118	70

In functionalized boehmite-epoxy nanocomposites there was an obvious improvement of the scratch resistance, with a penetration depth decreasing from 128μm (in neat polymer) to 72μm in FB-EP3 samples and the residual depth decreasing from 25 to 20 μm in FB-EP5. While in non-functionalized boehmite-epoxy nanocomposites the best result was recorded for BH-EP5 set with a penetration depth decreasing from 128 to 71μm. However no improvements were observed in residual depth. On the contrary it was increased, implying a non-uniform surface of these composites due to the presence of voids and agglomerates.

Also referring to the penetration and residual depth profiles given in figures A.16-18, as the scratching load increased the penetration occurred without much disturbance as in non-functionalized boehmite-epoxy polymers, in which the scratch resistance is much lower regarding the penetration depth as a factor. In figures A.19-21 disturbances in the depth profiles were observed, which is due to the voids and agglomerated particles on the surfaces of these nanocomposites. This could also be observed in the pictures taken from the tests in figure 4.27, in which the penetration profiles are shown.

| Pure | BH-EP3 | FB-EP3 | BH-EP5 | FB-EP5 | BH-EP10 | FB-EP10 |
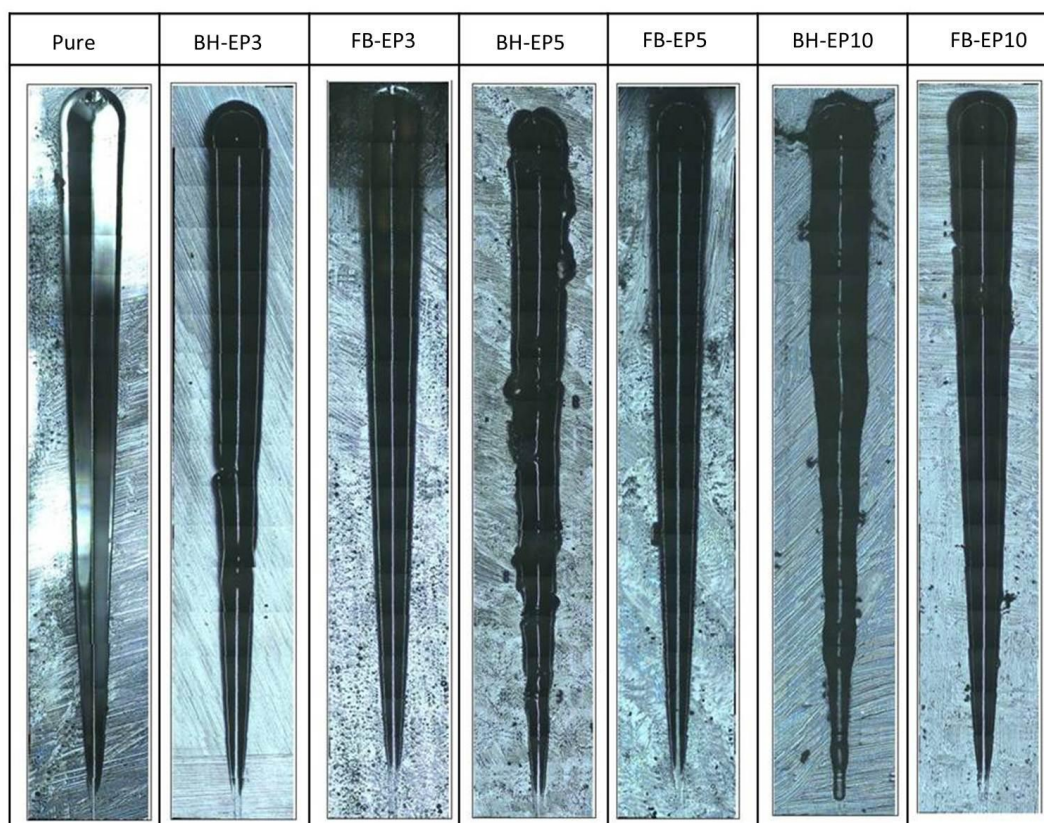
Figure 4.27 Images of scratch analysis, showing the scratch track for the different sets of polymers.

There was a significant difference in the penetration profiles between the non-functionalized and functionalized nanocomposites. Two trends were obtained. The first was the difference between functionalized and non-functionalized systems. The scratch track in functionalized nanocomposites was more uniform and not disturbed as in the non-functionalized boehmite-polymer samples. This also shows the adaptability of the functionalized boehmite particle to the polymer matrix, while this was not the case for the non-functionalized particles. The later showed very clearly aggregation phenomena instead of a close interaction with the polymer network and leaving space for void formations. The second trend was the decrease in quality of the samples as the weight ratio increased. Better profiles were observed in the lower weight ratios, with less interruption and more uniformity while in higher weight ratios these properties seemed to get worse.

CHAPTER V

CONCLUSIONS

1. In this study, nanoscale boehmite powders were produced via hydrothermal process from the raw material aluminum trihydroxide, $Al(OH)_3$ which can be locally supplied from Seydişehir Alüminyum factory for future studies.

2. In order to prevent agglomeration and obtain a uniform size distribution, the raw material was initially ground in a high energy ball mill without risking contamination of the feed.

3. Different from other researchers conducted in the same area, a two-step ageing process was developed. In the first stage the pH of medium was controlled by ammonia and acetic acid, under periodic ultrasonic mixing and ambient conditions. Different morphologies were obtained depending on the final pH attained in first ageing stage. Starting with an acidic media, needle-like morphologies were produced. On the other hand, an initial acidic treatment followed by a final step in basic media lead to hexagonal nanoplatelets with dimensions ranging from 100 to 500 nm upon hydrothermal digestion.

4. The hexagonal boehmite nanoplatelets were reacted with active epoxy monomers of bisphenol A diglycidyl ether with tin (II) chloride as catalyst. The FT-IR analysis and quantitative analysis of titration revealed that the boehmite platelets' surfaces were successfully modified.

5. In the functionalization step, effects of temperature and epoxy to boehmite weight ratio were studied. The optimum results were obtained at a reaction temperature of $80^{\circ}C$ and a weight ratio of 5:1. The inorganic/organic hybrid materials were then incorporated within epoxy/hardener resin mixture to obtain nano composites.

6. A comparative study was performed between functionalized boehmite/epoxy and non-functionalized boehmite/epoxy polymers. The nanocomposites were characterized with DMA, SEM, Hardness, micro scratch resistance, tensile test, impact test analyses.

7. The SEM analysis revealed that the functionalized boehmite-polymers were dispersed better when compared to its non-functionalized homologues which displayed agglomeration of the particles and an excessive degree of voids in the polymer matrix.

8. There was a distinct trend between the functionalized and non-functionalized boehmite-epoxy polymers, with the functionalized polymers showing better properties in most of the tests and analysis performed.

9. DMA analysis results revealed an improved glass transition temperature in the nanocomposites as well as in storage and loss modulus.

10. Hardness and scratch resistance tests showed an improvement of the hardness and scratch resistance of the functionalized boehmite/epoxy polymers in comparison to the neat polymer and the non-functionalized nanocomposites, which in turn showed a deterioration of these properties.

CHAPTER VI

RECOMMENDATIONS

1. In future studies, in hydrothermal synthesis, more parameters can be studied in order to obtain smaller nanoparticles with higher surface area to volume ratio but also with decreased agglomeration index. One can try different surface agents to prevent agglomeration and particle growth.

2. In functionalization step, in order to increase the number of epoxy functional groups, maybe a stronger ring opener catalyst can be utilized.

3. Considering the mixing order of epoxy resin, boehmite particles and hardener, the reverse sequence could have provided a higher incorporation degree of the functionalized boehmites into the epoxy resin.

4. Considering the process cycle of one sample of epoxy nanocomposite, significant time and effort is needed which requires a great deal of knowledge and analysis. This implies that the process becomes very complex and costly. Combining hydrothermal and functionalization steps in one can be recommended.

REFERENCES

1. Palucka T., Bensaude-Vincent B., *Composites Overview* , Hist. Recent.Sci. Technol., 2002.

2. Özdilek C.,Kazimierczak K., Van der Beek D., Picken S. J., *Preparation and properties of polyamide-6-boehmite nanocomposites*, Polymer, 45(15), 2004, pp. 5207-5214.

3. Corcione E., Frigione M., Maffezzoli A., Malucelli G., *Photo - DSC and real time - FT-IR kinetic study of a UV curable epoxy resin containing o-Boehmites*, Eur.Polym. J., 44(7), 2008, pp. 2010-2023.

4. Pawlowski, K.H., Schartel B. F., Mario A., Jäger Ch., *Flame retardancy mechanisms of bisphenol A bis(diphenyl phosphate) in combination with zinc borate in bisphenol A polycarbonate/acrylonitrile-butadiene-styrene blend,* Thermochim. Acta, 498(1-2), 2010, pp. 92-99.

5. Vogelson C.T., Koide, Alemany Y., Barron L. B., Andrew R., *Inorganic-organic hybrid and composite resin materials using carboxylate-alumoxanes as functionalized cross-linking agents*, Chem. Mater., 12(3), 2000, pp. 795-804.

6. Chen Q.,Udomsangpetch C., Shen S. C., Liu Y. C., Chen Z., Zeng X. T.., *The effect of AlOOH boehmite nanorods on mechanical property of hybrid composite coatings*, Thin Solid Films, 517(17), 2009, pp. 4871-4874.

7. Halbach, T.S., Mülhaupt, R., *Boehmite-based polyethylene nanocomposites prepared by in-situ polymerization*, Polymer, 49(4), 2008, pp. 867-876.

8. Florjańczyk Z.,Dębowski M., Wolak A., Malesa M., Płecha J., *Dispersions of organically modified boehmite particles and a carboxylated styrene–butadiene latix: A simple way to nanocomposites*, J. Appl.Polym. Sci., 105(1), 2007, pp. 80-88.

9. Ramos-Gallardo A., Vegas A., *The cation array in aluminum oxides, hydroxides and oxihydroxides. Zeitschrift für Kristallographie*, 211(5), 1996, pp. 299-303.

10. Christoph G. G.,Corbato Ch. E., Hofmann D. A.,Tettenhorst R.T., *Crystal structure of boehmite*, Clays Clay Miner., 27(2), 1979, pp. 81-86.

11. Milligan W.O., McAtee J.L., *Crystal structure of γ-AlOOH and γ-ScOOH*, J. Phys. Chem., 60(3), 1956, pp. 273-277.

12. Zeng W.M., Gao L., Guo J.K., *A new sol-gel route using inorganic salt for synthesizing Al2O3 nanopowders,* Nanostruct. Mat., 10(4), 1998, pp. 543-550.

13. Prodromou K.P. , Pavlatou-Ve A.S., *Formation of aluminum hydroxides as influenced by aluminum salts and bases*, Clays Clay Miner., 43(1), 1995, pp. 111-115.

14. Morgado E., Lam Y.L., Nazar L.F., *Formation of Peptizable Boehmites by Hydrolysis of Aluminum Nitrate in Aqueous Solution*, J. Colloid Interface Sci., 188(2), 1997, pp. 257-269.

15. Sato T., Sato K., *Preparation of gelatinous aluminium hydroxide from aqueous solutions of aluminium salts containing sulphate group with alkali*, J. Ceram. Soc. Jpn., 104(5), 1996, pp. 377-382.

16. Mishra D., Anand S., Panda, R. ., Das, R. P.., *Hydrothermal preparation andcharacterization of boehmites*, Mater. Lett., 42(1-2), 2000, pp. 38-45.

17. Bugosh J., *Colloidal alumia—The chemistry and morphology of colloidal boehmite*, J. Phys. Chem., 65(10), 1961, pp. 1789-1793.

18. Vallet-Regí M., Rodrígue-Lorenzo L. M.,Ragel C. V.,Salinas A. J., González-Calbet J. M., *Control of structural type and particle size in alumina synthesized by the spray pyrolysis method*, Solid State Ionics, 101-103, 1997, pp. 197-203.

19. Mathieu, Y., Lebeau, B.Valtchev, V., *Control of the morphology and particle size of boehmite nanoparticles synthesized under hydrothermal Cconditions*, Langmuir, 23(18), 2007, pp. 9435-9442.

20. Tsuchida, T., *Hydrothermal synthesis of submicrometer crystals of boehmite*, J. Eur. Ceram. Soc., 20(11), 2000, pp. 1759-1764.

21. Hakuta Y.,Ura H., Hayashi H., Arai K., *Effects of hydrothermal synthetic conditions on the particle size of [gamma]-AlO(OH) in sub and supercritical water using a flow reaction system*, Mater. Chem. Phys., 93, 2005, pp. 466-472.

22. Mousavand T., Ohara S.,Umetsu M., Zhang J., Takami S., Naka T., Adschiri T., *Hydrothermal synthesis and in situ surface modification of boehmite nanoparticles in supercritical water*, J. Supercrit. Fluids, 40(3), 2007, pp. 397-401.

23. Kannan, T.S., Panda, P.K., Jaleel, V.A., *Preparation of pure boehmite, alpha-Al_2O_3 and their mixtures by hydrothermal oxidation of aluminium metal*, J. Mater. Sci. Lett., 16(10), 1997, pp. 830-834.

24. Music, S., Dragcevic, D. and Popovic, S., *Hydrothermal crystallization of boehmite from freshly precipitated aluminium hydroxide*, Mater. Lett., 40(6), 1999, pp. 269-274.

25. Liu Y., Ma D., Han X., Bao X., Frandsen W., Wang D., Su D., *Hydrothermal synthesis of microscale boehmite and gamma nanoleaves alumina,* Mater. Lett., 62(8-9), 2008, pp. 1297-1301.

26. Liu Y., Li X., Xu Zh., Hu Zh., *Preparation of flower-like and rod-like boehmite via a hydrothermal route in a buffer solution*, J. Phys. Chem. Solids, 71(3), 2010, pp. 206-209.

27. Yanagisawa K., Gushi D., Onda A., Kajiyoshi K., *Hydrothermal synthesis of boehmite plate crystals,* J. Ceram. Soc. Jpn., 115(1348), 2007, pp. 894-897.

28. Buining P.A., Pathmamanoharan, Ch., Bosboom, M., Jansen J., Ben H.L., Hendrik N. W., *Effect of hydrothermal conditions on the morphology of colloidal boehmite particles: implications for fibril formation and monodispersity,* J. Am. Ceram. Soc., 73(8), 1990, pp. 2385-2390.

29. Bokhimi X., Toledo-Antonio J. A., Guzmán-Castillo M. L., Mar-Mar B., Hernández-Beltrán F., Navarrete J., *Dependence of boehmite thermal evolution on its atom bond lengths and crystallite size*, Journal of Solid State Chemistry, 161(2): p. 319-326.

30. Hamerton, Howlin, I., B.J., Jepson, P., *Metals and coordination compounds as modifiers for epoxy resins*, Coord. Chem. Rev., 224, 2002, pp. 67-85.

31. Segal, D., *Chemical synthesis of ceramic materials*, J. Mater. Chem., 7(8), 1997, pp. 1297-1305.

32. Chen, X. Y. , *Huh, H.S., Lee, S.W., Hydrothermal synthesis of boehmite (γ-AlOOH) nanoplatelets and nanowires: pH-controlled morphologies*, Nanotechnol., 18(28), 2007,p. 285608.

33. Sterte, J.P., Otterstedt, J.E., *A study on the preparation and properties of fibrillar boehmite*, Mater. Res. Bull., 21(10), 1986, pp. 1159-1166.

34. Zhu H.Y., Gao X. P., Song D. Y., Ringer S. P., Xi Y. X., Frost R. L., *Manipulating the size and morphology of aluminum hydrous oxide nanoparticles by soft-chemistry approaches*, Microporous Mesoporous Mater., 85(3), 2005, pp. 226-233.

35. Okada K., Nagashima T., Kameshima Y., Yasumori A., Tsukada T., *Relationship between formation conditions, properties, and crystallite size of boehmite*, J. Colloid Interface Sci., 253(2), 2002, pp. 308-314.

36. Suryanarayana, C., *Mechanical alloying and milling,*Prog. Mater Sci., 46(1-2), 2001, pp. 1-184.

37. Huang, B., Ishihara, K.N., Shingu, P.H., *Metastable phases of Al-Fe system by mechanical alloying*, Mater. Sci. Eng., A, 231, 1997, pp. 72-79.

38. Wolski K., Caër G. L., Delcroix P., Fillit R., Thévenot F., Coze J. Le., Influence of milling conditions on the FeAl intermetallic formation by mechanical alloying, Mater. Sci. Eng., A, 207(1), 1996, pp. 97-104.

39. Suryanarayana, C., Froes F.H., *Nanocrystalline titanium-magnesium alloys through mechanical alloying*, J. Mater. Res., 5(9), 1990, pp. 1880-1886.

40. Lu L., Lai M.O., Ng C.W., *Enhanced mechanical properties of an Al based metal matrix composite prepared using mechanical alloying*, Mater. Sci. Eng., A, 252(2), 1998, pp. 203-211.

41. Froyen L.,Delaey L., Niu X. P., Le Brun P., Peytour C., *Synthesizing aluminum alloys by double mechanical alloying*, JOM, 47(3), 1995, pp. 16-19.

42. Sezgiker, K., *Production of nano alumoxane from aluminum hydroxide*, Master thesis, Chemical Engineering Department, Middle East Technical University: Ankara, Turkey, 2010.

43. Lan T., Pinnavaia T.J., *Clay-reinforced epoxy nanocomposites,* Chem. Mater., 6(12), 1994, pp. 2216-2219.

44. Giannelis E.P., *Polymer layered silicate nanocomposites*, Adv. Mater., 8(1), 1996, pp. 29-35.

45. Tan F., Qiao X., Chen J., Wang H., *Effects of coupling agents on the properties of epoxy-based electrically conductive adhesives,* Int. J. Adhes. Adhes., 26(6), 2006, pp. 406-413.

46. Rong M., Zhang M., Liu, H., Zeng H., *Synthesis of silver nanoparticles and their self-organization behavior in epoxy resin*, Polymer, 40(22), 1999, pp. 6169-6178.

47. Tee D.I., Mariatti M., Azizan A., See C. H., Chong K. F., *Effect of silane-based coupling agent on the properties of silver nanoparticles filled epoxy composites*, Compos. Sci. Technol., 67(11-12), 2007, pp. 2584-2591.

48. Bajaj P., N.K. Jha, Kumar R.A., *Effect of coupling agents on the mechanical-properties of mica epoxy and glass-fiber mica epoxy composites*, J. Appl. Polym. Sci., 44(11), 1992, pp. 1921-1930.

49. Shukla, D.K., Kasisomayajula, S.V., Parameswaran, V*., Epoxy composites using functionalized alumina platelets as reinforcements*, Compos. Sci. Technol., 68(14), 2008, pp. 3055-3063.

50. Callender R.L., Harlan C. J.,, Shapiro N. M., Jones Ch. D., Callahan D. L., Wiesner M. R., MacQueen D. B., Cook R., Barron A. R., *Aqueous synthesis of water-soluble alumoxanes: environmentally benign precursors to alumina and aluminum-based ceramics,* Chem. Mater., 9(11), 1997, pp. 2418-2433.

51. Bauer F., Ernst H., Decker U., Findeisen M., Gläsel H.J., Langguth H., Hartmann E., Mehnert R., Peuker Ch., *Preparation of scratch and abrasion resistant polymeric nanocomposites by monomer grafting onto nanoparticles-FTIR and multi-nuclear NMR spectroscopy to the characterization of methacryl grafting*, Macromol. Chem. Phys., 201(18), 2000, pp. 2654-2659.

52. Kang S., Hong S., IlCh., Chul R., Park M., Rim S., Kim J., *Preparation and characterization of epoxy composites filled with functionalized nanosilica particles obtained via sol-gel process*, Polymer, 42(3),2001, pp. 879-887.

53. Ying-Ling, L., *A novel approach of chemical functionalization on nano-scaled silica particles*, Nanotechnol., 14(7), 2003, pp. 813.

54. Augustsson, C., *NM Epoxy Handbook*, 3rd ed., N.M. AB, 2004.

55. Shechter, L. and J. Wynstra, *Glycidyl ether reactions with alcohols, phenols, carboxylic acids, and acid anhydrides*,Ind. Eng. Chem., 48(1), 1956, pp. 86-93.

56. Messersmith, P.B. , Giannelis, E.P., *Synthesis and characterization of layered silicate-epoxy nanocomposites*, Chem. Mater., 6(10), 1994, pp. 1719-1725.

57. Yano K.,Usuki A., Okada A., Kurauchi T., Kamigaito O., *Synthesis and properties of polyimide–clay hybrid*, J. Polym. Sci., Part A: Polym. Chem., 31(10), 1993, pp. 2493-2498.

58. Bécu-Longuet L., Bonnet A., Pichot C., Sautereau H., Maazouz A., *Epoxy networks toughened by core–Shell particles: Influence of the particle structure and size on the rheological and mechanical properties*, J. Appl. Polym. Sci., 72(6), 1999, pp. 849-858.

59. Harani, H., Fellahi, S., Bakar., *Toughening of epoxy resin using hydroxyl-terminated polyesters*, J. Appl. Polym. Sci., 71(1), 1999, pp. 29-38.

60. Daniel I., Miyagawa H., Gdoutos E., Luo J., *Processing and characterization of epoxy/clay nanocomposites*, Exp. Mech., 43(3), 2003, pp. 348-354.

61. GojnyF.H., Wichmann M.H.G., Köpke U., Fiedler B., Schulte K., *Carbon nanotube-reinforced epoxy-composites: Enhanced stiffness and fracture toughness at low nanotube content*, Compos. Sci. Technol., 64(15 SPEC. ISS.), 2004, pp. 2363-2371.

62. Shahid N., Villate R.G., Barron A.R., *Chemically functionalized alumina nanoparticle effect on carbon fiber/epoxy composites*, Compos. Sci. Technol., 65(14), 2005, pp. 2250-2258.

63. Yusoff R., Aroua M.K., Nesbitt A., Day R.J., *Curing of polymeric composites using microwave resin transfer moulding (rtm)*, J. Eng. Sci. Technol., 2(2), 2007, pp.151-163.

64. Lee H., Neville K., *Expoxy Resins*, New York, McGraw-Hill Book Co., 1957.

65. ASTM D638, Standard Test Method for Tensile Properties of Plastics, 2003.

66. Wolfang Grellman, S.S., *Polymer Testing*, Hanser Gardnes Pubns, 2007.

67. Liu, H., Hu J., Xu J., Liu Z., Shu J., Mao H. K., Chen J., *Phase transition and compression behavior of gibbsite under high-pressure*, Phys. Chem. Miner., 31(4), 2004, pp. 240-246.

68. Bhattacharya I.N., Das S.C., Mukherjee P.S., Paul S., Mıtra P.K., *Thermal decomposition of precipitated fine aluminium trihydroxide,* Scand. J. Metall., 33(4), 2004, pp. 211-219.

69. Ruan H.D., Frost R.L. , Kloprogge J.T., *Comparison of Raman spectra in characterizing gibbsite, bayerite, diaspore and boehmite*, J. Raman Spectrosc., 32(9), 2001, pp. 745-750.

70. Wang, S.-L., *Water-vapor adsorption and surface area measurement of poorly crystalline boehmite*, J. Colloid Interface Sci., 260(1), 2003, pp. 26-35.

71. Dickie, S.A. and A.J. McQuillan, *In-situ infrared spectroscopic studies of adsorption processes on boehmite particle films: exchange of surface hydroxyl groups observed upon chelation by acetylacetone*, Langmuir, 20(26), 2004, pp. 11630-11636.

72. Christoph G.G.,Hofmann Ch., Douglas A., , Tettenhorst R. T., *The crystal structure of boehmite*, Clays Clay Miner., 27(2),1979, pp. 81-86.

73. Wolff D., Schlothauer K., Tänzer W., Fedtke M., Spevacek J., *Determination of network structure in butane-1,4-diol cured bisphenol A diglycidyl ether using 13C CP-MAS n.m.r. and i.r. spectroscopy*, Polymer, 32(11), 1991, pp. 1957-1960.

74. Li L., Wu Q., Li Sh., Wu P., *Study of the infrared spectral features of an epoxy curing mechanism*, Appl. Spectrosc., 62, 2008, pp. 1129-1136.

75. Colthup N.B., *Introduction to Infrared and Raman Spectroscopy*, New York, Academic Press, 1975.

76. Boerio F.J., Chen S.L, *Reflection-absorption infrared spectroscopy and ellipsometry of epoxy films on metals*, Appl. Spectrosc., 33, 1979, pp. 121-126.

77. Matsuura H., Yoshida H., *Calculation of Vibrational Frequencies by Hartree–Fock-Based and Density Functional Theory*, Handbook of Vibrational Spectroscopy, 2006.

78. Poisson N., Lachenal G., Sautereau, H., *Near- and mid-infrared spectroscopy studies of an epoxy reactive system*, Vib. Spectrosc., 12(2), 1996, pp. 237-247.

79. Walker F.H.,Dickenson J.B.H., Charles R.P., Frank R., *Cationic polymerization of emulsified epoxy resins*,Prog. Org. Coat., 45(2-3), 2002, pp. 291-303.

80. Chike K. E., *Raman and near-infrared studies of an epoxy resin*, Appl. Spectrosc., 47, 1993, pp. 1631-1635.

81. Mijovic J., Andjelic S., *Monitoring of reactive processing by remote mid infra-red spectroscopy*, Polymer, 37(8), 1996, pp. 1295-1303.

82. Choi J., Yee A.F., Laine R.M., *Organic/inorganic hybrid composites from cubic silsesquioxanes. epoxy resins of octa (dimethylsiloxyethylcyclohexylepoxide) silsesquioxane*, Macromolecules, 36(15), 2003, pp. 5666-5682.

83. Wu C.S., Liu Y.L., Chiu Y.S., *Epoxy resins possessing flame retardant elements from silicon incorporated epoxy compounds cured with phosphorus or nitrogen containing curing agents*, Polymer, 43(15), 2002, pp. 4277-4284.

84. Landel, R. F.,Nielsen, L.E., *Mechanical Properties of Polymers and Composites*, 2nd ed., CRC Press, 1993.

85. Pham, H.Q., Marks, M.J., *Epoxy Resins*, Encyclopedia of Polymer Science and Technology , John Wiley & Sons, 2002.

RESULTS

A.1 XRD test results

Table A.1 XRD data for the raw ATH and ground ATH powders with i-POH.

ATH powders (raw)			ATH fine powders (ground)		
°2θ	hkl	Intensity (%)	°2θ	hkl	Intensity (%)
18.38	002	100.0	18.4	002	100.0
20.36	110	25.9	20.38	110	15.9
20.60	200	13.5	20.56	200	8.3
26.90	112	9.2	26.94	112	5.2
36.68	021	15.1	36.68	021	10.4
37.12	311	7.0	37.16	311	8.4
37.74	213	21.7	37.74	213	11.7
44.20	313	19.6	44.24	313	9.7
50.58	314	16.0	50.6	314	8.5
52.24	024	17.3	52.2	024	8.7

Table A.2 XRD data for boehmite crystals produced by hydrothermal process for 5 and 7.5 hr as a reaction time.

HT5 (5hr operation)			HT6 (7.5 hr operation)		
°2θ	hkl	Intensity (%)	°2θ	hkl	Intensity (%)
14.56	020	94.4	14.52	020	87.7
28.22	120	92.6	28.20	120	88.6
38.38	140/031	100.0	38.38	140/031	100.0
45.82	131	13.0	45.76	131	13.1
48.96	051/200	94.0	48.96	051/200	95.6
51.56	220	19.1	51.56	220	17.7
55.2	151	34.9	55.22	151	35.6
60.6	080	16.1	60.60	080	17.4
64.06	231	40.9	64.06	231	41.8
64.98	002	26.6	64.96	002	26.2
66.98	171/022	9.9	66.98	171/022	9.2
71.92	251	44.7	71.88	251	46.3

Table A.3 XRD data for boehmite crystals produced by hydrothermal process for 10 hr as a reaction time.

HT7 (10 hr operation)		
°2θ	Hkl	Intensity (%)
14.58	020	98.2
28.26	120	86.9
38.42	140/031	100.0
45.84	131	12.8
49.00	051/200	94.8
51.62	220	17.9
55.26	151	35.7
60.60	080	18.7
64.10	231	42.0
65.02	002	26.9
67.02	171/022	9.4
71.94	251	46.5

A.2 Titration Analysis calculations

OH content in boehmite :

Materials :

Boehmite: 2g

0.05 N NaOH sln : 80 ml

0.05N HCl solution

Procedure :

From this solution, 10 ml are neutralized with 0.05N HCl solution, V_{HCl}: 30 ml

For a blank solution of 10 ml of 0.05 N NaOH solution, the neutralization HCl volume is : 5.5 ml.

In the following calculations, normality of titrating solution is equalized to molarity, C_{HCl}, since the neutralization reaction uses one proton per molecule of HCl and according to the equation for relation between normality and molarity :

$$Normality = molarity \times n \qquad \textbf{[Eqn.18]}$$

(where n = the number of protons exchanged in a reaction)

Moles of HCl consumed during neutralization of NaOH in the blank solution:

$$mole_{HCl} = V_{HCl} \times C_{HCl} \qquad \textbf{[Eqn.19]}$$

$$mole_{HClblank} = 5.5ml \cdot \frac{1L}{1000ml} \cdot \frac{0.05mol}{L} = 2.75 \cdot 10^{-4} moles HCl$$

$$mole_{HCl} = 30ml \cdot \frac{1L}{1000ml} \cdot \frac{0.05mol}{L} = 15 \cdot 10^{-4} moles HCl$$

Moles of OH reacted in titration reaction with HCl is:

$$n_{HCl} - n_{HClblanc} = (15 - 2.75) \cdot 10^{-4} = 12.25 \cdot 10^{-4} moles OH$$

Assuming that a perfect mixing was in the NaOH solution, then for 10 ml of NaOH contained:

$$m_{boehmite = \frac{2g}{80ml} \cdot 10ml = 0.25g}$$

So for 1 g of boehmite there are:

$$n_{OH} = \frac{12.25 \cdot 10^{-4} mole}{0.25 g boehmite} = \frac{0.0049 mol OH}{g Boehmite}$$

Epoxy Content on the boehmite surface

Materials:

Pyridine: 100 ml

12.2 M HCl solution: 1.7 ml

0.05 N NaOH solution

Functionalized Boehmite powder: 1 g

Procedure:

Blanc solution titration:

100 ml of pyridine where 1.7 ml HCl is diluted of 12.2 molarity of (HCl solution)

So in 100 ml pyridine, 0.02074 mole HCl is diluted.

The blank titration consumed 194 ml of 0.05 N NaOH:

$$n_{NaOHblank} = 194ml \cdot \frac{1L}{1000ml} \cdot \frac{0.05mol}{L} = 9.7 \cdot 10^{-3} moles NaOH$$

$$n_{NaOH} = 205ml \cdot \frac{1L}{1000ml} \cdot \frac{0.05mol}{L} = 10.25 \cdot 10^{-3} moles NaOH$$

Then in one gram of boehmite powders, the epoxy group moles reacted with excess NaOH is:

$$n_{NaOH} - n_{NaOHblanc} = (10.25 - 9.7) \cdot 10^{-3} = 5.5 \cdot 10^{-4} moles epoxy group$$

A.3 DMA results

In figures A.3.1-A.3.7 are shown the dynamic mechanical analysis results for each polymer set, from the pure epoxy polymer referred as "pure" to functionalized boehmite-epoxy polymer sets referred as EP3, EP5 and EP10 according to the weight percentage of boehmite crystals. Also the non-functionalized boehmite-epoxy polymer set, referred as BH3, BH5 and BH10. In all the graphs, the storage modulus E', the loss Modulus E" and tan delta are shown.

- **Pure epoxy polymer set**
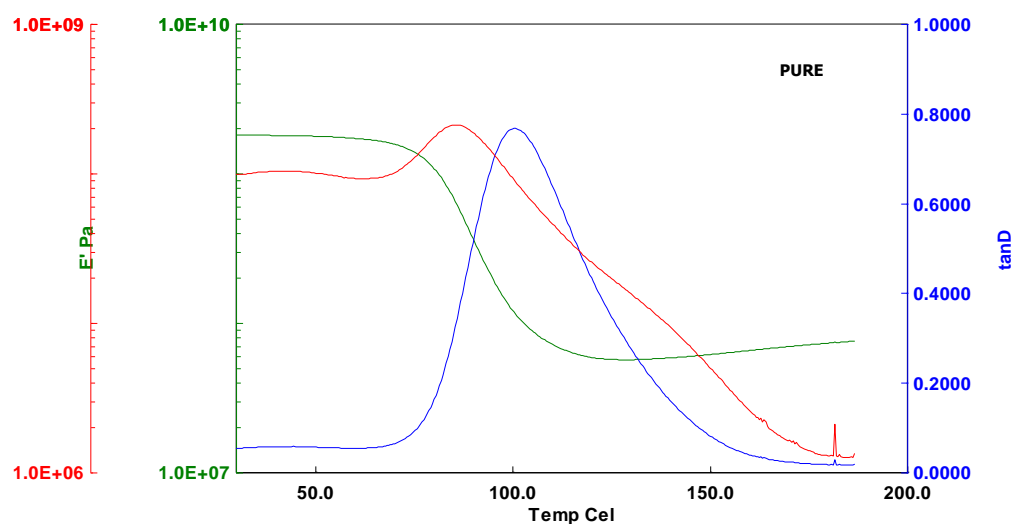
Figure A.1 Storage modulus, E', loss Modulus, E" and tan delta as a function of temperature for pure epoxy polymer set.

- **FB-EP3**

Figure A.2 Storage modulus, E', loss Modulus, E'' and tan delta as a function of temperature for 3 wt.% of epoxy functionalized boehmite-epoxy nanocomposite.

- **FB-EP5**

Figure A.3 Storage modulus, E', loss Modulus, E'' and tan delta as a function of temperature for 5wt.% of epoxy functionalized boehmite-epoxy nanocomposite.

- **FB-EP10**

Figure A.4 Storage modulus, E', loss Modulus, E'' and tan delta as a function of temperature for 10 wt.% of epoxy functionalized boehmite-epoxy nanocomposite.

- **BH-EP3**
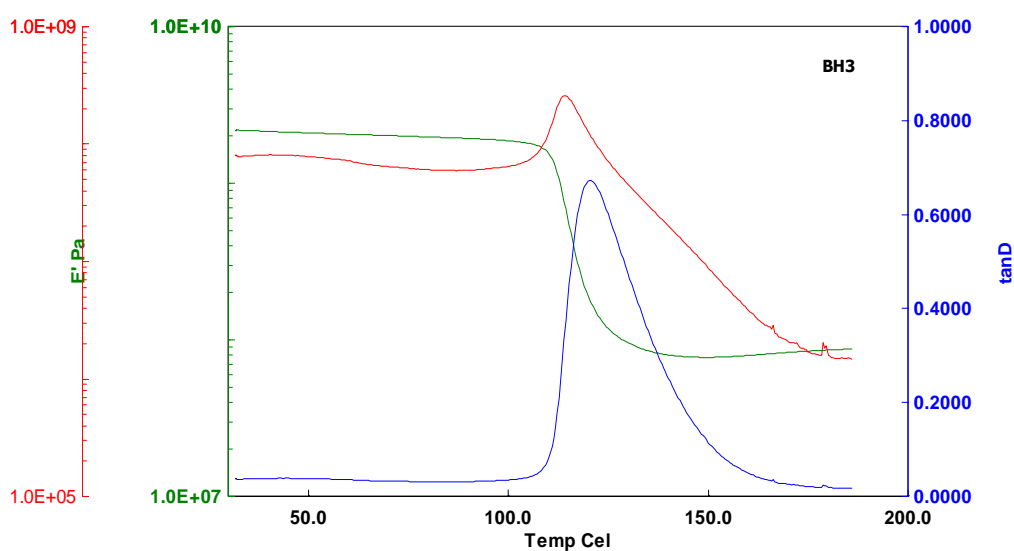
Figure A.5 Storage modulus, E', loss Modulus, E'' and tan deltaas function of temperature for 3 wt.% of non-functionalized boehmite-epoxy nanocomposite.

- **BH-EP5**
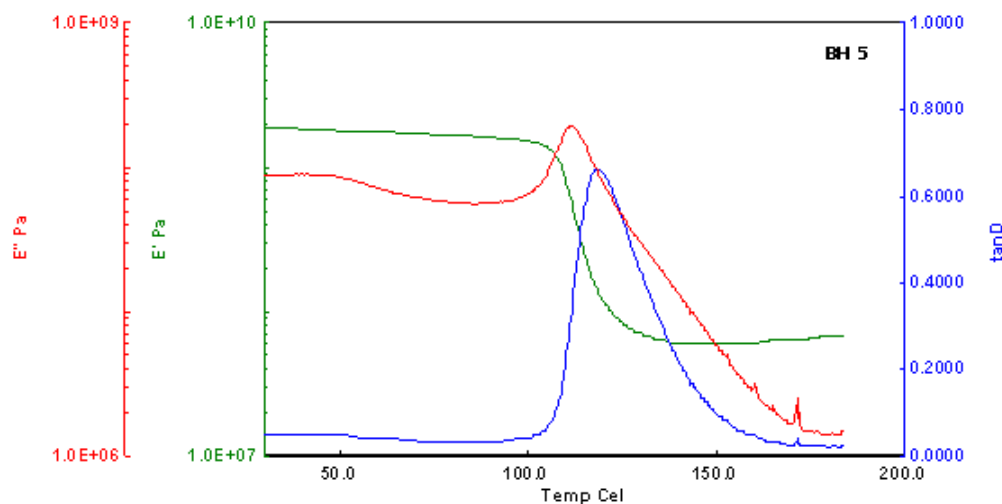
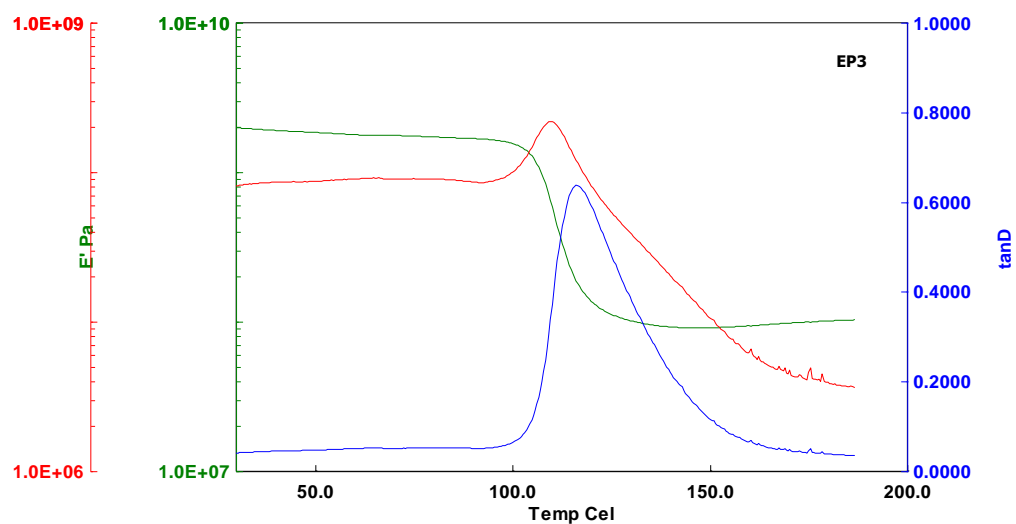**Figure A.6** Storage modulus, E', loss Modulus, E'' and tan deltaas function of temperature for 5wt.% of non-functionalized boehmite-epoxy nanocomposite.

- **BH-EP10**

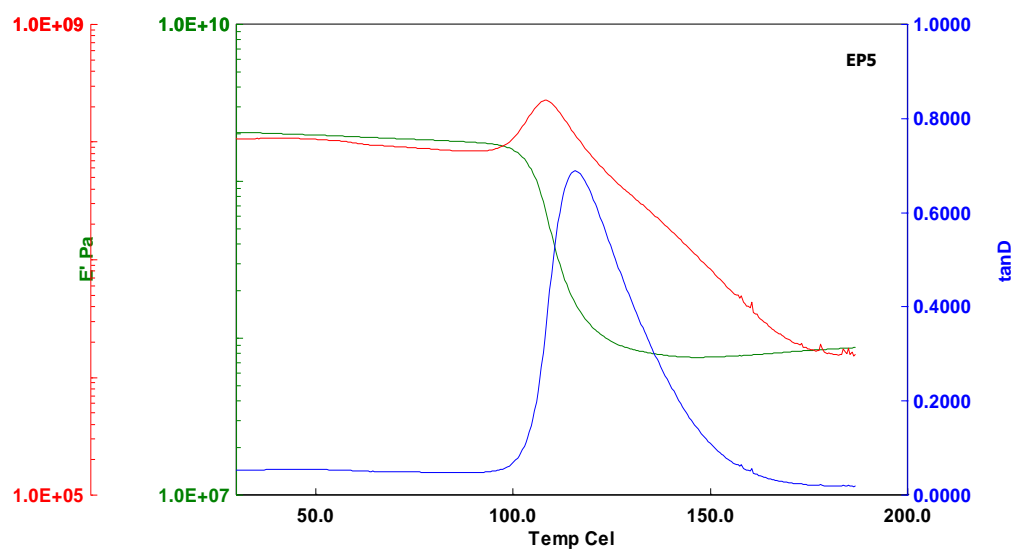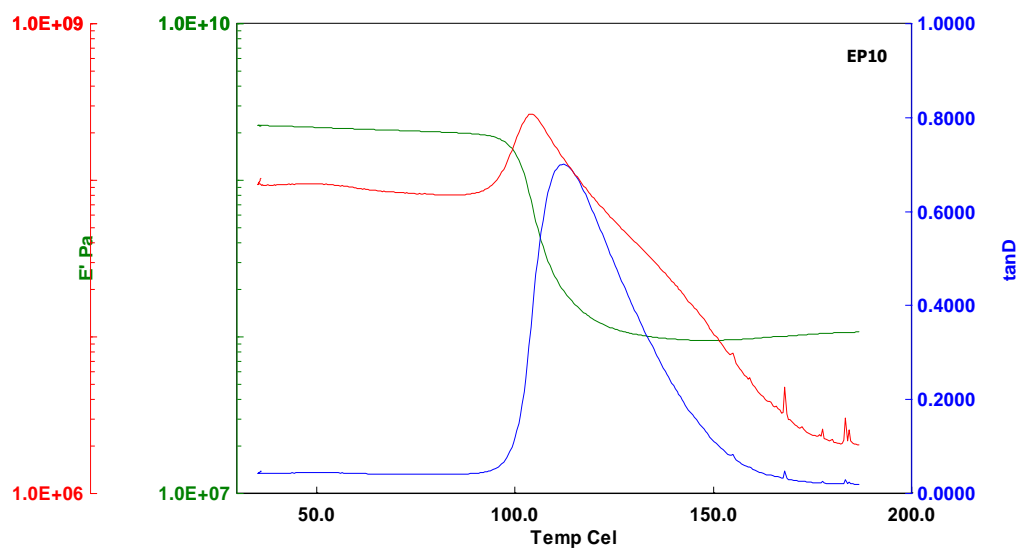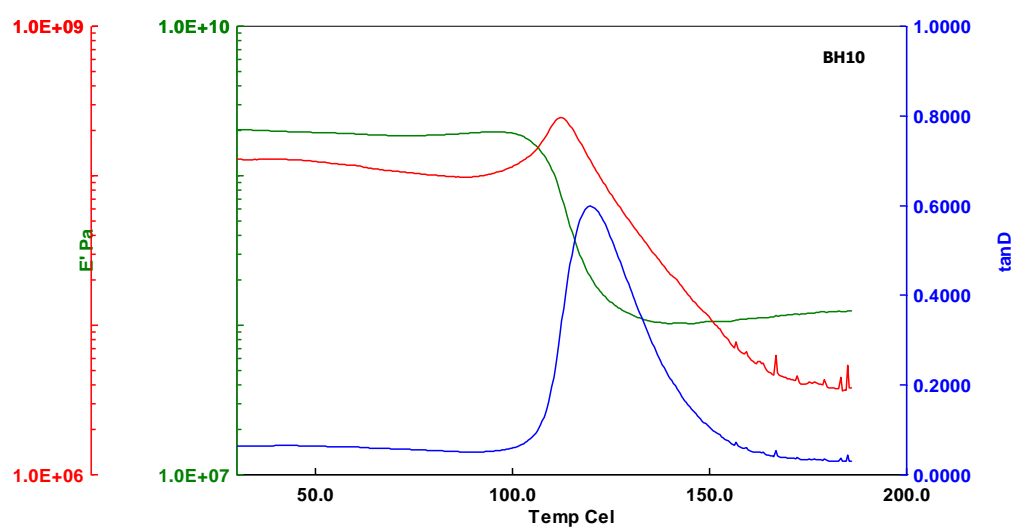**Figure A.7** Storage modulus, E', loss Modulus, E'' and tan deltaas function of temperature for 10wt.% of non-functionalized boehmite-epoxy nanocomposite.

A.4 Tensile Test Results

- **Pure**

Figure A.8 Aligned neat epoxy polymer dogbone samples after testing.

Table A.4 Tensile test results for the neat epoxy polymer.

Units	Max. Strength	Toughness	Max. Strain	Tensile Modulus
-	(MPa)	(10^6J/m^3)	(%)	(MPa)
1 - 1	63.1	2.85	14.5	743
1 - 2	62.7	2.46	10.7	831
1 - 3	62.7	2.48	10.9	841
1 - 4	61.3	2.84	13.0	645
1 - 5	69.5	3.90	13.7	704
Mean	63.9	2.91	12.6	753
Standard Deviation	3.25	0.58	1.68	83.8

- **FB-EP3**

Figure A.9   Aligned functionalized-boehmite/epoxy (3%wt) dogbone samples after testing.

Table A.5   Tensile test results for the functionalized boehmite (3%wt)/epoxy polymer.

Units	Max. Strength	Toughness	Max. Strain	Modulus
-	(MPa)	$(10^6 J/m^3)$	(%)	(MPa)
1 - 1	43.8	0.96	7.37	691
1 - 2	46.6	1.25	6.54	866
1 - 3	56.9	2.18	8.63	758
1 - 4	55.6	1.95	8.25	796
1 - 5	57.3	1.47	9.52	725
Mean	52.0	1.56	8.06	767
Standard Deviation	6.37	0.50	1.15	67.8

- **FB-EP5**

Figure A.10   Aligned functionalized-boehmite/epoxy (5%wt) dogbone samples after testing.

Table A.6 Tensile test results for the functionalized boehmite (5%wt)/epoxy polymer.

Units	Max. Strength	Toughness	Max. Strain	Modulus
-	(Mpa)	(10^6J/m^3)	(%)	(Mpa)
1 - 1	46.02	0.96	7.24	771
1 - 2	53.93	1.34	8.35	794
1 - 3	44.58	0.97	7.23	752
1 - 4	55.00	1.39	8.08	824
1 - 5	46.99	1.04	7.58	762
Mean	49.30	1.14	7.70	781
Standard Deviation	4.80	0.21	0.50	28.9

- **FB-EP10**

Figure A.11   Aligned functionalized-boehmite/epoxy (10%wt) dogbone samples after testing.

Table A.7   Tensile test results for the functionalized boehmite (10%wt) /epoxy polymer.

Units	Max. Strength	Toughness	Max. Strain	Modulus
-	(Mpa)	(10^6J/m^3)	(%)	(Mpa)
1 - 1	31.6	0.22	5.48	750
1 - 2	38.9	0.49	5.93	839
1 - 3	18.8	0.44	4.43	562
1 - 4	34.5	0.28	5.70	798
1 - 5	33.0	0.46	6.00	669
1 - 6	38.4	0.39	6.40	755
1 - 7	23.0	0.13	4.76	650
Mean	31.1	0.35	5.53	718
Standard Deviation	7.59	0.14	0.70	95.5

- **BH-EP3**

Figure A.12 Aligned non-functionalized-boehmite/epoxy (3%wt) dogbone samples after testing.

Table A.8 Tensile test results for non-functionalized boehmite (3%wt)/ epoxy polymer.

Units	Max. Strength	Toughness	Max. Strain	Modulus
-	(MPa)	(10^6J/m^3)	(%)	(MPa)
1 - 1	46.1	1.40	7.63	738
1 - 2	37.5	0.94	6.51	699
1 - 3	33.9	0.70	5.51	786
1 - 4	51.3	1.69	8.09	755
1 - 5	39.6	0.97	6.38	769
Mean	41.7	1.14	6.82	749
Standard Deviation	6.96	0.40	1.03	33.1

- **BH-EP5**

Figure A.13 Aligned non-functionalized-boehmite/epoxy (5%wt) dogbone samples after testing.

Table A.9 Tensile test results for non-functionalized boehmite (5%wt)/ epoxy polymer.

Units	Max. Strength	Toughness	Max. Strain	Modulus
-	(MPa)	(10^6J/m^3)	(%)	(MPa)
1 - 1	32.7	0.68	5.45	778
1 - 2	46.9	1.06	7.94	703
1 - 3	46.2	1.27	6.76	829
Mean	41.9	1.00	6.72	770
Standard Deviation	8.02	0.30	1.24	63.5

- **BH-EP10**

Figure A.14 Aligned non-functionalized-boehmite/epoxy (10%wt) dogbone samples after testing.

Table A.10 Tensile test results for non-functionalized boehmite (10%wt)/ epoxy polymer.

Units	Max. Strength	Toughness	Max. Strain	Modulus
-	(MPa)	$(10^6 J/m^3)$	(%)	(MPa)
1 - 1	39.4	1.07	7.11	681
1 - 2	29.5	0.62	5.58	678
1 - 3	40.3	1.03	6.54	776
1 - 4	29.5	0.57	5.08	738
1 - 5	31.2	0.42	5.97	738
1 - 6	38.7	0.94	6.17	768
1 - 7	38.3	0.67	6.60	725
Mean	35.3	0.76	6.15	729
Standard Deviation	4.94	0.25	0.68	38.2

A.5 Impact Test Results

- **Pure Epoxy polymer**

Table A.11 Impact test results for the neat epoxy polymer.

Units	Energy (J)	Impact strength (kJ/m^2)
1 - 1	1.15	30.3
1 - 2	0.651	17.1
1 - 3	0.749	19.7
1 - 4	0.440	11.6
1 - 5	0.933	24.6
Mean	0.785	20.7
Standard Deviation	0.271	7.14

- **FB-EP3**

Table A.12 Impact test results for the functionalized boehmite (3%wt)/ epoxy polymer.

Units	Energy (J)	Impact strength (kJ/m^2)
1 - 2	0.551	14.5
1 - 3	0.578	15.2
1 - 5	0.578	15.2
1 - 7	0.515	13.6
Mean	0.556	14.6
Standard Deviation	0.030	0.786

- **FB-EP5**

Table A.13 Impact test results for the functionalized boehmite (5%wt)/ epoxy polymer.

Units	Energy (J)	Impact strength (kJ/m^2)
1-1	0.371	9.76
1 - 4	0.274	7.21
1 - 5	0.304	8.00
1 - 6	0.236	6.21
1 - 9	0.197	5.18
Mean	0.276	7.27
Standard Deviation	0.066	1.75

- **FB-EP10**

Table A.14 Impact test results for the functionalized boehmite (10%wt)/ epoxy polymer.

Units	Energy (J)	Impact strength (kJ/m^2)
1-1	0.144	3.79
1 - 2	0.172	4.53
1 - 4	0.232	6.10
1 - 6	0.196	5.16
Mean	0.186	4.89
Standard Deviation	0.037	0.982

- **BH-EP3**

Table A.15   Impact test results for the non-functionalized boehmite (3%wt)/ epoxy polymer.

Units	Energy (J)	Impact strength (kJ/m^2)
1-1	0.594	15.6
1 - 2	0.498	13.1
1 - 3	0.578	15.2
1 - 4	0.573	15.1
1 - 5	0.759	19.9
Mean	0.600	15.8
Standard Deviation	0.096	2.53

- **BH-EP5**

Table A.16   Impact test results for the non-functionalized boehmite (5%wt)/ epoxy polymer.

Units	Energy (J)	Impact strength (kJ/m^2)
1 -2	0.292	9.13
1 - 4	0.362	11.3
1 - 5	0.246	7.69
Mean	0.300	9.38
Standard Deviation	0.058	1.83

- **BH-EP10**

Table A.17 Impact test results for the non-functionalized boehmite (10%wt)/ epoxy polymer.

Units	Energy (J)	Impact strength (kJ/m^2)
1-1	0.349	10.9
1 - 2	0.334	10.4
1 - 3	0.365	11.4
1 - 4	0.249	7.78
1 - 6	0.287	8.97
Mean	0.317	9.90
Standard Deviation	0.048	1.49

A.6 Scratching Test Results

In figures A6.1-7 are listed the scratch testing results for each set of polymers, precisely the graphs of penetration and residual depth profile versus the loaded force and the distance.

- **Pure**
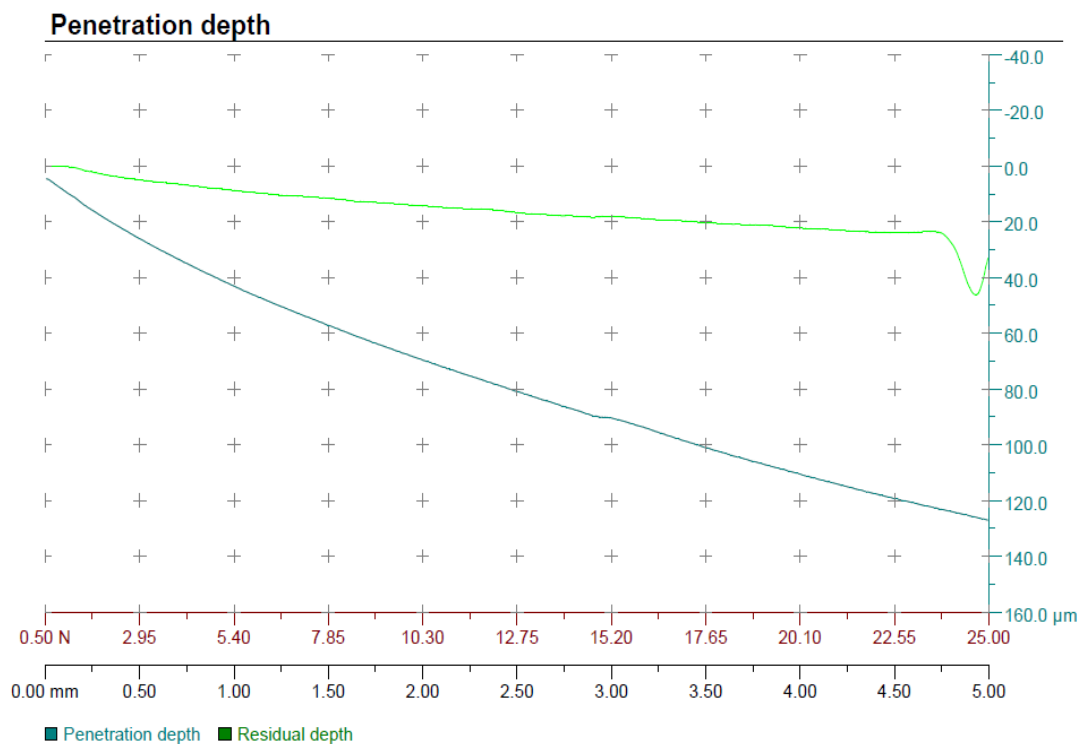
Figure A.15 Residual and penetration depth profiles with respect to the loaded force for pure epoxy polymer set.

Functionalized Boehmite- epoxy polymer set
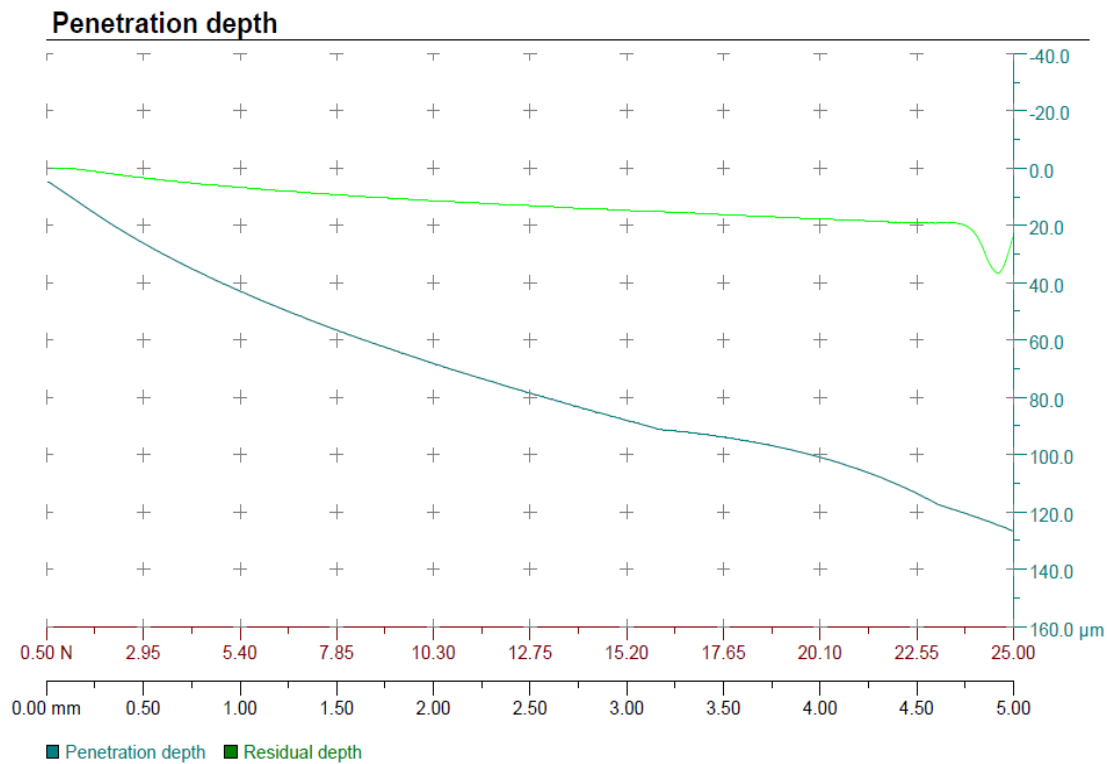
- **FB-EP3**

Figure A.16 Residual and penetration depth profiles with respect to the loaded force for 3 weight percent of epoxy functionalized boehmmite-epoxy nanocomposite.
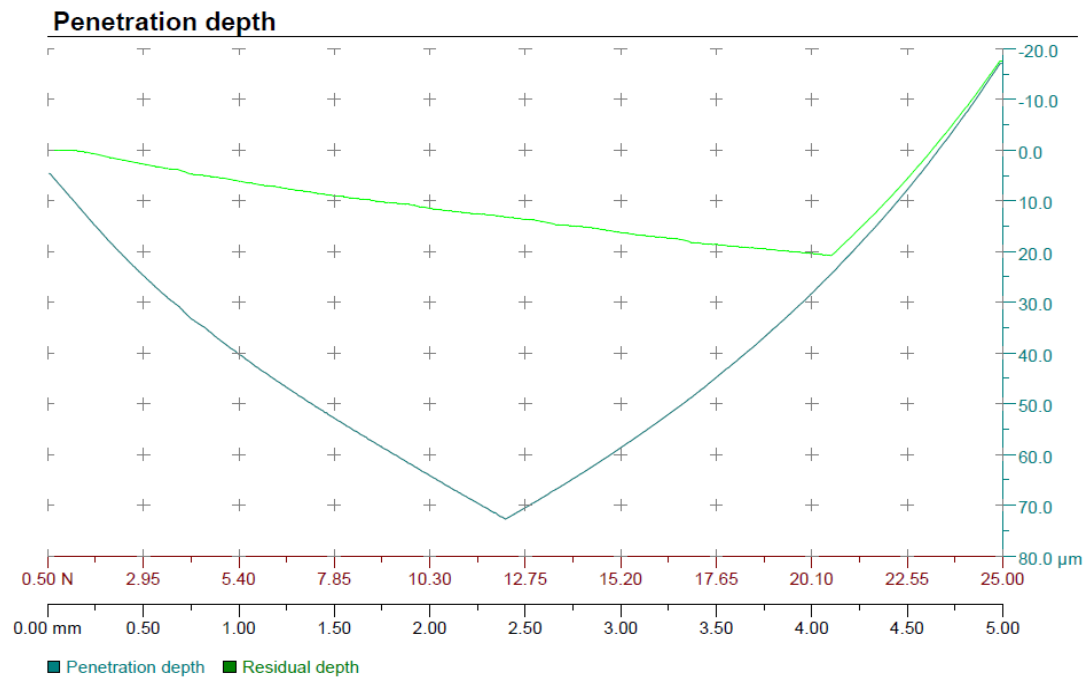
- **FB-EP5**

Figure A.17 Residual and penetration depth profiles with respect to the loaded force for 5 weight percent of epoxy functionalized boehmmite-epoxy nanocomposite.
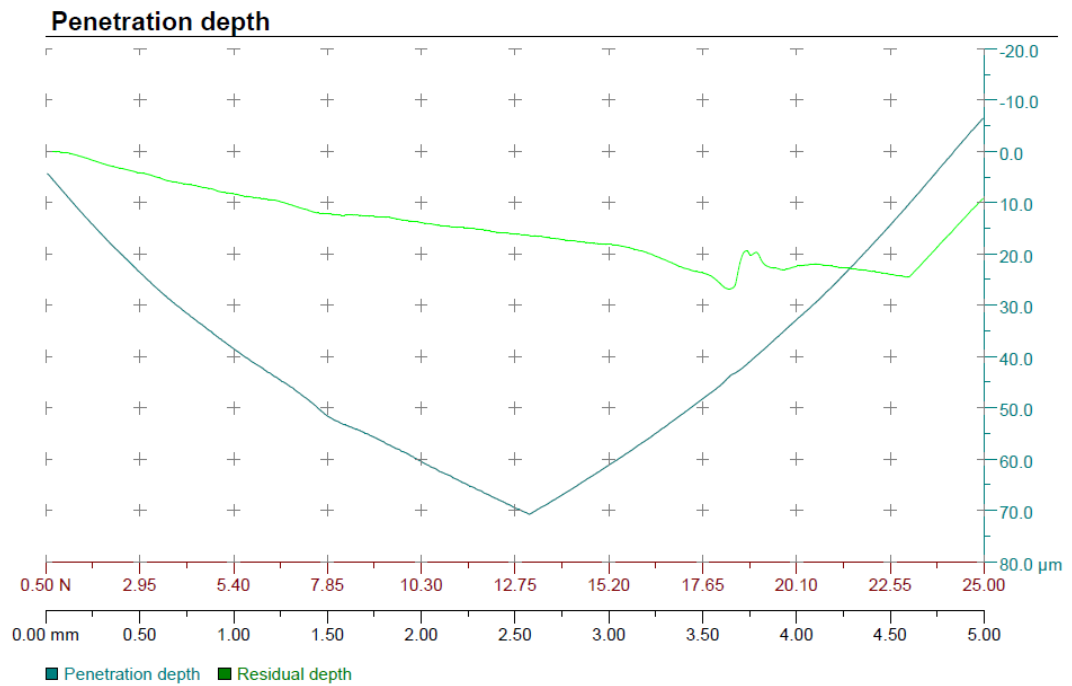
- **FB-EP10**

Figure A.18 Residual and penetration depth profiles with respect to the loaded force for 10 weight percent of epoxy functionalized boehmmite-epoxy nanocomposite.

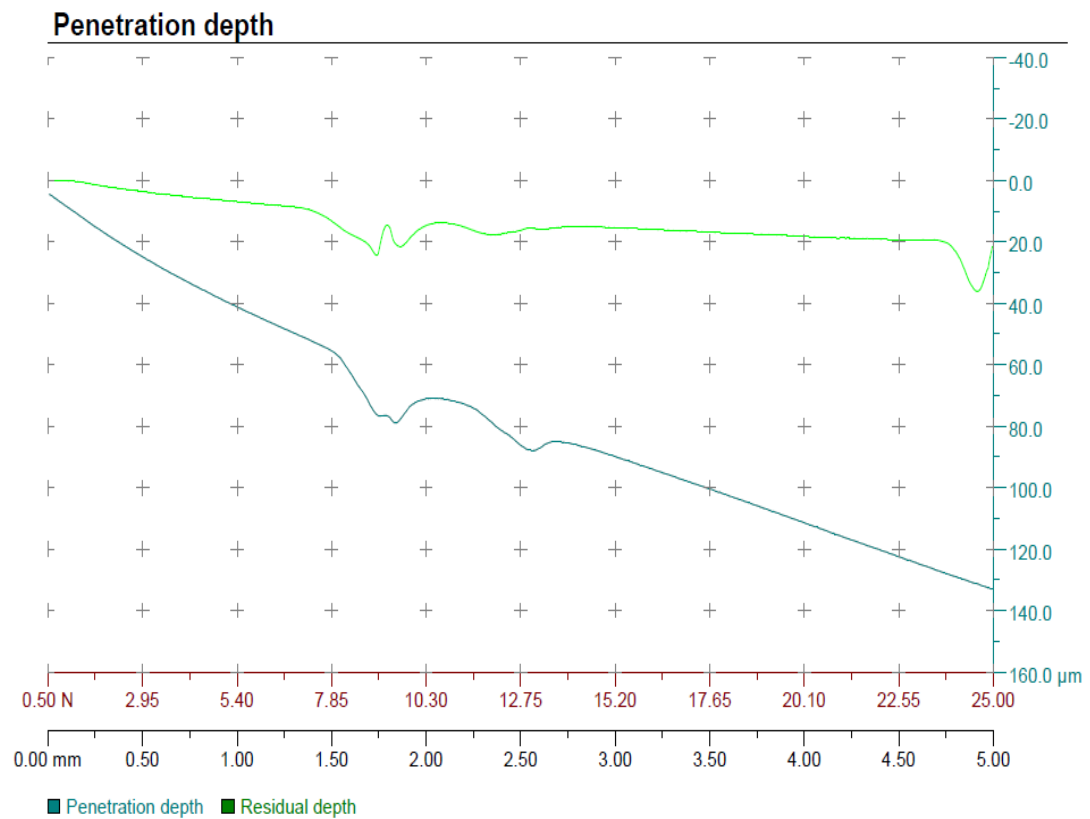**Non Functionalized Boehmite-epoxy polymer set**

- **BH-EP3**

Figure A.19 Residual and penetration depth profiles with respect to the loaded force for 3 weight percent of non-functionalized boehmmite-epoxy nanocomposite.
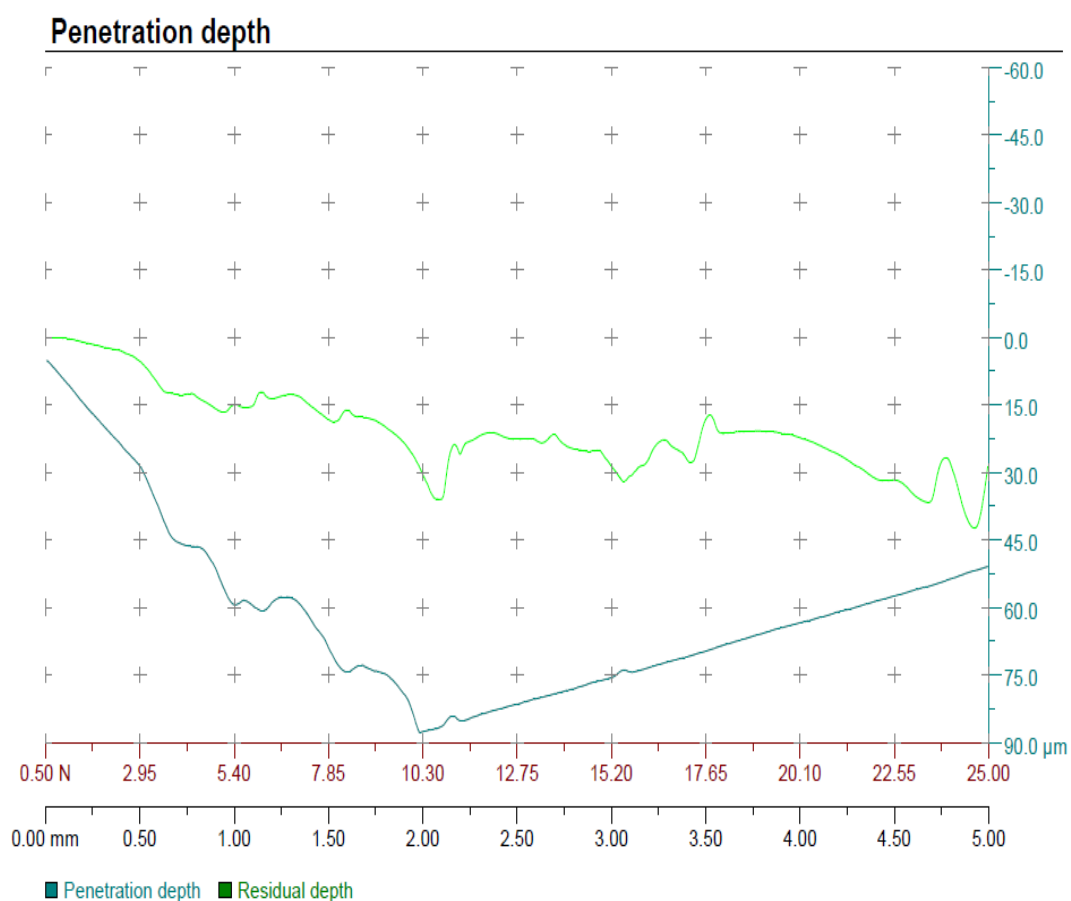
- **BH-EP5**

Figure A.20 Residual and penetration depth profiles with respect to the loaded force for 5 weight percent of non-functionalized boehmmite-epoxy nanocomposite.
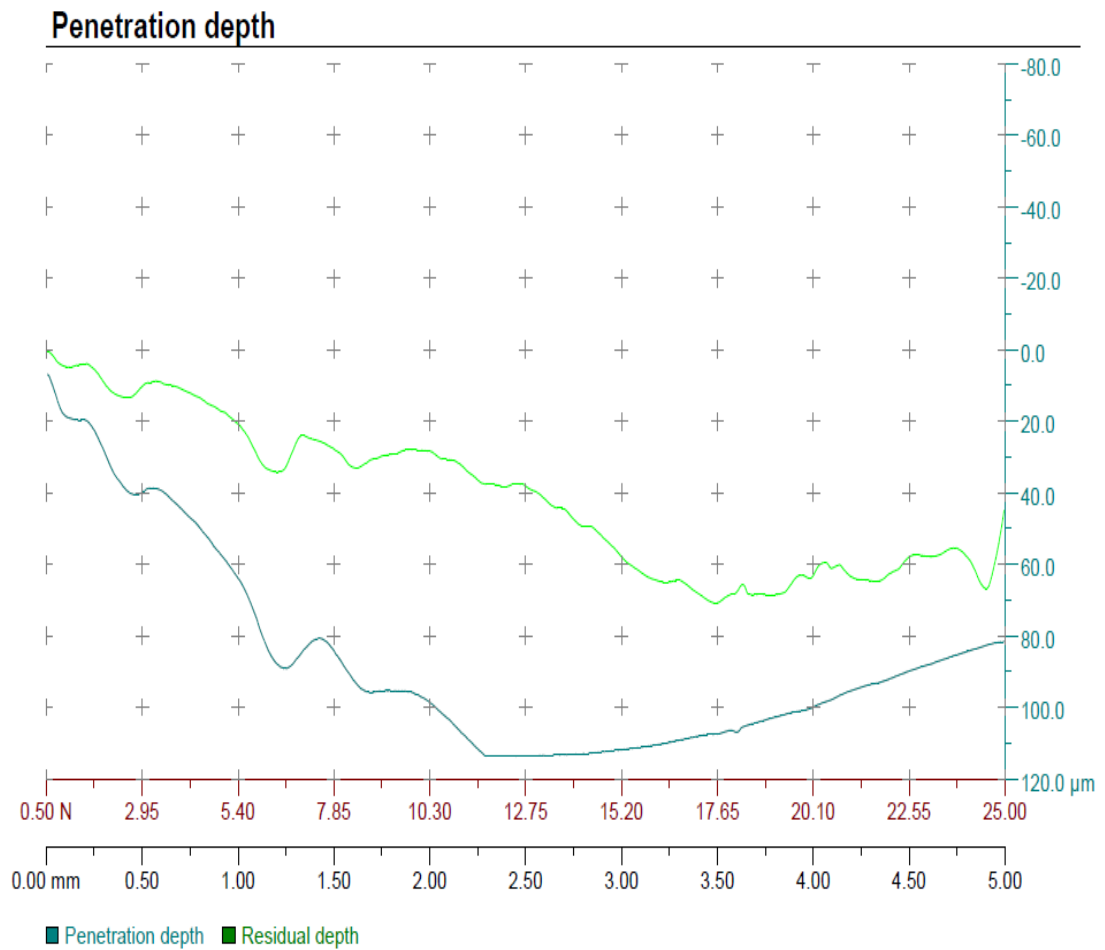
- **BH-EP10**

Penetration depth

Penetration depth   Residual depth

Figure A.21 Residual and penetration depth profiles with respect to the loaded force for 10 weight percent of non-functionalized boehmmite-epoxy nanocomposite.